

The author(s) shown below used Federal funds provided by the U.S. Department of Justice and prepared the following final report:

Document Title: Determination of Unique Fracture Patterns in Glass and Glassy Polymers

Author(s): Frederic A. Tulleners, John Thornton, Allison C. Baca

Document No.: 241445

Date Received: March 2013

Award Number: 2010-DN-BX-K219

This report has not been published by the U.S. Department of Justice. To provide better customer service, NCJRS has made this Federally-funded grant report available electronically.

Opinions or points of view expressed are those of the author(s) and do not necessarily reflect the official position or policies of the U.S. Department of Justice.

Determination of Unique Fracture Patterns in Glass and Glassy Polymers

Award Number **2010-DN-BX-K219**

Frederic A. Tulleners¹, MA, P.I.

John Thornton¹, D. Crim., Co-P.I.

Graduate Student Researcher

Allison C. Baca, BS¹

University of California - Davis,
Forensic Science Graduate Program,
1909 Galileo Ct., Suite B,
Davis, CA 95618

Disclaimer

“This project was supported by Award No. 2010-DN-BX-K219 awarded by the National Institute of Justice, Office of Justice Programs, U.S. Department of Justice. The opinions, findings, and conclusions or recommendations expressed in this publication/program/exhibition are those of the author(s) and do not necessarily reflect those of the Department of Justice.”

Abstract

The study of fractures of glass, glassy type materials, and plastic has long been of interest to the forensic community. The focus of this interest has been the use of glass and polymer fractures to reconstruct past events and to associate items of evidence. One example of this association is the matching of glass fragments from various locations where they can be shown to have come from a common origin. In the materials science community, fractography is the means and methods for characterization of fractured specimens or components in order to study or identify the mechanism of such failures, which is the focus on most of the literature on the subject. The ability to show that each and every fracture is, in fact, unique has not been a matter of consequence or of interest to the engineering or scientific community. In contrast, the basic premise that fractures are not likely to be reproducible is very relevant to the forensic science community. The issue arises when a given fracture pattern is restored or component pieces are physically fitted together and "matched" and the conclusion is drawn that this is unlikely to be possible unless all the components were derived from the same part. Despite the importance of this assumption, very limited research has actually been done to confirm that this is indeed the case. This study documented the very controlled fracture patterns of 60 glass panes, 60 glass bottles, and 60 plastic tail light lens covers. The pane and bottle specimens were fractured with three different types of penetration tips: sharp tip, round tip, and blunt tip. Two basic methods were used to initiate the fractures—dynamic impact from a dropping weight and static pressure from an Instron[®] 4204 Tensile Tester. The fracture patterns were then documented in great detail in such a manner that allowed the analyst to inter-compare the fracture patterns. This subsequent comparison illustrated the uniqueness of all of the fracture patterns we observed in

window glass, bottle glass, and plastic lens materials. Thus, we are substantiating the individuality of glass and polymer fractures under closely controlled conditions.

KEY WORDS

Fractography, Physical Match, Glass Fracture, Instron[®] Tensile

Table of Contents

Executive Summary.....	6
Introduction.....	15
Statement of the problem.....	15
Literature citations and review.....	17
Forensic Studies.....	17
Engineering Studies.....	24
Statement of hypothesis.....	27
Materials and Methods.....	28
Glass Panes.....	31
Dynamic Impact Procedure.....	31
Static Pressure Procedure.....	33
Glass Bottles.....	36
Dynamic Impact Procedure.....	36
Static Pressure Procedure.....	38
Plastic Lenses.....	41
Dynamic Impact Procedure.....	41
Static Pressure Procedure.....	43
Velocity Measurements.....	45
Inter-comparison of Fracture Patterns.....	49
Results.....	50
Glass Panes.....	50
Glass Bottles.....	53

Plastic Lenses.....	57
Conclusions.....	59
Discussion of findings.....	59
Implications for policies and practice.....	61
Implications for future research.....	62
References.....	64
Dissemination of Research Findings.....	66
Appendix A Fracture Images.....	A-1
Appendix B High Speed Fracture Video.....	B-1
Appendix C Testing Device Design.....	C-1
Appendix D Timing System.....	D-1

Determination of Unique Fracture Patterns in Glass and Glassy Polymers

EXECUTIVE SUMMARY

Synopsis

The study of fractures of glass, glassy type materials, and plastic has long been of interest to the forensic community. The focus of fracture research was mainly driven by the need to determine the various reasons for the failure of a brittle material. In the forensic science community, study of glass fractures has focused on reconstruction of the fracture mechanism by observing the presence of Wallner lines (arcing lines on the fracture surfaces) and Hackle marks (marks are parallel with stair-step structures) as well as the overall fracture patterns defined by radial (fractures radiating from the point of impact), concentric (fractures formed in a circular pattern around the point of impact), and conchoidal patterns (fractures with a beveled edge illustrating side of penetration). The forensic community currently relies on analytical techniques such as density measurements, refractive index measurements, and various elemental analyses to describe the chemical composition in an effort to determine if glass fragments share a common origin. Currently, most of the engineering research articles that specialize in fractures, discuss the formation of fractures and analytical observations postulate that all fractures are unique. The focus of most of the engineering literature is the explanation and mechanism of fractures. The ability to show that each and every fracture is, in fact, unique has not been a matter of consequence or interest to the engineering or general scientific community. A review of the forensic and engineering literature on glass fracture shows very little has been done that proves that each and every glass or polymer fracture is unique. Most researchers postulate that due to

matrix imperfections, fractures propagate randomly, but no significant research has been published in this area. Some research that has been done looked at the fracture of glass rods and glass microscope slides. However, these studies do not simulate forensic science case work involving fracture pattern analysis of window pane glass and glass bottles.

For the forensic community, the ability to piece together glass fragments in order to show a physical fit or a “Physical Match” is the strongest evidentiary finding of an association. The usual statement is that "the evidence glass fragment was physically matched to another glass establishing thus both share a common origin." The opinion is usually conclusive but lacks objective criteria to determine the uniqueness of a fit. In the area of glassy polymers, which are increasingly being used as glass substitutes, forensic reconstruction of polymer fracture has been investigated to a much lesser extent than glass. Some research has focused on the production of hackle marks and pseudo-conchoidal marks with high velocity projectile impacts. In essence, little research exists that looks at replication of fracture patterns in an attempt to objectively define uniqueness.

Purpose

The purpose of this research is to provide a first, objective scientific background that will illustrate that repetitive fractures, under controlled conditions on target materials such as glass window panes and glass bottles, are in fact different and unique. In this phase of our study, we fractured glass window panes, glass bottles (clear wine bottles), and polymer tail light lens covers. Each and every fracture was documented in detail for subsequent inter-comparison and to illustrate the uniqueness of the fracture pattern.

Research Design – Glass Fracture

We used 60 double strength glass (nominally 1/8" thick) window panes and 60 clear glass wine bottles for the glass portion of the fracture. The window panes were cut into 8" x 8" sections from a single sheet of double strength glass. Each pane was numbered as to its location on the original sheet. The glass wine bottles were 750 ml clear, flint glass bottles donated by the Gallo Wine Bottling Company in Modesto, CA. These bottles were manufactured in a two-step molding process and were taken from the line of a single day's work to ensure that the bottles were all manufactured from the same batch of glass. For the glass pane and glass bottle component, this research used two methods for fracture initiation:

1. A dynamic impact that used a dropping weight
2. A static impact which used an Instron[®] 4204 Tensile Tester

Each of these fracture methods was done with three different types of tips to initiate the fracture—a sharp tip, a round tip, and a blunt tip.

Dynamic Impact Experimental Design

The purpose of the dynamic impact was to have sufficient force to initiate a fracture and then stop the falling weight from penetrating the glass and causing excessive destruction of the window pane. In order to accomplish this, we designed a fracture device that allowed for a weight to be dropped at various heights and also allowed for the positioning of the glass pane so that the fracture tip only penetrated in a fraction of an inch, after which its further movement was absorbed by the fracture device. The 8" x 8" glass panes were placed on a 2" thick foam block. The flexibility of the foam was intended to allow for the formation of concentric fractures, as well as radial fractures.

The glass bottles were internally coated with RTV Urethane and allowed to set overnight. The purpose of the coating was to maintain the bottle structure for subsequent documentation after fracture. The bottles were aligned in a custom semi-circular stand, oriented by using the bottle mold line to ensure a 12 o'clock position for the fracture tip. The bottle was then rotated so that the bottle mold lines were at the 3 and 9 o'clock positions.

Static Impact Experimental Design

For the static tests, we used an Instron[®] 4204 Tensile Tester that can track force in both the compression and extension directions. A custom indenter was attached to the Instron[®] 4204 Tensile Tester with a 50 kN load cell. The indenter tips were the same three interchangeable fracture tips used for the dynamic impact experiments. These tips proved to be satisfactory in initiating fractures for both the glass panes and bottles. The force applied by the Instron[®] was documented as the maximum indenter extension in mm versus load in kN (kiloNewtons). For the glass panes, we initially tried using a foam backing but that technique caused problems with the Instron[®] unit. Therefore, we placed the glass panes in frames with a 1/2" lip around all 4 sides of the 8" x 8" section of glass window pane.

Fracture Documentation

After the glass panes were fractured, they were assembled and covered with clear tape for subsequent documentation. The fracture patterns were then documented in the following sequence:

- Hand sketching using an acetate overlay over the glass pane
- Scanning the glass at 600 dpi

- Translating the fracture on the glass panes by using a digitizer tablet which imported the data to a CAD.DWG file.

For the glass bottles, the fracture pattern was likewise documented by hand sketching using an acetate overlay, and the overlay was scanned at 600 dpi. The fractures on the glass bottle were not amenable to direct scanning or use of a digitizing tablet.

Velocity Documentation of the Dropping Weights

We used two methods to determine the velocity of the dropping weights. Using a high speed Phantom Video Camera (V 7.3), we were able to track the velocity of the weights using MATLAB[®] software that was able to track the position of a high contrast black circle on a white background (this circle was placed on the weight). The software provided the X, Y position of the black circle, frame by frame, and from this data, the software routine calculated the velocity. The second method for determining velocity of the weight involved the use of a series of specific wavelength sensors and an accurate timing mechanism. The distance between the start and stop sensor was measured to $\pm 1/16$ ". This distance was within one inch of the indenter travel.

Research Design – Polymer Fracture

For the polymer tail light lens cover, we used Bargman from Cequent[™] Electrical Products. They are composed of an acrylonitrile butadiene styrene (ABS) plastic, amber in color, and part number of 34-84-016. The lens covers are 5 5/8" x 4 1/4" and are used on trucks and motor homes. They were selected because of their uniform size, availability, and suitable configuration for fracture documentation.

We initially intended to use the same fracture tips that had been used for fracturing the glass panes and bottles. However, in the dynamic impact system, we could not obtain sufficient velocity to break the polymer lenses. The tips that did penetrate left a round hole the size of the fracture tip with minimal, if any, fracture lines. This also applied to static impact test with the Instron[®] 4204 Tensile Tester series of tests. We changed the indenter mechanism to a 2” diameter flat disc to conduct the static pressure tests. In reality, this may be more reflective of tail light lens breaking in an actual vehicle accident environment. A total of 30 plastic lenses were fractured using this method.

For the dynamic impact tests, we used a dropping pipe device set up at the California Criminalistics Institute (CCI). This device is used to induce filament deformation in automotive lamps. The 5 5/8" x 4 1/4" plastic lens was placed at the base of the CCI dropping pipe device. The lens was left in its original plastic packaging so that the fragments would remain contained. The pipe was raised to a predetermined height and released, striking the lens to initiate the fracture. This process was repeated at three different drop heights (3, 6, and 9 ft.), fracturing 10 plastic lenses per height. A total of 30 plastic lenses were fractured using the dynamic impact method.

Findings

Each fracture pattern was compared to that of every other fracture pattern within its category (pane, bottle, or lens). This was performed by overlaying one fracture pattern on top of another, in the same orientation for all patterns. This inter-comparison of fracture patterns was conducted in order to determine if the overall fracture pattern was duplicated. The 60 glass panes required a

total of 1,770 pairwise comparisons. Likewise, the 60 glass bottles required a total of 1,770 pairwise comparisons.

The plastics lenses were also subjected to two types of breaking routines. The analyses of the 60 fractures required total of 1,770 pairwise comparisons. The total number of comparisons that were made for glass panes, glass bottles, and plastic lenses in this study were 5,310.

In producing the glass fractures on the glass panes and the glass bottles, it can be seen that the blunt fracture tip required the highest velocity to initiate the fracture and the round fracture tip required the least. The force required to initiate the fracture was also reflected in the appearance of fracture pattern. The fracture patterns produced by the sharp tip had fewer fracture lines than that of the either the round or blunt tips. The fracture pattern produced by the blunt tip had the most fracture lines, and required the largest amount of load applied to the glass. Also noted was that the blunt tip produced a star-shaped fracture pattern, completely unlike the patterns produced by the sharp and round fracture tips.

Conclusions

No overall fracture patterns were duplicated in the glass window panes or the glass bottle experiments. Some similarities were noted in a limited number of specific fracture lines; however, the overall patterns were not duplicated.

The plastic lenses did exhibit some general similarities in fracture patterns, such as the center of many of the lenses breaking completely out of the lens. They also had a tendency to fracture along the mold lines of the lens. However, there were no duplicates of overall fracture patterns. Thus, one must use caution in looking at plastics lens fracture since the breaking of plastic lens

showed a tendency to fracture in specific areas, like along mold lines. More caution should be exercised in evaluating the uniqueness of fracture in this type of material.

Implications for Policy and Practice

These results support the theory that coincidental duplicate fracture patterns are highly unlikely to occur. This finding supports the reliability of physical match findings and fracture pattern interpretation when dealing with broken glass and plastic objects. This research should aid the practitioner in any court testimony involving the significance of fracture matching of broken glass and polymers materials.

One other issue to consider in our research is that we documented with 2-dimensional fractured images. In real time forensics fracture reconstruction, the analyst is generally working with a 3-dimensional fragment. Thus, they will have more discriminating capabilities.

Dissemination

This research has been presented at the American Academy of Forensic Sciences and a UC Davis graduate off-site seminar. Intentions are to present at a regional forensic science meeting in the Southwest and a regional meeting in Northern California. The research will also be condensed and submitted for publication in a suitable forensic science peer reviewed journal.

Future Research Suggestions

This study of 180 fractures (5,310 pairwise comparisons) was done by a graduate student researcher (GSR) with little forensic experience. But during the 1.5 years of the project, the GSR

gained extensive experience in documenting fractures. This study could be replicated by forensic examiners trained in physical matching.

High speed video could be helpful in assessing fracture formation or propagation. In our research, we saw some unusual fracture propagation in two glass bottles. Further research effort needs to be made in the area of mathematical assessment and analysis of the fracture features. If we can use mathematical techniques, we minimize possible bias or error caused by lack of attention to detail by an analyst in this type of research. Several options are available for image analysis using existing algorithms but would require some custom programming commands. Mathematical software exists which allows one to perform various mathematical operations on digital images. These routines enable one to extract significant information from a given fracture image. Future research opportunities exist for areas using such digital image software on our current fracture images. Some of the concepts that could be applied in order to explore match quality are:

- Document all the segments in a particular glass fracture and provide a pixel based area count of each segment in the form of a histogram.
- Document the glass segments by measuring its pixel circumference. When two segments have the same circumference, use other mathematical routines to evaluate the difference or similarity of segment shape.
- Count the length of each fracture line until it ends or intersects and plot this as histogram suitable for inter-comparison.

In conclusion, there remains a continuing need for more research effort in the area of physical matching of glass/polymer fractures using larger databases and their reduction to a suitable form of inter-comparison using mathematical algorithms.

Introduction

Statement of the problem

Glass and polymers are ubiquitous in our environment, and as a consequence, fractured glass and glassy polymers are encountered as evidence materials in both criminal and civil investigations. We are surrounded by glass and glassy polymers – in architectural situations, in automobile windows, in beverage bottles and other liquid containers, in incandescent light bulbs – and any of these may break under certain conditions. Certainly from a forensic standpoint, the presiding property of glass, and to a somewhat lesser extent with glassy polymers, is its susceptibility to breakage. The possibilities are legion. The glass may be broken purposefully, as with the forced entry into a building through a window, or it may be inadvertent, or incidental to a struggle. Within the forensic science community, glass fracture has been a consideration for more than 80 years. The fracture of polymers, because of their later introduction, is somewhat less researched.

From the very outset, it was appreciated that many torn or fractured materials could be fitted back together, and that an intimate fit of broken pieces would provide strong evidence that the pieces had at one time been joined. This was seen to apply to a fairly wide variety of materials – wood, ceramics, fabrics, paper, metals, and certainly glass. When an object is separated into two or more pieces with irregular margins and then reconstructed by fitting the pieces back together, it is said that a *physical match* exists between the items. A complementary and palpable physical match between separated items has historically been construed as proving that the items had originally been joined. Unambiguous physical matches are commonly considered to be the zenith of all forensic identifications.

This does not mean that physical matches, of all types and descriptions, are unassailable with respect to their validity. Physical matches of surface contours, particularly those of three dimensions, have an established basis in common sense and everyday experience. Everyone fitting a broken cracker back together is quickly convinced of the premise that the pieces were at one time an intact whole. For many people, this process may have started at an early age, perhaps with a broken toy.

But with few exceptions, the assumption of the significance of a physical match has not been subjected to rigorous scientific testing. If a fractured surface is unique, then one may make a reasonable posit that there exists a physical explanation for why it is unique. But the common experience of fitting broken pieces back together, with the acceptance of uniqueness, has resulted in a situation where any urgent necessity of proving fracture uniqueness by formal scientific studies has not been recognized.

This is no longer the case, and this situation cannot endure. The National Academy of Sciences Report – *Strengthening Forensic Science in the United State* [1] – has stressed the need for research to establish a firm scientific basis for many aspects of physical evidence that heretofore have been taken for granted. The uniqueness of fractured glass and polymers would fall in this category. And the *Daubert* decision [2], which either governs, or at least influences, the acceptance of scientific evidence in courts of law demands that scientific evidence be placed on a solid footing.

Hence the need and justification for the present research. It is appropriate, however, to first review the history of fractured glass and glassy polymers within the forensic science domain, as the interpretation of fractures is driven by the manner in which forces are applied and the manner in which the fractures are expressed, that is, their appearance. It is appropriate as

well to consider the subject from the engineering standpoint, as it is within the engineering discipline that fracture phenomena have been critically studied and described.

Literature citations and review

Forensic Studies

Early work within the forensic sciences was with respect to glass alone, and was directed toward the development of an explanation for why glass fractures in the manner in which it does rather than a detailed consideration of the appearance of the fractures themselves or the assessment of whether two pieces of fractured glass constituted an acceptable physical match.

In the forensic science literature, one of the earliest recorded interest in glass fracture was that reported by Preston [3]. The issue addressed by Preston was how flaws in glass were created using stationary, rolling, and sliding spheres and glazier's diamonds and wheels. Here he found that these flaws extend far below the surface irregularities. Further experiments by Preston [4] focused on blunt contact cracks. He described that some fracture marks surrounded an "explosion center." He goes on to say that he also observed "hackly features" surrounding a semicircular area of "polished" fracture. Based on these features, Preston concluded that explosion center was representative of a pre-existing flaw and the fracture spread over the small, semicircular area. These features have become known as the fracture origin, hackle lines, and fracture mirror, respectively [5].

Another early record of glass fracture interest was that reported by Matwejeff [6]. The issue addressed by Matwejeff was whether a glass window was broken from the inside of a room or from the outside. Matwejeff reported that he was unable to locate any previously published work on this issue, and as a consequence performed his own experiments. His conclusions remain valid to this date.

Matwejeff noted the presence of arcing lines on the fracture surfaces of broken piece of glass, the appearance of which bore a relationship to the side from which the force was applied to the glass pane. (These lines are now referred to in both engineering literature and forensic literature as Wallner Lines.) These lines, which are in relief, vary in the extent of their curvature. They are nearly parallel to one edge of the broken glass, and nearly perpendicular to the other. Matwejeff correctly understood that these lines were not due to some inherent property within the glass itself, but rather were a manifestation of the fracture process. Matwejeff also noted that fractures of window panes resulted in two discernibly different types of fractures. One type of fracture radiated away from the point of application of force, and these were termed *radial* fractures. Another type of fracture was concentric around the point of application of force, and were termed *concentric* fractures. Concentric fractures were not invariably observed, but tended to be seen with greater applications of force. Matwejeff recognized that the arcing lines (Wallner Lines) show a different orientation with radial and with concentric fractures.

Matwejeff was also armed with the knowledge that the tensile strength of glass is much lower than the compressive strength, *i.e.*, that glass breaks under tension, not compression. To explain the breaking of glass, Matwejeff then concluded:

- As a force is applied to glass, the glass deforms elastically until the elastic limit on the far side of the glass is exceeded. With the glass on the far side under tension, the near surface is under compression.
- The glass fails under tension, with the fracture initiating on the far side and radiating out from the fracture origin.
- If the force cannot be accommodated by radial fractures alone, the additional force will push in on the radial fractures, causing tension on the near surface.

- The glass will then break again under tension, this time from the near side. The fractures will then extend between the initial radial fractures, tending to form the boundary of a circle concentric around the fracture origin.
- The arcing lines (Wallner Lines) will indicate the direction of application of force if the analyst knows whether it is a radial or a concentric fracture surface that is being examined.

In 1936, the work of Matwejeff was confirmed by the FBI Laboratory [7]. (It should be stressed that this work, as with the original work of Matwejeff, was directed toward determining the direction of application of force to a broken window; the uniqueness of fracture surfaces was not at issue). The FBI Laboratory reported that in over 200 glass fracture experiments, no difficulty was encountered in determining the direction of application of force.

In the same year, Tryhorn [8] affirmed the work of Matwejeff, and elaborated on the issue of radial and concentric fractures. Tryhorn described radial fractures as occurring when a sharp pointed force was applied to the glass, while concentric fractures may be expected when blunt objects are involved. Tryhorn noted that concentric fractures may be absent when the original force is insufficient to break out pieces of glass. Tryhorn used the term conchoidal ('shell like') fractures to describe the arcing lines on fracture surfaces, and described the reverse relationship between the orientation of the lines on radial and concentric fractures. Tryhorn reported on some anomalous conchoidal lines on some radial fractures, remote from the point of impact. These anomalous lines were reversed from the typical radial/concentric orientation. Tryhorn speculated that these anomalous lines were the result of the window being rigidly held near supporting window frames.

A year later, in 1937, Nicholls [9] offered another explanation for anomalous lines, that in the fracture process, the glass may bend in a wave form with the reversal occurring at the wave nodes. Nicholls concluded that only the fracture surfaces between the point of origin and the first concentric fracture should be considered reliable for determining the direction of force.

Another fracture feature was described in the 1949 text by O'Hara and Osterberg [10]. In this text, *hackle marks* are described as a series of parallel marks in relief on fracture surfaces. The discussion of the interpretation of hackle marks in this work is no longer considered valid, but hackle marks clearly contribute to the “fit” of a physical match between fracture surfaces.

In 1936, the FBI advanced the “3R” rule [11] to summarize the relationship of arcing (conchoidal or Wallner Lines) to the direction of force applied to breaking glass, that a radial fractures produces arcs at right angles (i.e., perpendicular) to the rear (i.e., far) surface of the window.

Nelson discussed the value of hackle marks in the interpretation of direction of force from an operational standpoint [12]. Hackle marks are parallel, and may be more easily photographed than Wallner Lines, which are curved and do not provide a single angle from which the lines may be illuminated to illustrate their entirety. As Thompson pointed out, however, they are of themselves somewhat difficult to photograph [13]. Thompson considered hackle marks in greater detail, noting that hackle marks often present themselves as varying stair-step structures, with a shelf at the top (fracture edge) and base of the deeper marks. The shelves at the top are parallel to each other, and the same may be said for the shelves at the bottom of the hackle. But those at the top are typically at a different angle than those at the bottom, causing one type or the other to be more prominent visually, but not both at the same time.

In 1973, the entire subject of glass fracture was reviewed by McJunkins and Thornton [14]. In this review, the fracture-related properties of glass were developed, including processes in glass formation, the atomic arrangement in glass structure, glass composition, and mechanical and physical properties of glass. Fracture surface markings were discussed, including mirror, mist or fine hackle, coarse hackle, and conchoidal or Wallner Lines. The relationship of stress conditions to fracture surface properties was developed.

The subject was again approached in 1986 by Thornton and Cashman [15]. The principal thrust of this work was to clarify the assumption and attitudes within the forensic science community that the fracturing of glass centers around the tensile failure of the glass. Frequently that was described as the “bending” of the glass, a holdover from Matwejeff. Thornton and Cashman pointed out that while this is not conceptually incorrect, current developments within the engineering community have shown that deflection of glass represents only one case of a more universal phenomenon in which the tensile failure of glass does not necessarily involve actual deflection. Tensile failure can result with either quasi-static or dynamic loading of the glass. In quasi-static loading, tensile failure will be initiated at the weakest point. This weakest point will be a so-called *Griffith Crack*. A Griffith crack is a hypothetical flaw, the sides of which may be in optical contact with one another. With the conceptualization of a Griffith crack, no actual deformation of the glass would be required before failure. (As developed by Thornton and Cashman, dynamic loading will explain the “cratering” observed with moderate to high-velocity projectile impact, an aspect of fracturing which is not relevant to the present work).

The interpretation of the physical aspects of glass was again reviewed by Thornton in 2001 [16]. Fracture-related surface features were discussed, but also the uniqueness of glass

fracture was addressed. The rationale for the uniqueness of a glass fracture was summarized as follows:

- Glass is an amorphous solid, with no definite structure and with no favored cleavage as determined by a crystalline lattice. A fracture is a rupture of atomic bonds, but since the atoms in glass are arranged in no consistent order, the fracture is therefore between atoms that are uniquely positioned in the glass. In another sample of glass, the atoms will again be uniquely positioned, but there is no mechanism advanced by chemical or physical phenomena that would suggest that the positioning of the atoms in one sample would mimic the positioning in another sample.

Other considerations of glass fracture have been addressed in the forensic literature, such as thermal fractures and fractures resulting from the impact of high-velocity projectiles, or the production of very small fragments of glass in a direction retrograde to the application of force, that is, a “backward” cascade of very small particles if a window is broken. Tempered or disannealed glass is entirely a separate area. With one exception, these issues are not relevant to the present study and will not be discussed here. The one exception is that fractures, of whatever sort, will not cross. A fracture that approaches another fracture will be immediately arrested and will not extend beyond the first fracture. This is because the continuity of the material has been disrupted by the first fracture, thus prohibiting the second fracture from continuing any further. This has implication in establishing a temporal sequence to a series of fractures, but is also relevant to the general appearance of a pattern of glass fractures.

Although glassy polymers are increasingly being used as glass substitutes, within the forensic science discipline the fracture of glassy polymers has been investigated to a much lesser

extent than glass. Rhodes and Thornton studied glassy polymers from the standpoint of high-velocity impact, that is, projectile impact [17]. While high-velocity projectile impact is not relevant to the present study with respect to glass, one observation developed in this study may be relevant to glassy polymers. Rhodes and Thornton observed that pronounced, high curved hackle marks may be observed on fracture surfaces. These have the potential of being mistaken for conchoidal marks (Wallner Lines). If glass fracture considerations were projected onto the glassy polymer fracture phenomena, a determination of the direction of force based on these *pseudo-conchoidal* marks would be in error.

Katterwe [18] illustrates several examples of plastics and glass fractures and their subsequent visual comparison. He describes a series of fractures on glass by using a Vickers Hardness tester. The fractures were initiated using three different loads and were generated under reproducible point sources. He was able to show that, under the same experimental conditions, the fractures resulted in randomly distributed cracks: crack numbers, lengths, propagations, directions, shapes, and orientations. However, the glass specimens he used were microscope slides. The number of these samples was not specified in this paper but appear to be at least 5 specimens. He stated that there is a close association between fracture origins and surface flaws. These surface flaws are a result of the production process and are randomly distributed from sample to sample. This random distribution of irregularities is the basis for the randomly distributed cracks in the specimens. Sglavo [19] used cyclic loading with Vickers indentation on commercial soda-lime-silica glass bars to look at crack propagation and its subsequent examination by fractography. He was able to correlate experimental results with theoretical predictions. These predictions were obtained on the basis of indentation fracture mechanics and a sub-critical crack propagation mechanism.

Engineering Studies

From an engineering and materials science standpoint, the fracturing of glass has been the subject of numerous studies. Conspicuous among these in terms of detail and appropriateness to the issue of fracture uniqueness are those of Shinkai [20], Orr [21], Ropp [22], Mecholsky [23], Kepple and Wasylyk [24], and Quinn [25]. It should be recognized, however, that the engineering and materials science concerns are directed toward durability and manufacturing considerations. While the fracturing of glass and the phenomena associated with it are important concerns, the question of the uniqueness of fractures isn't countenanced. Stated differently, while engineers, material scientists, glass and ceramic chemists, and glass and polymer manufacturers have actively pursued research into fracture mechanisms, they all have assumed that fractures are unique and consequently have not directly addressed that issue. In a sense, they have taken for granted that fractures are unique in the same manner that forensic scientists have taken it for granted.

Engineering studies have developed considerable information that is germane to the subject of glass fracture. Glass breaks under tension, not compression. (In somewhat imprecise terms, but in terms that may be more meaningful to a lay jury or other users of forensic information, when a piece of glass is pushed, it doesn't break from the side that has been pushed, but rather from the back side, which has been stretched. As stress is applied to the glass, the tensile limit will invariably be reached before the compression limit. Glass may certainly break under compression, but before it has an opportunity to do so, it has already broken under tension).

Engineering studies have not in all respects resolved certain competing theories concerning glass fracture. The Griffith Theory of fracture propagation [26] anticipates that a

flaw or defect must be present before a fracture can be initiated. This defect may be so small as to be undetected by any reasonable means. Griffith flaws are generally conceded to exist, but evidence for them is largely indirect and their existence may be conceptual rather than actual. Poncelet [27] has advanced a theory requiring only that the application of stress for a critical amount of time. In the Poncelet Theory, there is a normal equilibrium rate of atomic bond rupture and reformation. This rate is influenced by stress, and when the rate of bond rupture exceeds the rate of bond formation, a fracture will be induced. There has not been an entirely adequate resolution of these two theories, but both appear to have merit. In the practical interpretation of glass fracture and fracture uniqueness, it is not essential that either of these theories would need to be favored.

Features may be observed on the fracture edges that illustrate a relationship between fracture behavior and the topology of the surface. These are mirror, mist, hackle, and Wallner Lines. These are not chaotic, but have different characteristics that are capable of being interpreted in terms of the fracture process. There is no universally accepted nomenclature, and unfortunately there is some confusion in the engineering literature, where hackle is occasionally seen as “striations,” and Wallner Lines as both “conchoidal marks” and “ripple”. An effort at standardization is seen, however, in an ASTM Standard [28] on the subject of definitions related to glass.

Mirror. Near the fracture origin, the propagation of the fracture is relatively slow. When the fracture edge is observed, it will be flat and virtually featureless. This area may exist for only a few millimeters with moderate impact, but for several centimeters with very low impact force. Since the surface is flat and reflects light efficiently, it is termed mirror. Two pieces of glass of the same thickness but from different fractures could conceivably be fitted together tightly, but

only if a very small extent of the fracture were to be considered. Given the fact that mirror operates over a very small domain, this is not a credible attack on the validity of a palpable physical match.

Mist. As the fracture continues from the origin and picks up speed, the fracture tip cannot dissipate the accumulated stress efficiently. As a consequence, the fracture edge will increase its surface area in order to decrease its surface free energy. Very small cracks will develop, but they are so small that even under magnification they are poorly resolved. Under low magnification they appear as a “frosted” or “misty” area, and are termed “mist.” Although mist areas do not provide much relief, there is not a definite relief aspect to the fracture edge. The fracture edge now has a three dimensional character, and two pieces of glass of the same thickness but from different fracture will not result in a palpable physical match.

Hackle. Hackle consists of rather coarse parallel marks, and the relief aspect is significant. The processes leading to the formation of hackle are not altogether settled in the engineering literature. It is unclear whether it is formed as a result of a further extension of the phenomenon of reduction of surface free energy by an increase in surface area, or whether it is formed on a fracture surface as a result of a localized realignment in an effort for the fracture propagation to remain perpendicular to the tensile stress. In the consideration of the uniqueness of glass fracture for forensic purposes, it isn't necessary to chose between these competing explanations. Hackle in which a particular mark extends outward from the fracture surface must have a complementary area of depression in its fracture mate. Stated differently, wherever there is a “zig” on one piece, there must be a “zag” in the other. Consequently, when hackle exists, it contributes significantly to a palpable physical match.

Wallner Lines. The conchoidal lines which are referred to in the engineering literature as Wallner Lines are the most conspicuous of all fracture edge markings. The relief aspect of these lines is considerable, and certainly greater than the fracture markings previously described. As with hackle, an area on one fracture surface that extended away from the fracture margin would require a complementary retreat from the fracture surface on its fracture mate.

The significance of these fracture surface markings is that a fracture is not solely a two-dimensional affair, (although that is the principal focus of the present study). A broken piece of glass may have an exclusive pattern of fracture, with irregular contours and an inimitable arrangement of radial and concentric fracture. But in glass of any appreciable thickness, it will also have a three-dimensional aspect which may be exploited to determine if two pieces had at one time been joined. Both considerations are significant in the assessment of fracture uniqueness.

Statement of hypothesis

In this research, it is hypothesized that every fracture forms a unique and non-reproducible fracture pattern. Alternately, it may be that some fracture patterns may be reproduced from time to time. If it is found that each fracture forms a unique and non-reproducible fracture pattern, then this finding will support the theory that coincidental duplication of fracture patterns cannot be attained. However, if duplicate fracture patterns are found, this would falsify the null hypothesis and show that some fracture patterns may be reproduced from time to time.

Materials and Methods

The materials used in this study were 60 panes of double strength glass, 60 glass bottles, and 60 polymer tail light lenses. Double strength glass is 1/8" thick, whereas single strength glass is 3/16" thick. The glass panes were 1/8" thick and cut into 8" x 8" sections from a single sheet of double strength glass, in order to maintain uniformity of the glass and were numbered as to their location on the original sheet. The glass wine bottles were 750 ml clear, flint glass bottles donated by the Gallo Wine Bottling Company in Modesto, CA. These bottles were manufactured in a two-step molding process and were taken from the line of a single day's work to ensure that the bottles were all manufactured from the same batch of glass. The molding process began by melting the glass along with recycled cullet in the furnace. The molten glass was then extracted from the bottom of the furnace as a molten glob and taken up by the assembly line to fill the bottle mold. Air was blown into the molten glob to form the head, neck, and shoulder of the bottle. The mold was then inverted and air was blown in to form the rest of the bottle. The inversion of the mold caused some of the molten glass to settle toward the base of the bottle. This is known as the "settle wave" and the glass here is usually thicker and looks slightly distorted.

For the polymer tail light lenses, we used Bargman from CequentTM Electrical Products. They were composed of an acrylonitrile butadiene styrene (ABS) plastic and amber in color with part number 34-84-016.

Fractures were initiated using two methods: dynamic impact and static pressure. The materials used for the dynamic impact method included a custom built fracture device with an adjustable top to accommodate both the glass panes and bottles (Fig.1). This device sat at the bottom of a 12' polycarbonate tube which acted as a guide for the dropping weight. The dropping weight

consisted of a set of weights, totaling 965g, with three interchangeable impact tips—round, sharp, and blunt (Fig. 2). The fracture device was built such that the dropping weight impacted the glass only a fraction of an inch, so upon fracture initiation, no secondary impact would occur. Thus, most of the subsequent kinetic energy was absorbed by the fracture device.

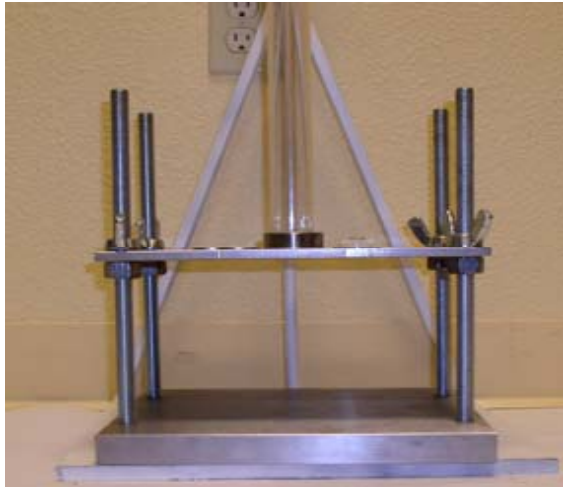


Figure 1 Fracture device



Figure 2 Dropping weight with interchangeable impact tips (round and sharp shown)

Although suitable for the glass panes and bottles, this fracture device did not prove to be sufficient in initiating fractures in the plastic lenses. Instead, a dropping pipe (normally used for the deformation of headlamps) was used at the California Criminalistics Institute. The setup consisted of the dropping pipe with guide wires on each side to keep it aligned, which impacted a steel plate (Figs. 3 & 4).

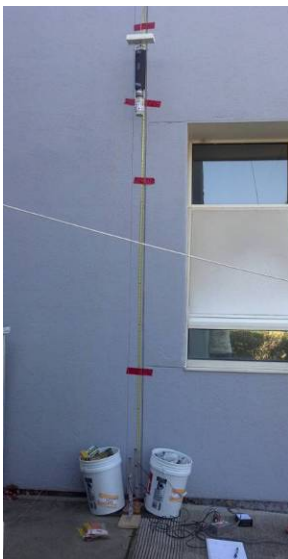


Figure 3 Dropping pipe setup



Figure 4 Close-up of impact site

The weighted buckets shown in Figures 3 and 4 were placed on the impact plate in order to maintain tension on the wires allowing for an almost friction free drop. The pipe, originally weighing 2,094 grams, was filled with a lead ingot to add additional weight, bringing the total to 2,359 grams. This pipe was then placed in a drop cage which kept the pipe in line with the wire guides (Figs. 5-7).



Figure 5 Drop cage



Figure 6 Dropping pipe



Figure 7 Base cap of dropping pipe

The instrument used for the static pressure method was an Instron[®] 4204 Tensile Tester with a 50 kN load cell (Fig. 8). The acrylic container pictured in Figure 8 was used as a precaution in order to contain any glass shards that resulted from the compression tests. The indenter that was used in the Instron[®] was custom built similar to that of the dropping weight in the dynamic impact method. It too had three interchangeable fracture tips of the same type. These tips proved to be satisfactory in initiating fractures for both the glass panes and bottles; however, a wider tip had to be used to initiate fractures in the plastic lenses (Fig. 9). The narrower tips penetrated the plastic lens, creating a hole, without making any significant fractures.



Figure 8 Instron® 4204 Tensile Tester (glass bottle setup shown)



Figure 9 Indenter with wide fracture tip (right side)

Glass Panes

Dynamic Impact Procedure: An 8" x 8" glass pane was placed on a 2" thick foam block. The flexibility of the foam was intended to allow for concentric fractures, along with the expected radial fractures. The foam block and glass pane were then placed under the fracture device which was adjusted so that the impact tip was just slightly in contact with the glass. The dropping weight was raised to a predetermined height and released to initiate the fracture. This process was repeated for each of the three impact tips, fracturing 10 glass panes per tip. A total of 30 glass panes were fractured using the dynamic impact method.

After each pane was fractured, it was reassembled and the fracture pattern was secured with clear packing tape on either side of the glass. The fracture pattern was then documented by hand sketching using an acetate overlay, scanned at 600 dpi, and translated to a CAD DWG file using a digitizer tablet. Subsequent velocities were then calculated using high speed video and an electronic timing system. This is further discussed in the "Velocity Measurements" section. Figures 10-12 are representative fracture patterns for each of the three impact tips.

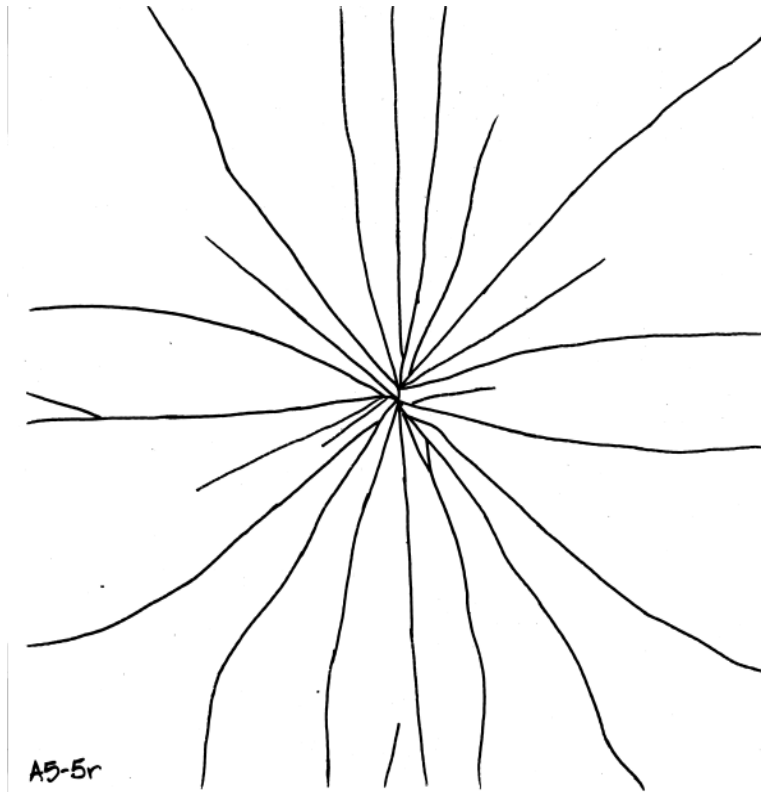


Figure 10 Fracture pattern using round impact tip

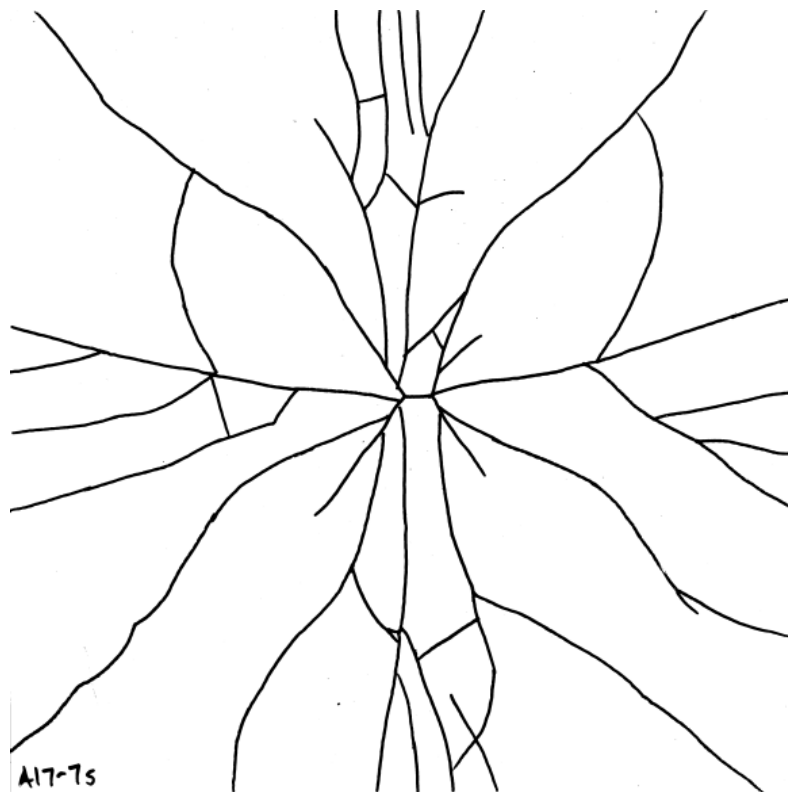


Figure 11 Fracture pattern using sharp impact tip

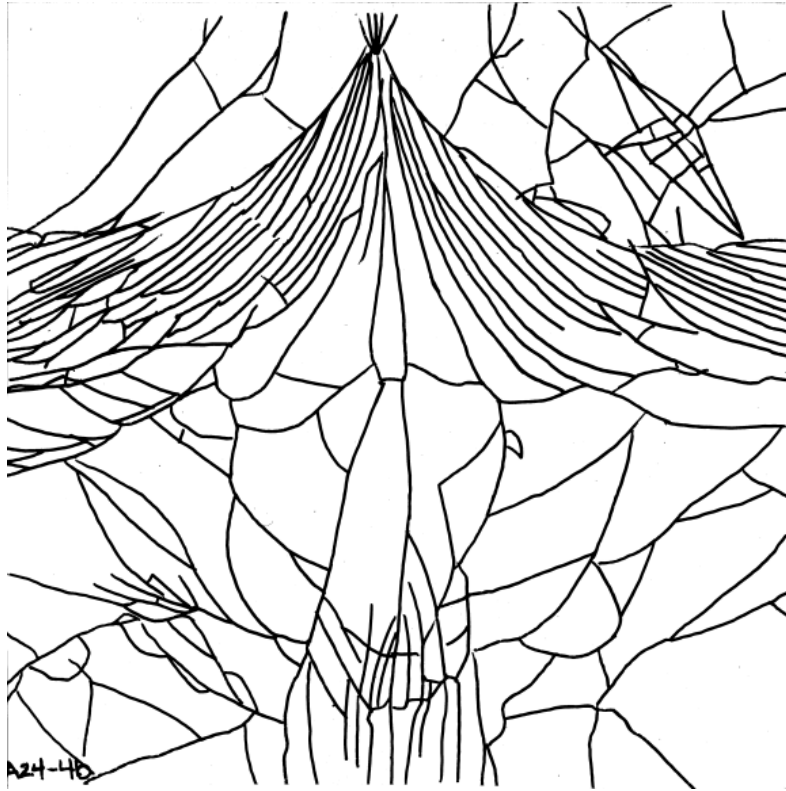


Figure 12 Fracture pattern using blunt impact tip

Static Pressure Procedure: An 8" x 8" glass pane was placed in a wood frame. The foam block was not used for these experiments because it did not prove to be suitable and did not work with the Instron[®] tester. The wood frame, however, allowed for the flexibility necessary to obtain concentric fractures along with the expected radial fractures. Once the glass pane was placed in the frame, it was placed under the indenter of the Instron[®]. An acrylic container was placed around the glass to ensure that any shards were safely collected. The indenter crosshead speed was set to 10 mm/min and would automatically stop compression when the fracture occurred. As the indenter began to apply compression to the glass pane, the Instron[®] software recorded load versus extension. Once the initial fracture occurred, the indenter stopped and the software produced a load profile of the fracture. This process was repeated for each of the three fracture

tips, fracturing 10 glass panes per tip. A total of 30 glass panes were fractured using the static pressure method.

After each pane was fractured, it was removed from the frame and reassembled. The fracture pattern was subsequently secured with clear packing tape on each side of the glass. The fracture pattern was documented by hand sketching using an acetate overlay, scanned at 600 dpi, and translated to a CAD DWG file using a digitizer tablet. Figures 13-15 are representative fracture patterns for each of the three fracture tips.

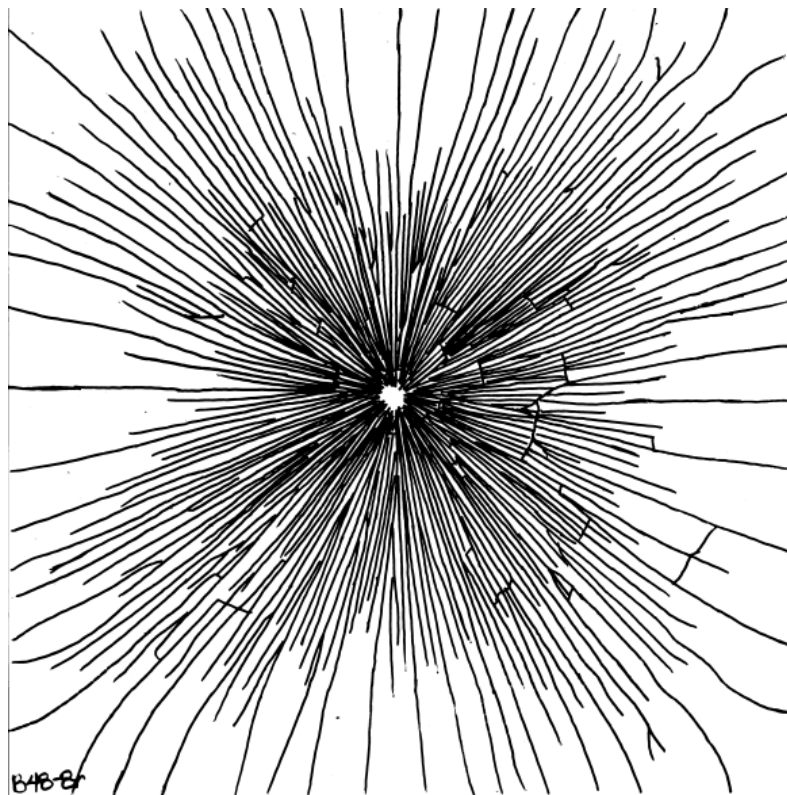


Figure 13 Fracture pattern using round fracture tip

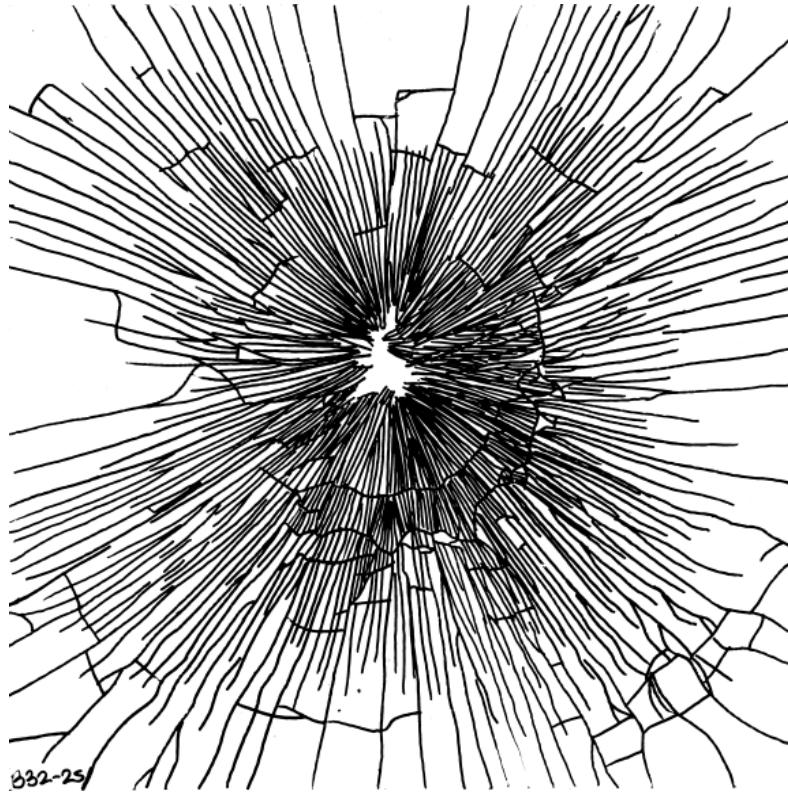


Figure 14 Fracture pattern using sharp fracture tip

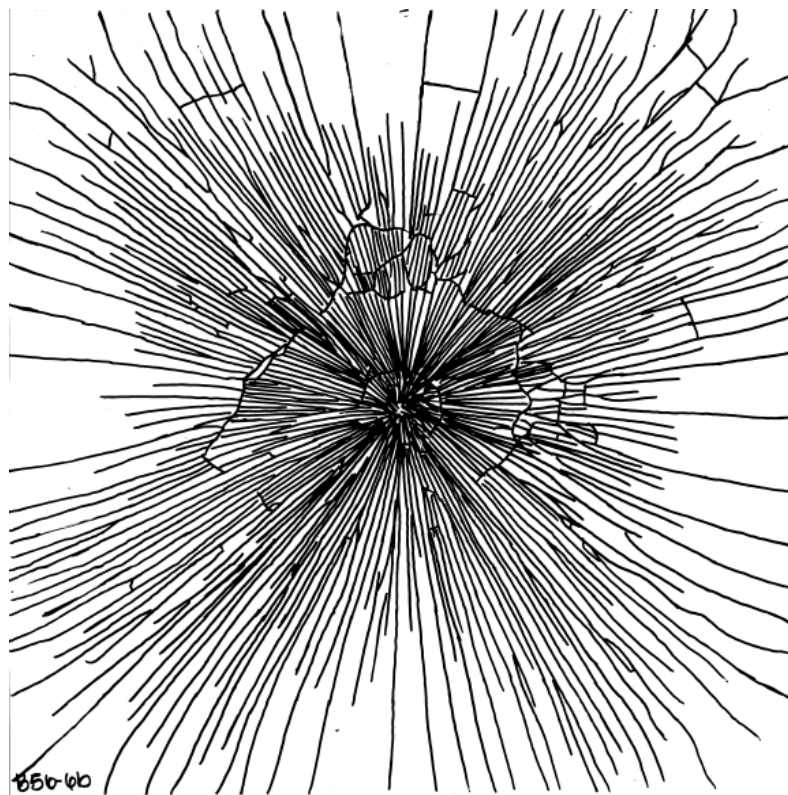


Figure 15 Fracture pattern using blunt fracture tip

Glass Bottles

Dynamic Impact Procedure: Each glass bottle was internally coated with RTV Urethane and allowed to set overnight. This coating was flexible enough that it did not impede the fracture, yet strong enough that it retained the shape and fracture pattern of the bottle. Once the urethane had set, the bottle was placed in a custom built bottle cradle that prevented the bottle from shifting as the bottle was impacted. The bottle was initially placed in the cradle such that the seam was at the 12 o'clock position. Here, the impact tip was lined up so that it just slightly contacted the glass. Subsequently, the bottle was rotated 90° so that the seams were at the 3 and 9 o'clock positions. The dropping weight was raised to a predetermined height and released to initiate the fracture. This process was repeated for each of the three impact tips, fracturing 10 glass bottles per tip. A total of 30 glass bottles was fractured using the dynamic impact method. After each bottle was fractured, the fracture pattern was secured with clear packing tape. The fracture pattern was then documented by hand sketching using an acetate overlay. Due to the shape of the specimen, it did not lend itself to documentation by scanning or translating to CAD files. Subsequent velocities were then calculated using high speed video and an electronic timing system. This is further discussed in the "Velocity Measurements" section. Figures 16-18 are representative fracture patterns for each of the three impact tips.



Figure 16 Fracture pattern using round impact tip

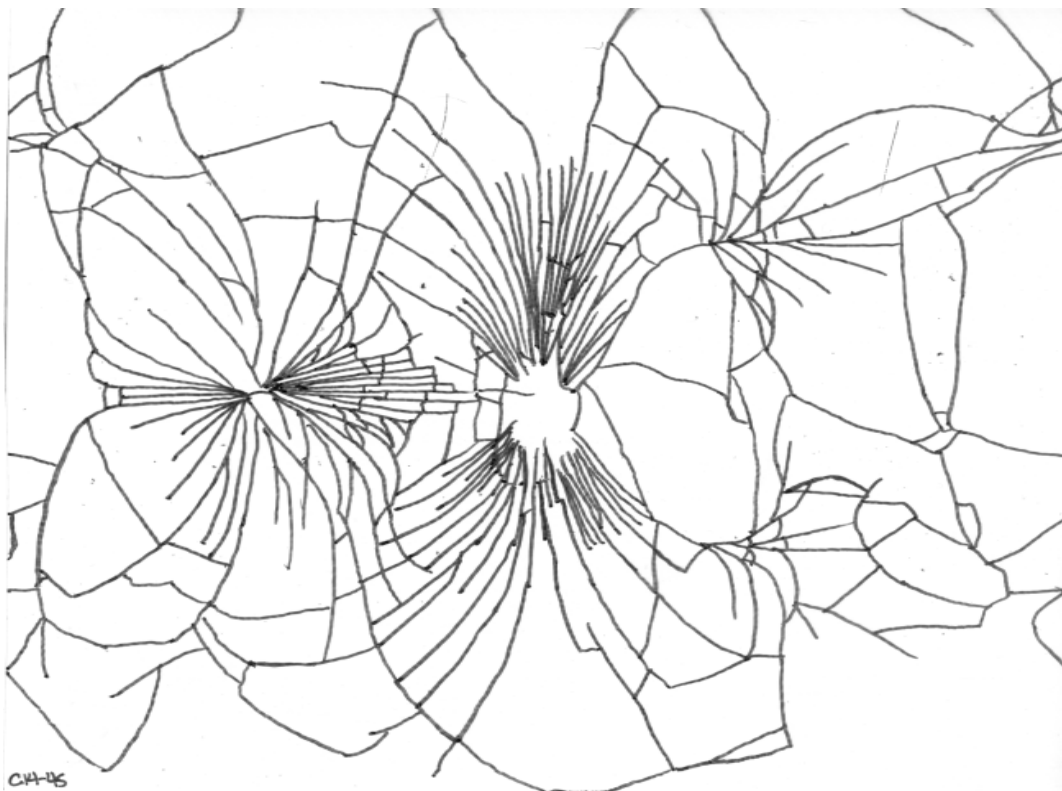


Figure 17 Fracture pattern using sharp impact tip

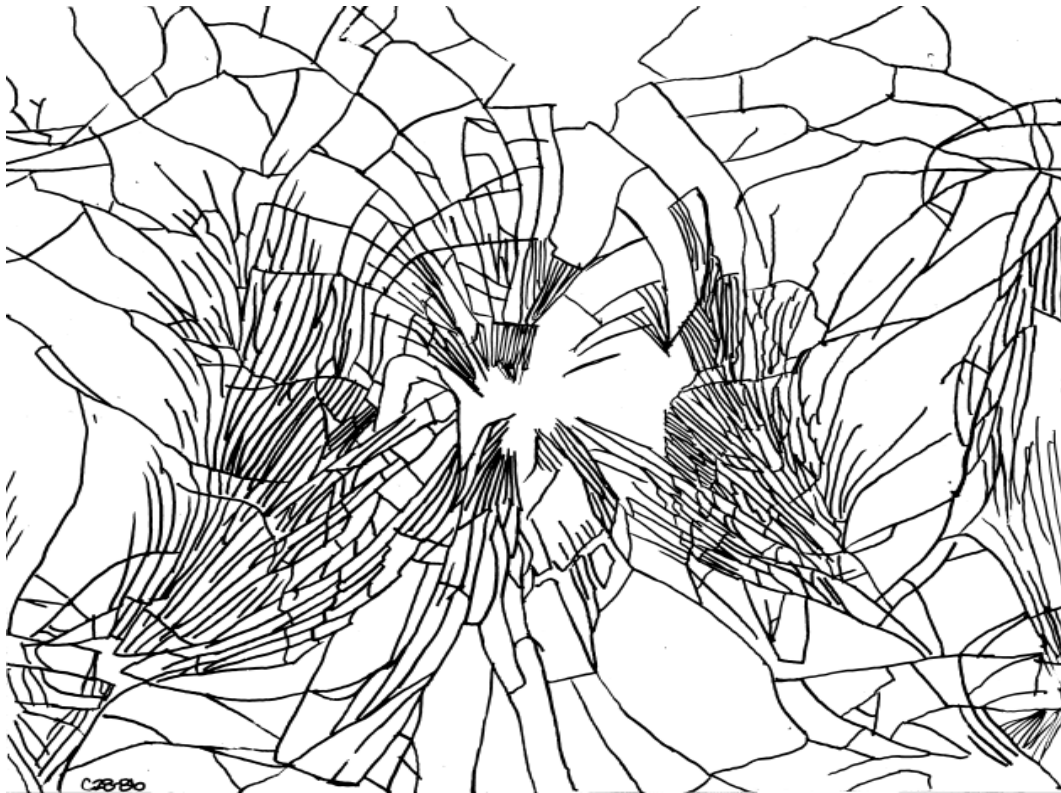


Figure 18 Fracture pattern using blunt impact tip

Static Pressure Procedure: Like for the dynamic impact, each glass bottle was internally coated with RTV Urethane and allowed to set overnight. This coating was flexible enough that it did not impede the fracture, yet strong enough that it retained the shape and fracture pattern of the bottle. Once the urethane had set, the bottle was placed in a custom built bottle cradle that prevented the bottle from shifting as compression was applied. The cradle and bottle were then placed under the indenter of the Instron[®]. The acrylic container was again used to collect any resulting glass shards. The indenter crosshead speed was set to 10 mm/min and would automatically stop compression when the fracture occurred. As the indenter began to apply compression to the glass bottle, the Instron[®] software recorded load versus extension. Once the initial fracture occurred, the indenter stopped and the software produced a load profile of the

fracture. This process was repeated for each of the three fracture tips, fracturing 10 glass bottles per tip. A total of 30 glass bottles was fractured using the static pressure method.

After each bottle was fractured, the fracture pattern was secured with clear packing tape. The fracture pattern was then documented by hand sketching using an acetate overlay. Figures 19-21 are representative fracture patterns for each of the three fracture tips.

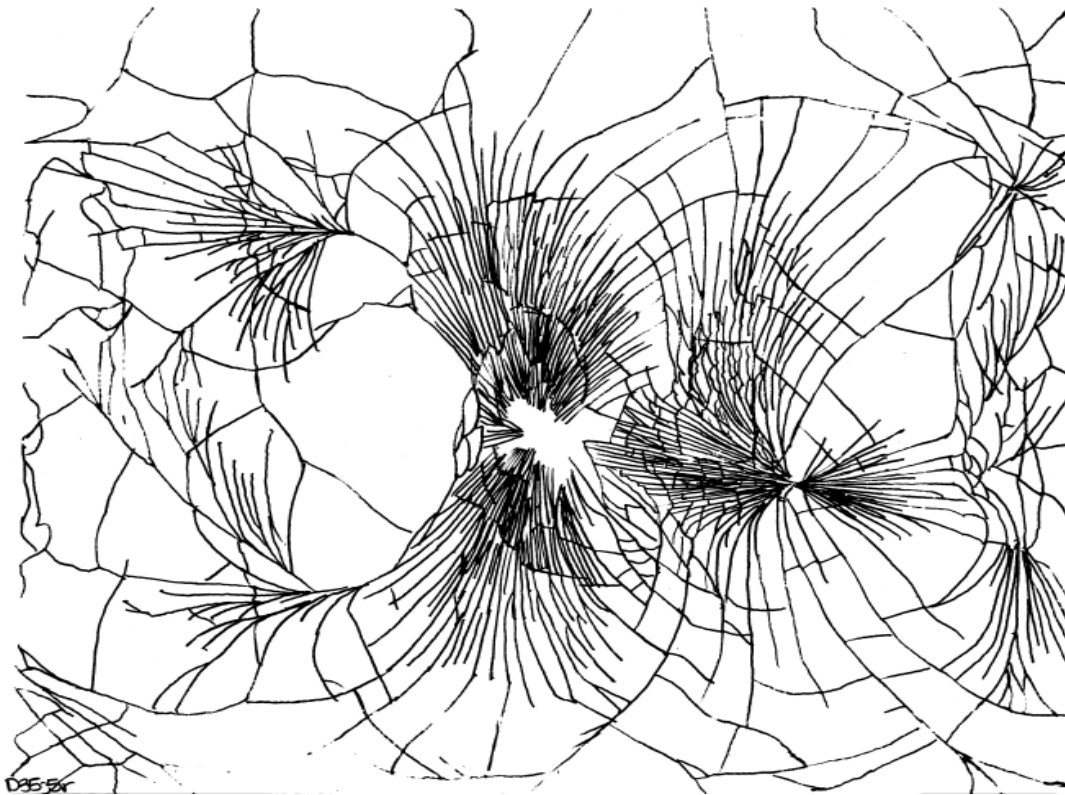


Figure 19 Fracture pattern using round fracture tip

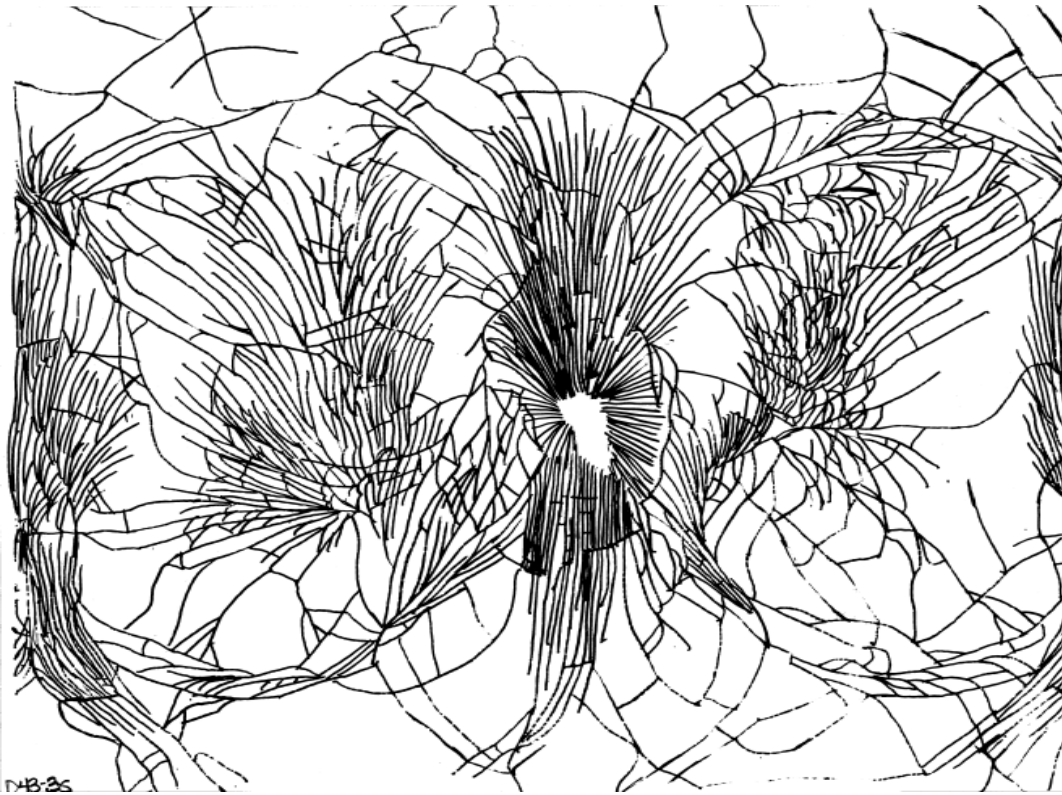


Figure 20 Fracture pattern using sharp fracture tip

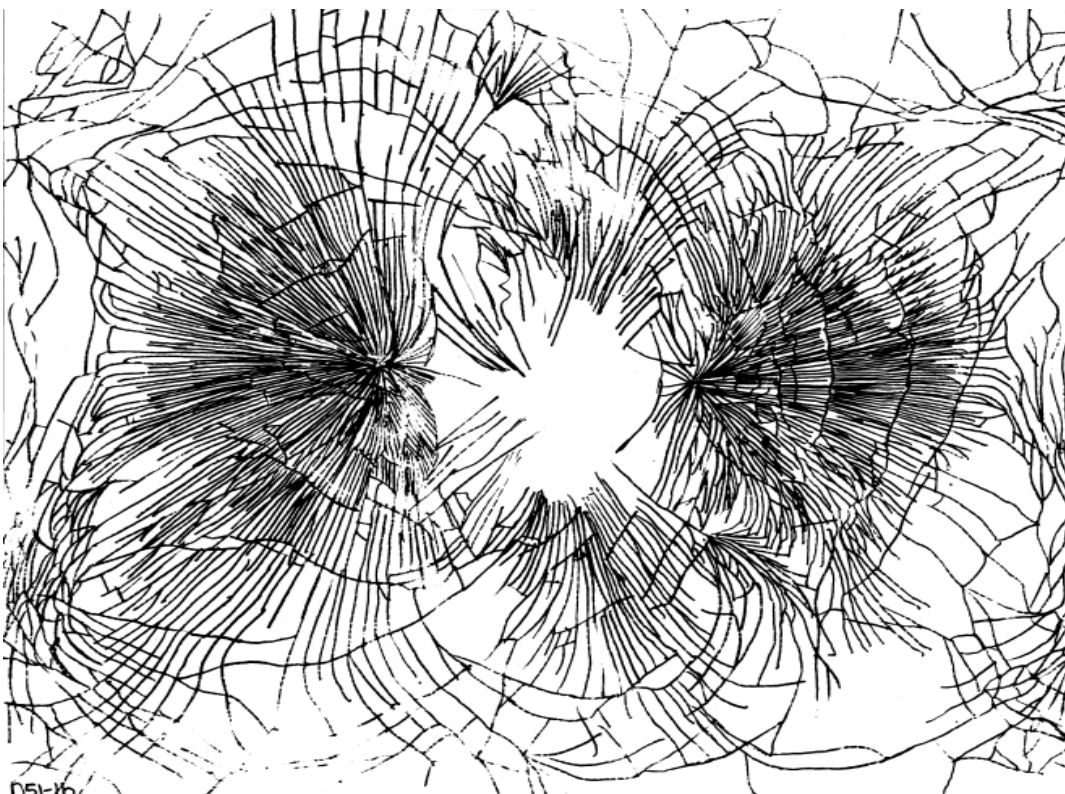
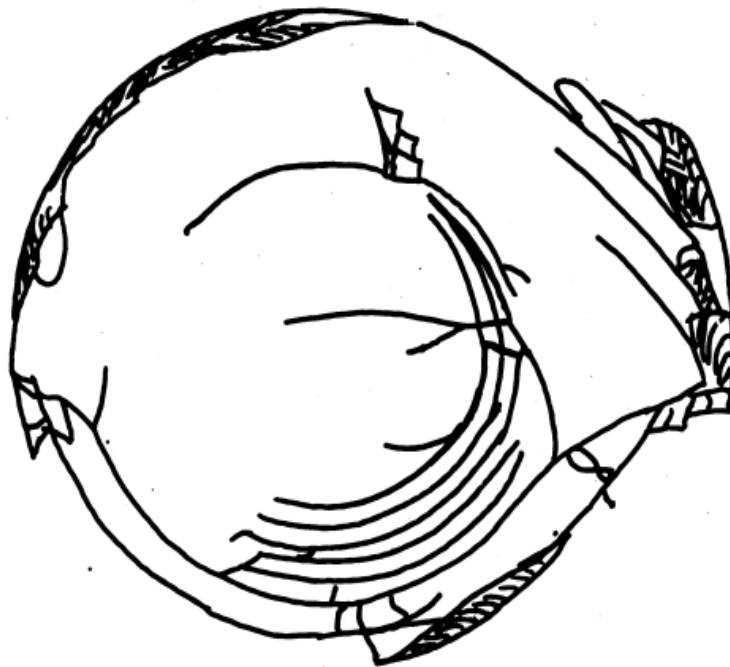


Figure 21 Fracture pattern using blunt fracture tip

Plastic Lenses

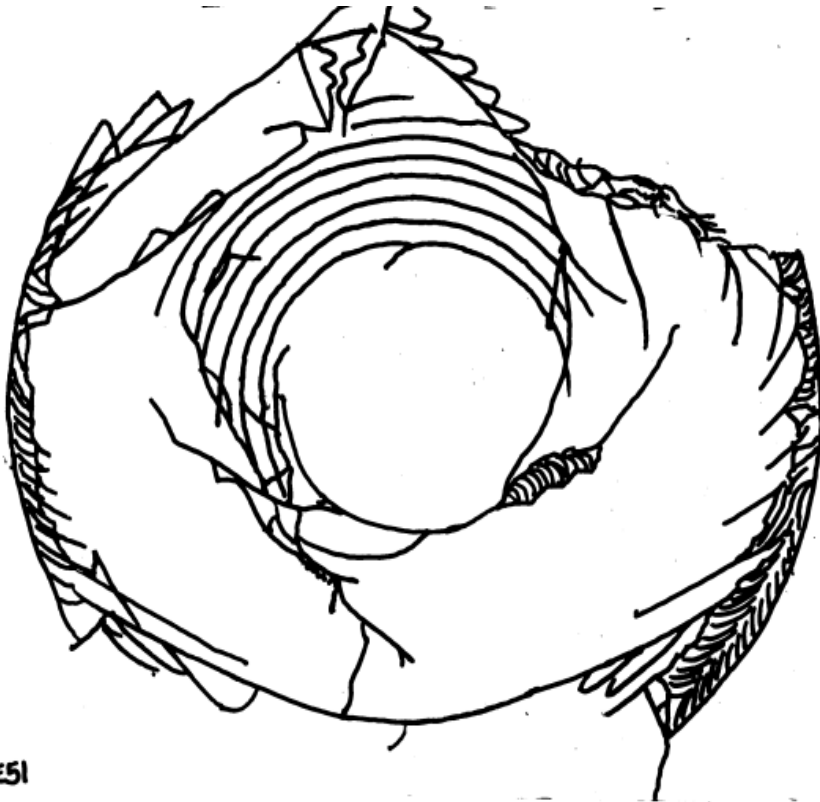
Dynamic Impact Procedure: A 5 5/8" x 4 1/4" plastic lens was placed at the base of the CCI dropping pipe setup. The lens was left in its original plastic packaging so that the fragments would remain contained. The dropping pipe was raised to a predetermined height and released to initiate the fracture. This process was repeated at three different drop heights (3, 6, and 9 ft), fracturing 10 plastic lenses per height. A total of 30 plastic lenses were fractured using the dynamic impact method.

After each lens was fractured, it was reassembled and the fracture pattern was secured with clear packing tape. The fracture pattern was then documented by hand sketching using an acetate overlay. Subsequent velocities were then calculated using high speed video and an electronic timing system. This is further discussed in the "Velocity Measurements" section. Figures 22-24 are representative fracture patterns for each of the drop heights.



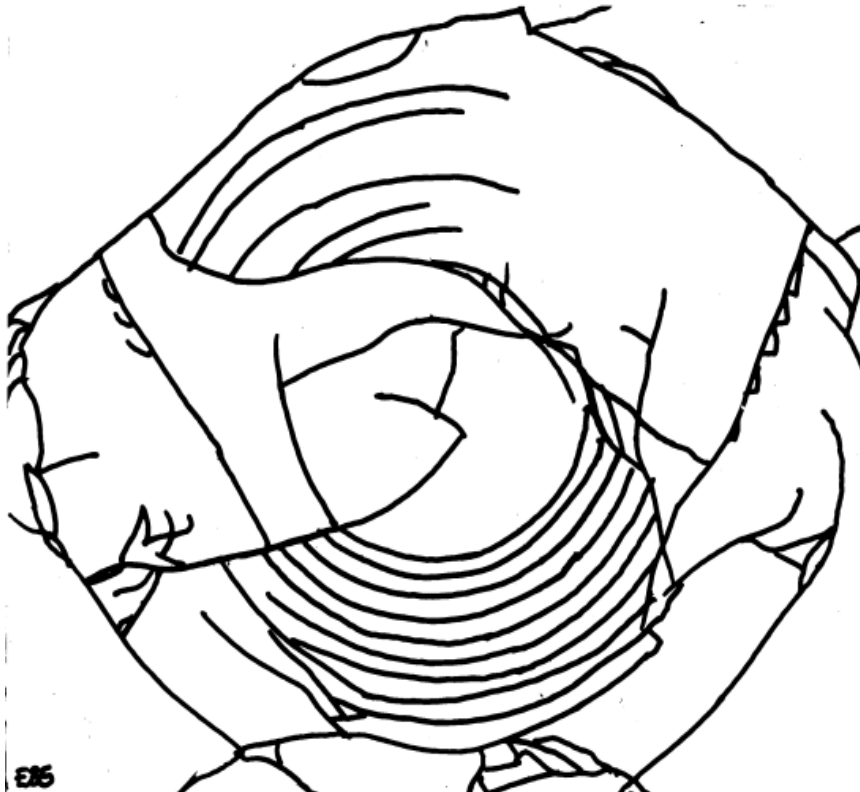
EH2

Figure 22 Fracture pattern at 3 ft



E51

Figure 23 Fracture pattern at 6 ft



E56

Figure 24 Fracture pattern at 9 ft

Static Pressure Procedure: A 5 5/8" x 4 1/4" plastic lens was placed under the indenter of the Instron® within the acrylic container to collect any plastic shards. The indenter crosshead speed was set to 10 mm/min and would automatically stop compression when the fracture occurred. As the indenter began to apply compression to the plastic lens, the Instron® software recorded load versus extension. Once the initial fracture occurred, the indenter stopped and the software produced a load profile of the fracture. Since only the wide fracture tip was used, all 30 lenses were fractured under the same conditions.

After each lens was fractured, it was reassembled and the fracture pattern was secured with clear packing tape. The fracture pattern was then documented by hand sketching using an acetate overlay. Only the top of the lens (4 1/4" x 3 3/4") was documented due to the slanting edges of the lens. Figures 25-27 are representative fracture patterns of these plastic lenses.

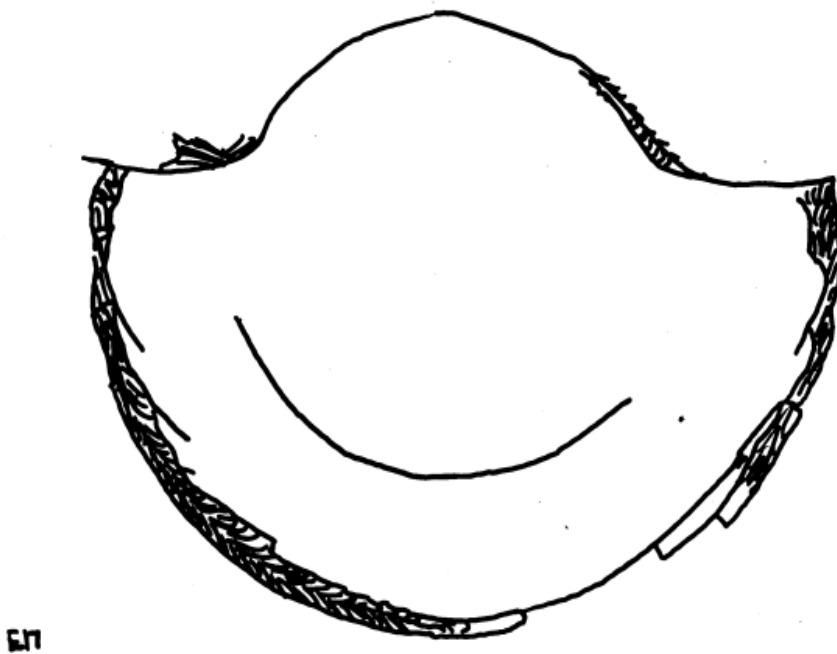
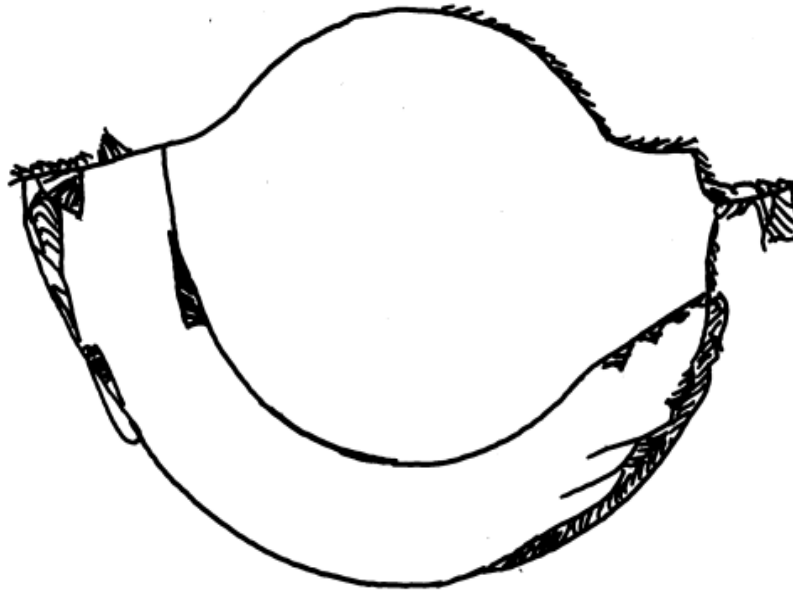
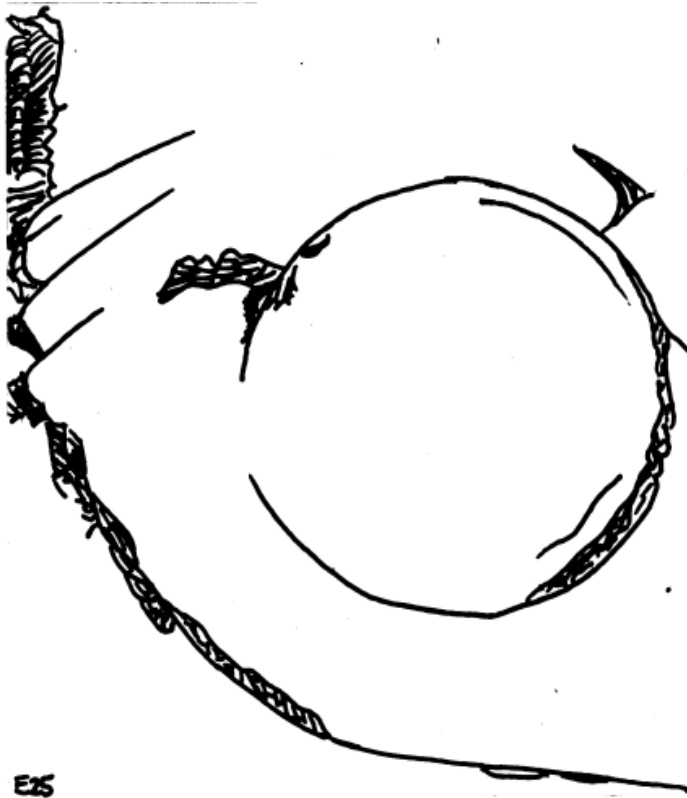


Figure 25 Fracture pattern using wide fracture tip



E9

Figure 26 Fracture pattern using wide fracture tip



E25

Figure 27 Fracture pattern using wide fracture tip

Velocity Measurements

Velocity measurements were made using both high speed video and an electronic timing system. To calculate the velocity using high speed video, a ½" diameter black dot was taped to the dropping weight. The camera was setup such that the dropping weight entered the field of view approximately eight inches before impact. With the black dot facing the camera, the entrance and impact of the dropping weight was recorded. This process was repeated in triplicate for four different drop heights—3, 6, 9, and 12 ft. Once all trials were complete, the videos were analyzed by MATLAB[®]. We developed a program that tracked a black dot placed on the dropping weight with a contrasting white background. The program tracked this dot, frame by frame, producing a plot describing the X and Y positions versus time (Fig. 28). By then taking the derivative of this plot, or the change in position over the change in time, a velocity magnitude profile was produced (Fig. 29). An average velocity was calculated for each of the four drop heights using these plots.

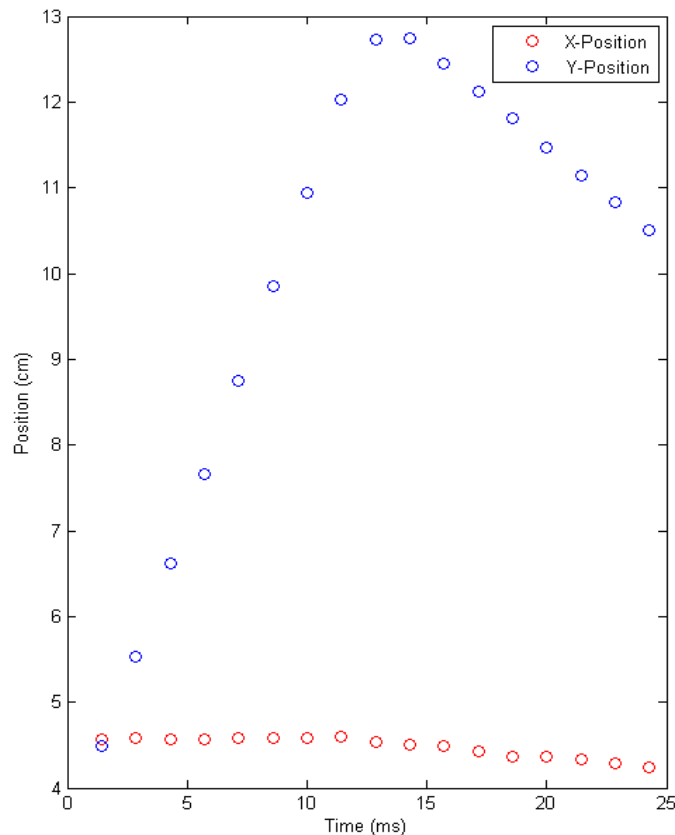


Figure 28 Plot showing change in X and Y positions of the indenter versus time using high speed video.

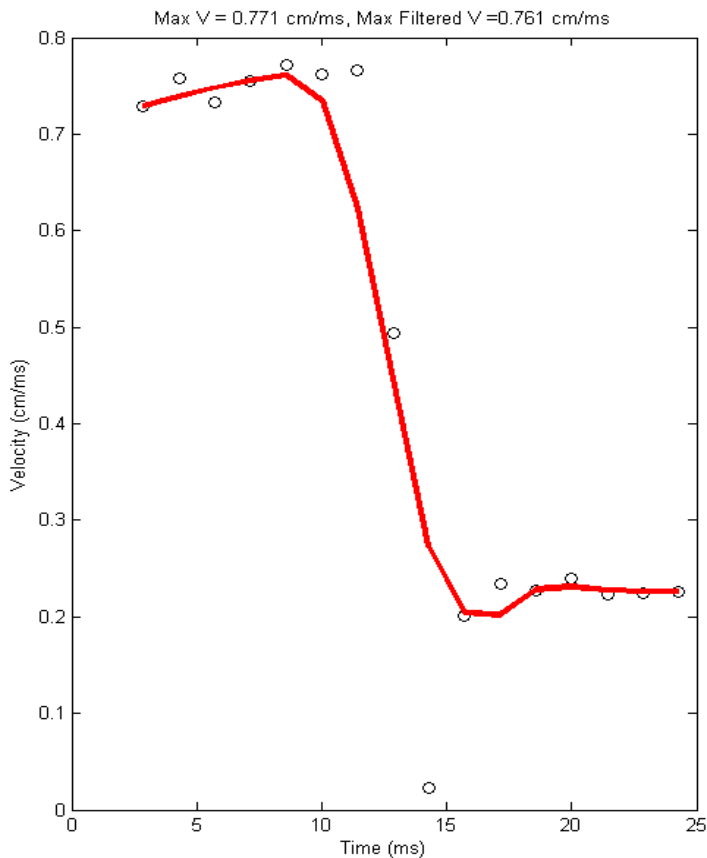


Figure 29 Derivative of plot in Figure 28. The change in position over the change in time will give the maximum velocity of the indenter.

To calculate the velocity using the electronic timing system, we developed a custom timing system which included sensors with microsecond sensitivity. They were used to start and stop a timer. The sensors were attached to one inch wide metal brackets which had the option to position the sensors up or down in three inch sections (Fig. 30). The brackets were then placed on either side of the fracture device. The sensors were positioned so that as the dropping weight was released, it would break the beam path of the first sensor which would start the timer. Then as the dropping weight continued down toward impact, it would break the beam path of the second sensor, which would stop the timer. In order to obtain a more precise beam path, a one inch wide metal panel with 1/16th of an inch holes was placed in front of the detector sensors (Fig. 31). This collimated beam light allowed for more accurate position measurements.

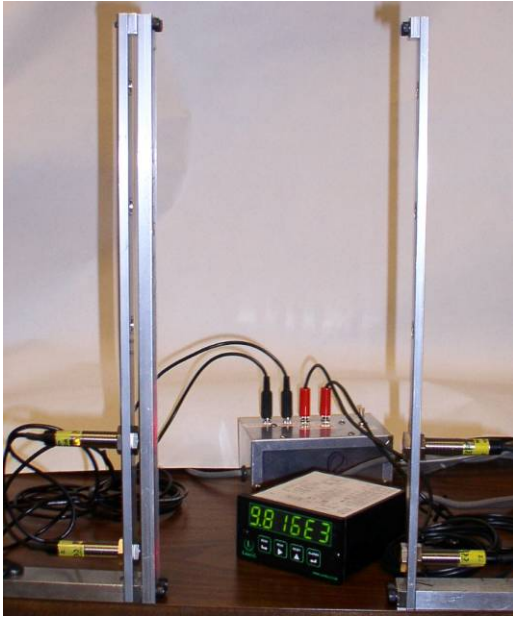


Figure 30 Electronic timing system



Figure 31 Collimated beam light

Timings were recorded in triplicate for the same four drop heights measured using the high speed video. An average time was calculated for each of the drop heights and converted to feet per second. These same processes were repeated for the dropping pipe setup to fracture the plastic lenses. Figure 32 illustrates the relationship between the theoretical and calculated velocities for the dropping weight as determined from the high speed video and the electronic timing system.

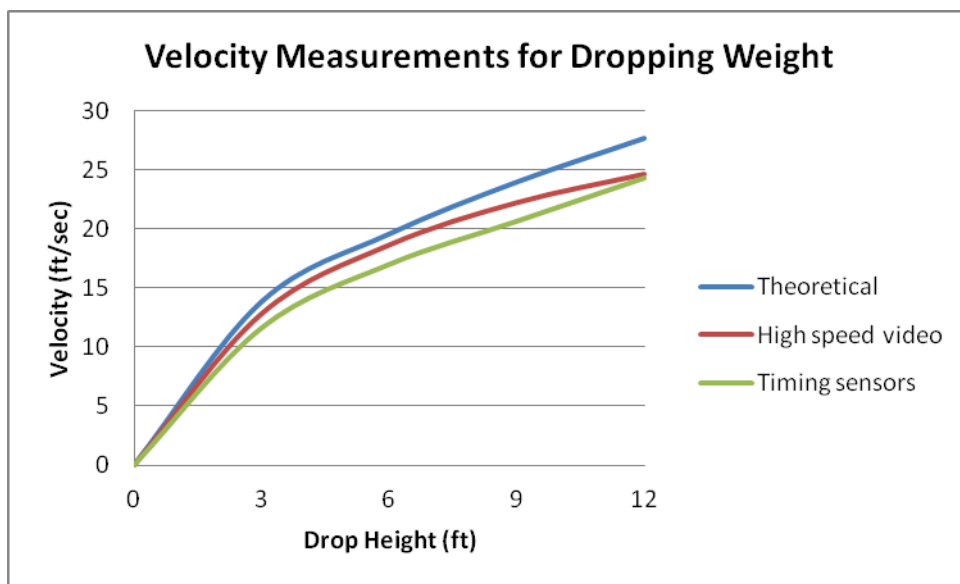


Figure 32 Comparison of theoretical velocity vs. calculated velocities for dropping weight

As can be seen in Figure 32, there is a divergence from the theoretical. This is due to the fact that theoretical velocity values assume a vacuum, but the high speed video and timing sensor trials were completed in a closed system. The dropping weight was inside a tube, which caused a partial compressing of air, causing the values to diverge slightly. However, this was still a reasonable estimation of the force required to initiate the fracture.

Figure 33 illustrates the relationship between the theoretical and calculated velocities for the dropping pipe as determined from the high speed video and the electronic timing system.

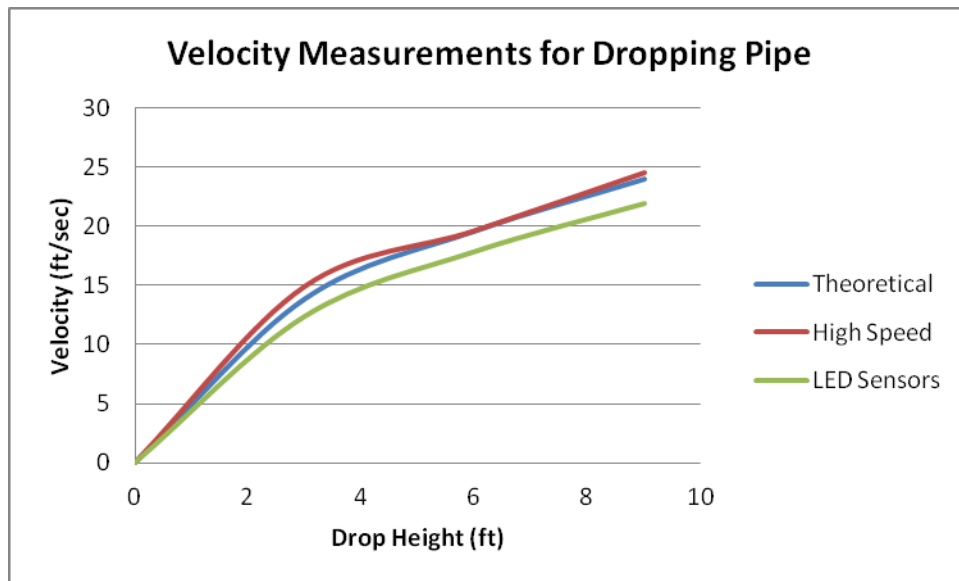


Figure 33 Comparison of theoretical velocity vs. calculated velocities for dropping pipe

As can be seen in Figure 33, there is a divergence from the theoretical. This is due to the fact that theoretical velocity values assume a vacuum, but the high speed video and timing sensor trials were completed using guide wires with minimal friction. As the dropping pipe traveled down these guide wires, some friction was produced causing the values to diverge slightly. However, this was still a reasonable estimation of the force required to initiate the fracture.

Figure 34 illustrates the relationship between the kinetic energy and the velocity of the dropping pipe. Not all of the kinetic energy was transferred to the fracture. This was a partial elastic collision because the pipe did rebound after impact.

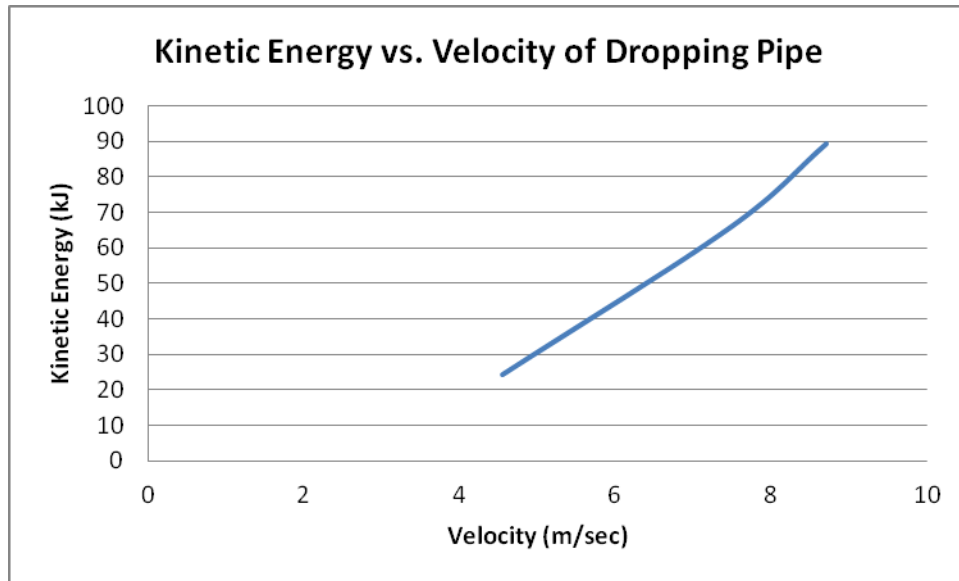


Figure 34 Kinetic energy vs. velocity of dropping pipe

Inter-Comparison of Fracture Patterns

Once all the fracture experiments were complete, each fracture pattern was compared to that of every other fracture pattern within its category (pane, bottle, or lens). This was done by sketching each pattern using an acetate overlay then overlaying one fracture pattern on top of another, in the same orientation for a one-to-one comparison (Fig. 35) for all 60 patterns. For example, fracture pattern 1 for the glass panes was compared to fracture patterns 2-60, individually. Fracture pattern 2 was then compared to patterns 3-60, individually until comparisons were completed for all 60 patterns.

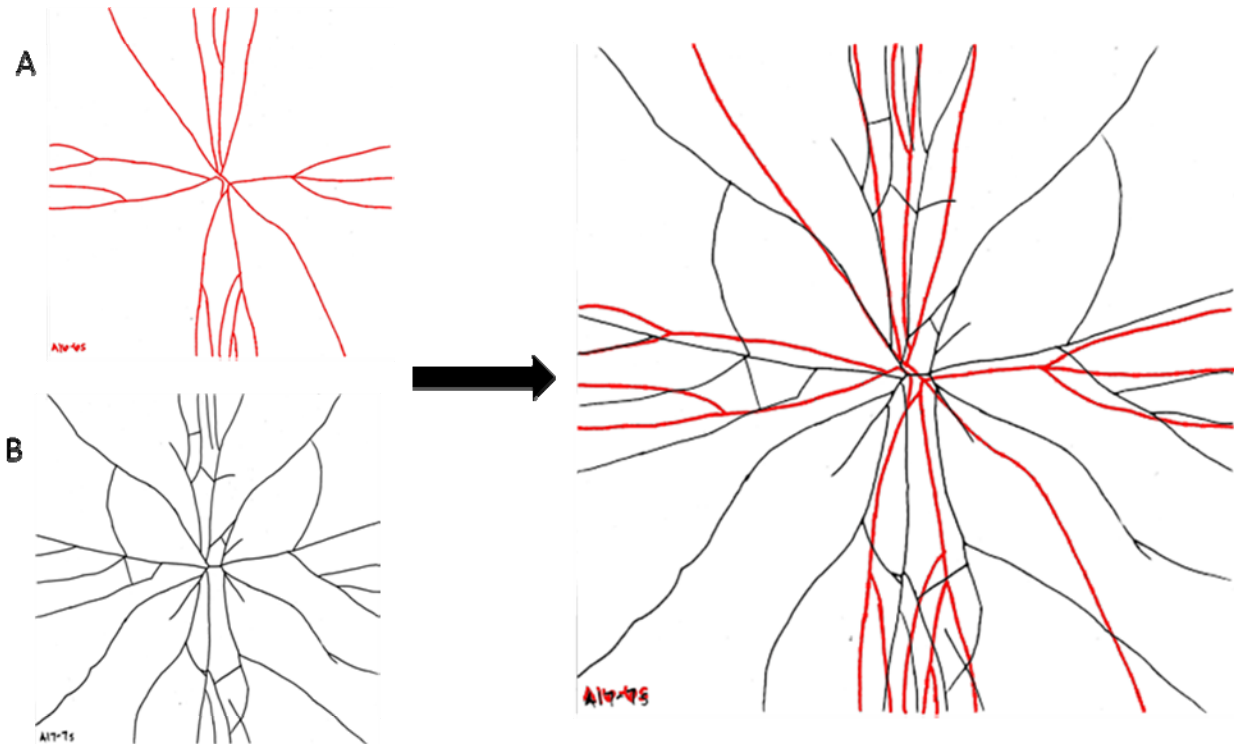


Figure 35 Inter-comparison of fracture patterns (window pane shown)

This inter-comparison of fracture patterns was conducted in order to determine if the overall fracture pattern was duplicated in any instance. A total of 1,770 pairwise comparisons were made for each category for an overall total of 5,310 pairwise comparisons. The mathematical relationship of these comparisons can be described by Equation 1 where n is the total number of specimens.

$$\sum_{i=1}^{n-1} \frac{n(n-1)}{2}$$

Eq. 1

Results

Glass panes

Dynamic Impact: Tables 1-3 are summaries of the velocity required to fracture each glass pane using the specified impact tip. These velocities were used to ensure consistent breakage. From the data, it can be seen that the blunt fracture tip required the highest velocity to initiate the

fracture while the round fracture tip required the least. This is most likely due to the fact that the round tip concentrated the velocity to a single point, whereas the blunt fracture tip caused the velocity to be distributed on the glass pane more widely.

Impact Fracture Velocities - Sharp Tip		
Glass Pane #	Height to fracture (ft)	Velocity (ft/s)
A11	5.5	18.76
A12	6.0	19.60
A13	5.0	17.89
A14	6.0	19.60
A15	6.0	19.60
A16	6.0	19.60
A17	6.0	19.60
A18	6.5	20.40
A19	6.0	19.60
A20	6.0	19.60

Table 1 Impact fracture velocities using sharp fracture tip

Impact Fracture Velocities - Round Tip		
Glass Pane #	Height to fracture (ft)	Velocity (ft/s)
A1	5.0	17.89
A2	2.0	11.31
A3	2.0	11.31
A4	2.5	12.65
A5	3.5	14.97
A6	4.5	16.97
A7	4.5	16.97
A8	5.0	17.89
A9	6.0	19.60
A10	5.0	17.89

Table 2 Impact fracture velocities using round fracture tip

Impact Fracture Velocities - Blunt Tip		
Glass Pane #	Height to fracture (ft)	Velocity (ft/s)
A21	6.0	19.60
A22	6.5	20.40
A23	6.0	19.60
A24	7.0	21.17
A25	7.0	21.17
A26	6.0	19.60
A27	6.5	20.40
A28	6.0	19.60
A29	6.5	20.40
A30	6.0	19.60

Table 3 Impact fracture velocities using blunt fracture tip

The force required to initiate the fracture was also reflected in the fracture pattern. The fracture pattern produced by the sharp tip had fewer fracture lines than that of either the round or blunt tips. The fracture pattern produced by the blunt tip had the most fracture lines, consistent with the amount of load applied to the glass. It should also be noted that the blunt tip produced a star-shaped fracture pattern, completely unlike the patterns produced by the sharp and round fracture tips.

Instron[®] Static Pressure: Table 4 is a summary of the maximum load and extension at failure for the static pressure tests. An average load and extension were calculated for each of the three fracture tips.

Static Pressure Test Values		
	Maximum extension (mm)	Maximum load (kN)
Sharp Tip	3.39	1.47
Round Tip	3.82	1.72
Blunt Tip	3.93	1.79

Table 4 Static pressure test values for glass panes

In viewing that data in Table 4, it can be seen that the sharp tip required the least amount of force, while the blunt tip required the most. This is most likely due to the fact that the sharp tip

had the force focused to single point on the glass, whereas the blunt tip spread out the force by having a larger surface area in contact with the glass. Figure 36 is an example of a load profile produced from the fracture initiation in a glass pane. A straight line would be expected for the load profile as the extension and load increase. However, a curvature can be seen, which is most likely attributed to a combination of the stiffness of the Instron[®] setup and the flexing of the glass.

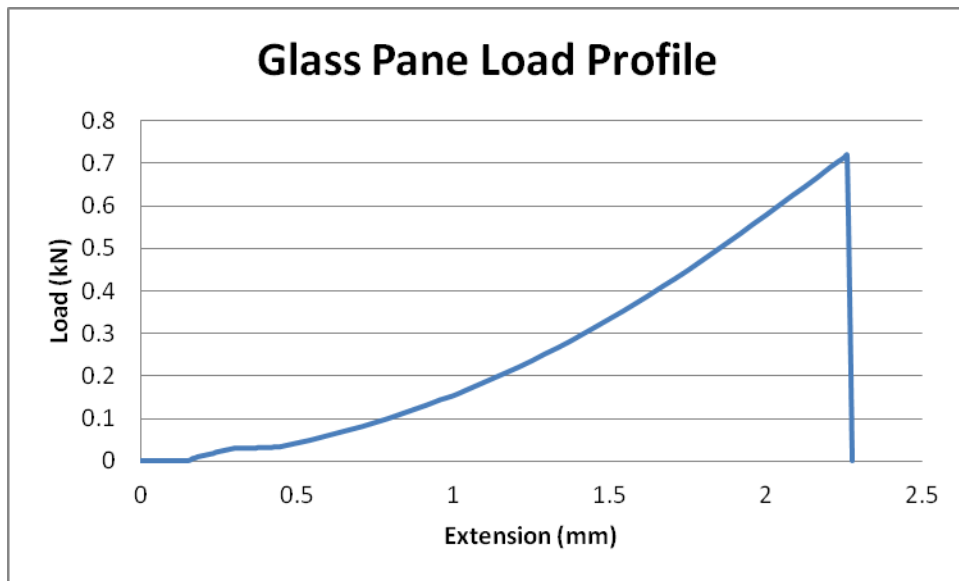


Figure 36 Load profile for glass pane

Glass Bottles

Dynamic Impact: Figure 37 illustrates the slight variability in the thickness of glass from the shoulder of the bottle to the base of the bottle. The bottles were positioned such that each was impacted at the midpoint between the shoulder and the base.

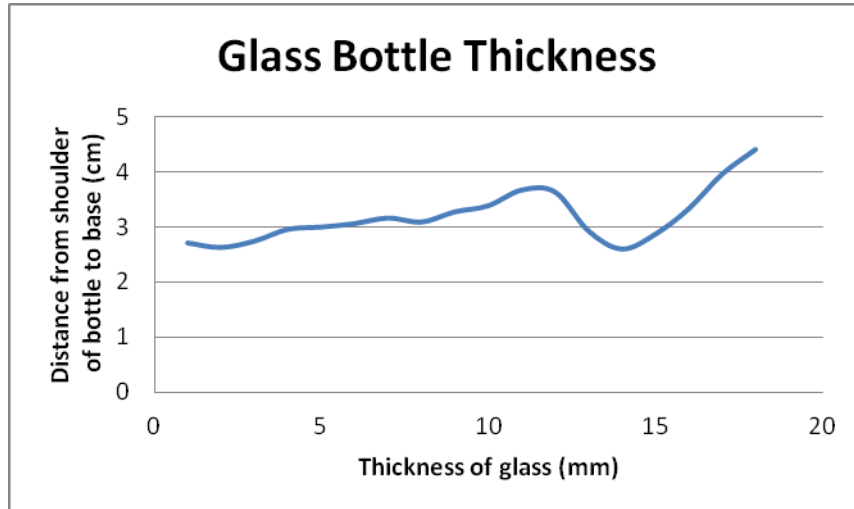


Figure 37 Variation in glass thickness from shoulder to base of bottle

Tables 5-7 are summaries of the velocity required to fracture each glass bottle using the specified impact tip. These velocities were used to ensure consistent breakage. From the data, it can be seen that the blunt fracture tip required the highest velocity to initiate the fracture while the sharp fracture tip required the least. This is most likely due to the fact that the sharp tip concentrated all the force to a single point on the glass bottle, whereas the blunt tip spread out the force, requiring more velocity to initiate the fracture.

Impact Fracture Velocities - Sharp Tip		
Bottle #	Height to fracture (ft)	Velocity (ft/s)
C11	6.5	20.40
C12	4.0	16.00
C13	6.5	20.40
C14	4.0	16.00
C15	4.0	16.00
C16	4.0	16.00
C17	7.0	21.17
C18	4.0	16.00
C19	4.0	16.00
C20	4.0	16.00

Table 5 Impact fracture velocities using sharp fracture tip

Impact Fracture Velocities - Round Tip		
Bottle #	Height to fracture (ft)	Velocity (ft/s)
C1	7.0	21.17
C2	5.0	17.89
C3	6.0	19.60
C4	5.0	17.89
C5	5.0	17.89
C6	6.0	19.60
C7	5.5	18.76
C8	5.0	17.89
C9	5.5	18.76
C10	5.0	17.89

Table 6 Impact fracture velocities using round fracture tip

Impact Fracture Velocities - Blunt Tip		
Bottle #	Height to fracture (ft)	Velocity (ft/s)
C21	10.0	25.30
C22	9.0	24.00
C23	10.0	25.30
C24	10.0	25.30
C25	10.0	25.30
C26	10.0	25.30
C27	10.5	25.92
C28	10.5	25.92
C29	10.0	25.30
C30	10.0	25.30

Table 7 Impact fracture velocities using blunt fracture tip

The force required to initiate the fracture was also reflected in the fracture pattern. The fracture pattern produced by the sharp tip had fewer fracture lines than that of the either the round or blunt tips, whereas the fracture pattern produced by the blunt tip had the most fracture lines, consistent with the amount of load applied to the glass. The fracture lines produced using the blunt tip, were much more concentrated than the fracture lines of either the sharp or round tips.

Instron[®] *Static Pressure*: Table 8 is a summary of the average maximum extension and load at failure produced by each of the three fracture tips in the static pressure tests.

Static Pressure Test Values		
	Maximum extension (mm)	Maximum load (kN)
Sharp Tip	3.76	9.63
Round Tip	3.59	10.12
Blunt Tip	4.08	11.39

Table 8 Static pressure test values for glass bottles

In viewing the data in Table 8, the trend in required force to initiate the fracture is similar to that of the glass panes. Here too, the sharp tip required the least amount of force, while the blunt tip required the most force. Again, this is most likely due to the amount of surface area of the tip that made contact with the glass. However, the separation in force between each of the tips is much more significant here than with the glass panes. Figure 38 is an example of a load profile produced from the fracture initiation in a glass bottle.

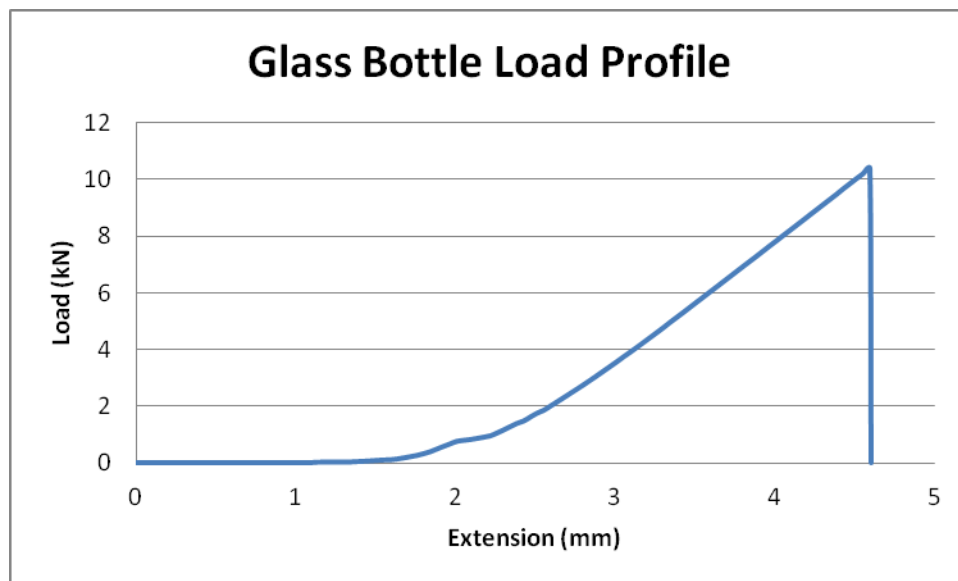


Figure 38 Load profile for glass bottle

Plastic lenses

Dynamic Impact: Table 9 is a summary of the velocity required to fracture the lenses at various drop heights.

Impact Fracture Velocities	
Drop Height (ft)	Velocity (ft/sec)
3	12.35
6	17.81
9	21.87

Table 9 Impact fracture velocities for plastic lenses

Instron[®] Static Pressure: Table 10 is a summary of the maximum extension and load required to initiate a fracture. Since only the wide tip was used, due to limitations using the other tips, an average extension and load of all 30 lenses was calculated.

Plastic Lenses		
	Maximum extension (mm)	Maximum load (kN)
Wide Tip	9.84	0.941

Table 10 Static pressure values for plastic lenses

In viewing the data in Table 10, it can be seen that although the maximum extension value exceeds that of both the glass panes and bottles, the maximum load is relatively minimal. This is due to the fact that as the lens began to fracture, it would give slightly, causing the load to drop. The indenter would continue to apply compression, building up the load again, until the fracture was fully initiated. Figure 39 is an example of a load profile produced from the fracture initiation in a plastic lens.

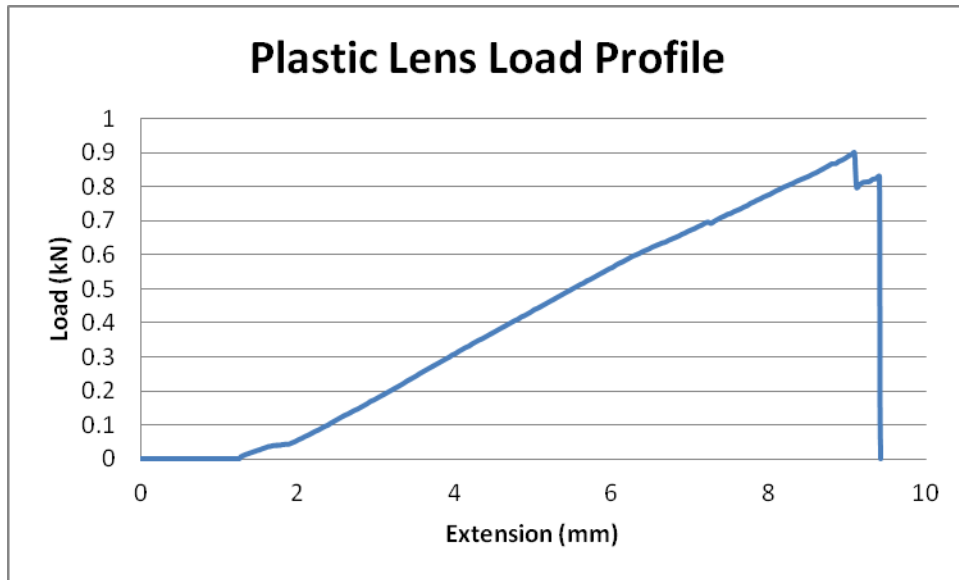


Figure 39 Load profile for plastic lens

It was determined in the inter-comparison of the overall fracture pattern of the glass window panes that no duplicate patterns were found. There were some similarities as far as specific fracture lines were concerned; however, the overall patterns were not duplicated. It was also determined that no duplicate fracture patterns were found in the inter-comparison of the overall fracture pattern of the glass bottles. Viewing these fracture patterns, there were similarities in the shape of the pattern, however, the overall fracture pattern was not duplicated. The plastic lenses did exhibit many similarities in fracture patterns, such as the center of many of the lenses breaking completely out of the lens. They also had a tendency to fracture along the mold lines of the lens. However, the inter-comparison showed that there were no duplicates of overall fracture patterns.

High Speed Video Observations

We were able to use a Phantom color high speed video camera (V. 7.3) to observe two bottle fractures (see Appendix B). The two bottle fractures were recorded by high speed video and it was determined that the fracture was initiated at the impact point, but due to the angle at which

the bottle was fractured, only the reflection of the fracture from the base to the shoulder could be observed. Figure 40 illustrates this fracture sequence. This was observed on two bottle fractures.

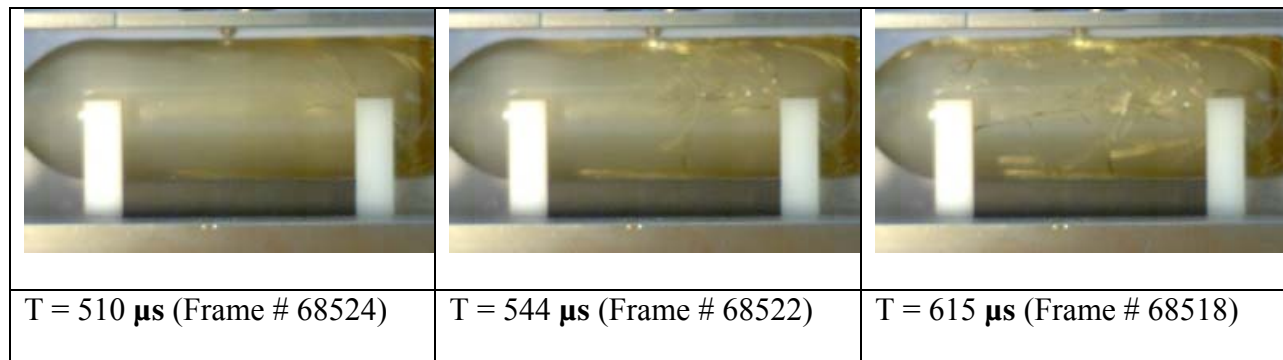


Figure 40 High speed video images

Conclusions

Discussion of findings

The concept of uniqueness of fracture patterns in glass and glassy polymers was examined through dynamic impact and static pressure experiments. For the dynamic impact experiments, the glass panes, glass bottles, and plastic lenses were each subjected to a high velocity dropping weight to initiate the fracture. For the static pressure experiments, each material was subjected to compression using an Instron[®] Tensile Tester to initiate the fracture.

Glass Panes

Analyzing the fracture patterns for the dynamic impact experiments, we found that the blunt fracture tip required the highest velocity to initiate the fracture, whereas the round fracture tip required the least. It was also observed that the blunt tip produced a much higher number of fractures with a distinctly different pattern than that of the sharp or round tips.

Analyzing the fracture patterns for the static pressure experiments, we found that the blunt tip required the most force to initiate the fracture, whereas the sharp tip required the least force. The

blunt tip produced a higher number of both radial and concentric fractures than either the sharp or round tips produced.

The fracture patterns produced using dynamic impact were much simpler than the fracture patterns produced using static pressure. The static pressure fracture patterns had more radial fractures and almost all contained concentric fractures, whereas the dynamic impact patterns contained significantly less radial and concentric fractures. This is because the stress field is being modified rather than simply depleting as it does in the impact case.

Glass Bottles

Analyzing the fracture patterns for the dynamic impact experiments, we found that the blunt fracture tip required the highest velocity to initiate the fracture, whereas the sharp fracture tip required the least. The blunt tip produced a significantly higher number of fractures than that of the sharp or round tips. Also, due to the greater velocity, the blunt tip caused much more of the glass at the impact site to be blown out when compared to the impact sites of the bottles fractured using the sharp and round tips.

Analyzing the fracture patterns for the static pressure experiments, we found that the blunt tip required the most force to initiate the fracture, whereas the sharp tip required the least force. The number of fractures produced by each of the three impact tips was more evenly distributed, however, it appears that the blunt and round tips produced a larger number of fractures than that of the sharp tip.

The fracture patterns produced using dynamic impact are somewhat similar to the fracture patterns produced using static pressure. The patterns of the two fracture methods did not differ as greatly as the glass pane patterns. However, overall, the static pressure fracture patterns had a larger number of fractures than the dynamic impact patterns.

Plastic Lenses

Analyzing the fracture patterns for the dynamic impact experiments, we determined that the impact site of the dropping pipe on the lens crushed rather than splintered the lens. It was also seen that some of the fractures in the lens did not break clean, but rather sheared. The fractures toward the outer edges of the lens had tendency to follow the ridges in the molding of the lens.

Analyzing the fracture patterns for the static pressure experiments, we determined that the fractures had tendency to follow the ridges in the molding of the lens just larger than that of the impact tip. In some instances, the center of the lens separated completely from the rest lens. Shearing fractures were also seen in combination with compression fractures. This is because the stresses were higher in the thin areas of the lens.

The fracture patterns produced using dynamic impact contained more fractures than the fracture patterns produced using static pressure. Although in both methods the fractures tended to follow the ridges in the molding, the static pressure fractures tended to be more concentrated toward the center of the lens, whereas the dynamic impact fractures extended all the way to the edge of the lens.

Based on the limited specimens tested in this study, the results appear to indicate that the patterns could be unique. However, more studies under very controlled conditions would be needed to fully determine that each fracture forms a unique and non-reproducible fracture pattern.

Implications for policy and practice

These results support the theory that coincidental duplicate fracture patterns are highly unlikely to occur. This finding will add to the reliability of physical match findings and fracture pattern

interpretation when dealing with glass and plastic objects. This research should enhance the capability of the analyst to testify in a court of law as to the uniqueness of a fracture.

Implications for further research

Recommendations for further research are several with a focus on developing mathematical routines. We need a mechanism to mathematically describe each fracture pattern and allow for its objective mathematical comparison to other fracture patterns. The glass could also be examined under cross polar filters to view the stress birefringence of the fracture to determine how the fracture pathways are related.

Increase Sample Size

Increase the number of fractures using one method of fracture initiation in order to enhance numbers and statistics.

High Speed Video

Use a high speed video to record fracture sequences in order to ascertain if there is a predisposition to certain fracture propagation.

Mathematical Analysis – Boundary or Segment Histogram

Ideally, in order to illustrate the uniqueness of a fracture, one could use a mathematical algorithm that would evaluate the fracture surface and provide an area histogram of the different fracture segments. For some fractures that have closed boundaries, this could be a solution. This has been successfully implemented on a much smaller scale for determining the area distribution of blood stain patterns. If one looks at Figure 38 Image A, this image could be amenable to such analysis. However, most fractures have the appearance of Figure 38 Image B wherein some fracture lines extend a limited amount and do not intersect any other fracture or boundary. This

type of fracture may not be amenable to closed boundary analysis. Note that in this case the edge of the glass panes have been highlighted as a black rectangle. When we apply mathematical analysis to Image B we attain the results shown in Figures 39 and 40. In Figure 39, the partitioning of Image B is shown as colored segments with different pixel areas. The subsequent Figure 40, shows the histogram of the pixels areas. So we can illustrate this partitioning, but it still does not account for the fracture lines that do not end in a contact.

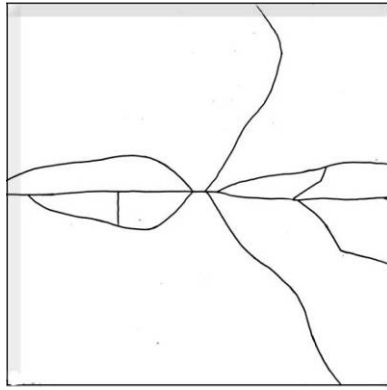


Figure 38 Image A

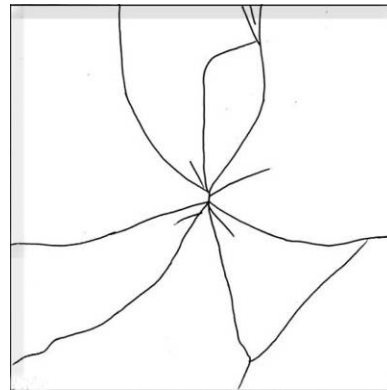


Figure 38 Image B

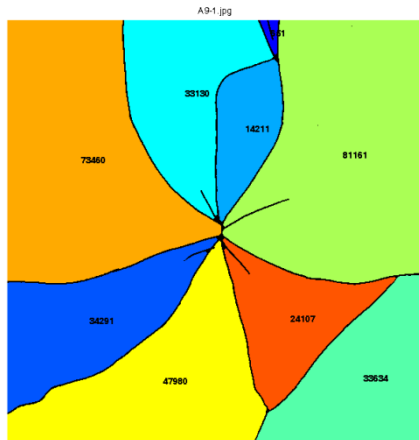


Figure 39 Segmentation of Image B (numbers correspond to pixel areas)

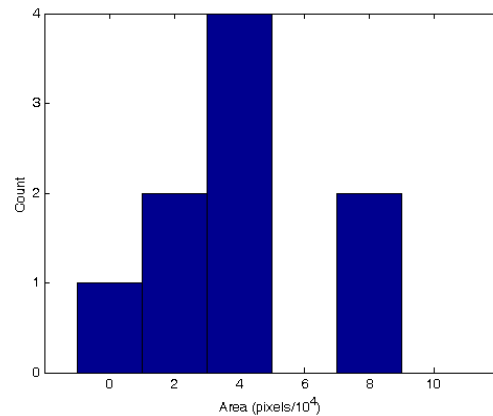


Figure 40 Area Histogram of Image B

Segment analysis routines could also be used to evaluate the size and shape distribution of the fragments that are formed. Using this approach would allow for the determination of the probability of matching an evidence fragment to a particular event.

Mathematical Analysis Segment Circumference

In glass fractures, one can be asked to illustrate that a given glass fragment fits into place into another glass fracture. So assuming we had a fracture such as illustrated in Figure 41, one could perform a perimeter profile or pixel count. This count could then be compared to all other segments in a series of fracture exemplars. For those segments that have the same pixel circumference, we could conduct an analysis that differentiates the different segment shapes. The end result would be the interpretation that a particular glass segment is unique and not reproduced in other glass fractures.

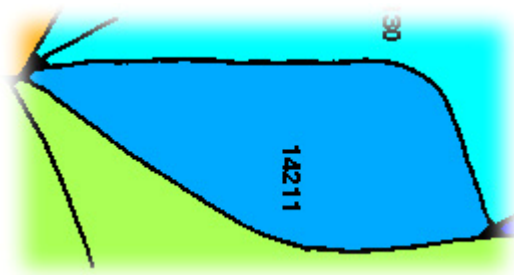


Figure 41 A segment of a glass fracture

References

1. National Research Council of the National Academies, Strengthening Forensic Science in the United States – A Path Forward, National Academies Press, Washington, D.C., 2009.
2. Daubert v. Merrell Dow Pharmaceuticals, Inc., 509 U.S. 579 (1993).
3. Preston FW. The Structure of Abraded Glass Surfaces. Transactions of the Optical Society 1921-22 No. 3, p. 141.

4. Preston FW. A Study of the Rupture of Glass. J. Soc. Glass Techn. 1926 Vol. 10, p. 234.
5. Quinn GD. A History of the Fractography of Brittle Materials. Key Engineering Materials 2009 Vol. 409, p. 4.
6. Matwejeff SN. Criminal Investigation of Broken Window Panes. Amer. J. Police Sci 1931; 2:148.
7. Federal Bureau of Investigation, Evidence of Fractured Glass in Criminal Investigations, FBI Law Enforcement Bulletin, October 1936, p. 2.
8. Tryhorn FC. The Fracture of Glass. Forensic Science Circular 1936 No. 2, p. 1.
9. Nicholls LC. Anomalous Fracture in Glass. Forensic Science Circular 1937 No. 3, p. 7.
10. O'Hara CE, Osterberg, JW. An Introduction to Criminalistics. MacMillan, New York, 1949., p. 239.
11. Federal Bureau of Investigation, Glass Fracture Examinations Aid the Investigator, FBI Law Enforcement Bulletin, October 1936, p. 2.
12. Nelson DF. Illustrating the Fit of Glass Fragments. J. Crim. Law, Criminol. Police Sci 1959; 50:312.
13. Thompson JW. The Structure of Hackle Lines on Glass. Intern. Crim. Police Rev March 1969; p. 62.
14. McJunkins SP, Thornton JI. Glass Fracture Analysis – A Review. Forensic Science 1973; 2:1-27.
15. Thornton JI, and Cashman PJ. Glass Fracture Mechanism – A Rethinking. J. Forensic Sciences 1986; 31:818-824.
16. Thornton JI. “Physical Examination of Glass Evidence”, in Forensic Examination of Glass and Paint, ed. B. Caddy, Taylor & Francis, London, 2001, p. 97-121.
17. Rhodes EF, Thornton JI. The Interpretation of Impact Fractures in Glassy Polymers, J. Forensic Sci 1975; 20:274-282.
18. Katterwe HW. Fracture Matching and Repetitive Experiments: A Contribution of Validation, AFTE Journal 2005; 37(33):229-241.
19. Sglavo VM, Gadotti M, Micheletti T. Cyclic Loading Behavior of Soda- Lime Silicate Glass using Indentation Cracks, Fatigue Fract. Engng. Mater. Struct 1997; 20(8):1225-1234.

20. Shinkai N. "Fracture and Fractography of Flat Glass," in Fractography of Glass, ed. R. Brandt and R. Tressler. Plenum, New York, 1995.
21. Orr L. Practical Analysis of Fractures in Glass Windows. Materials Research and Standards 1998; 12:21-23, 47-48.
22. Ropp RC. Handbook of Glass Fractography. Author House, Bloomington, IN, 2008.
23. Mecholsky J. "Fracture Analysis of Glass Surfaces," in Strength of Inorganic Glass, ed. C. Kurkjian, Plenum, New York, 1986.
24. Kepple J, Wasylyk J. "The Fracture of Glass Containers," in Fractography of Glass, ed. R. Brandt and R. Tressler, Plenum, New York, 1995.
25. Quinn GD. Fractography of Ceramics and Glasses, Special Publication 960-16, National Institute of Standards and Technology, U.S. Government Printing Office, 2007.
26. Griffith A. Phenomena of Rupture and Flow in Solids. Philosophical Transactions of the Royal Society of London, 221, Series A:163-204 (1920).
27. Poncelet E. The Markings of Fracture Surfaces. Journal of the Society of Glass Technology 1958; 42:279-288.
28. ASTM Method C162-85a, Vol. 15.02, "Standard Definitions of Terms Relating to Glass and Glass Products". American Society for Testing and Materials, Philadelphia, 1985.

Dissemination of Research Findings

We intend to disseminate this research by presentation talks at various seminars and by submission a technical peer reviewed article to the Journal of Forensic Sciences (JFS). The JFS article will be an abridged version and will be submitted by GSR A. Baca as part of her thesis requirement. Once an article is reviewed and approved by the Journal of Forensic Sciences, it may take 1.5 years before the results are in print.

So far we have presented this research in the following locations/seminars:

- American Academy of Forensic Sciences 64th Annual Meeting, February 25, 2012
Abstract A196. “Determination of Unique Fracture Patterns in Glass and Glassy Polymers” by Allison Baca

- UC Davis off-site seminar, Granlibakken, Lake Tahoe, May 6, 2012 Determination of Unique Fracture Patterns in Glass and Glassy Polymers” by Allison Baca

- Future location for proposed oral presentations:
 - California Association of Criminalists Semi-Annual Seminar, San Jose, CA
November 2012

 - Southwest Association of Forensic Scientists (SWAS) Scottsdale, AZ.
October 2012

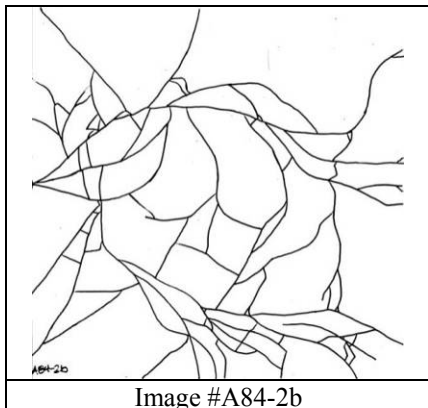
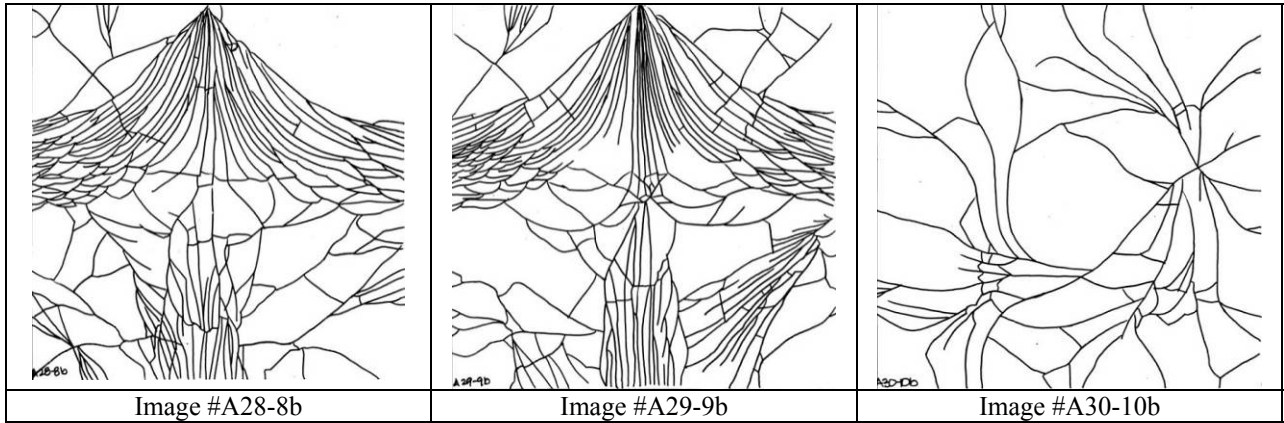
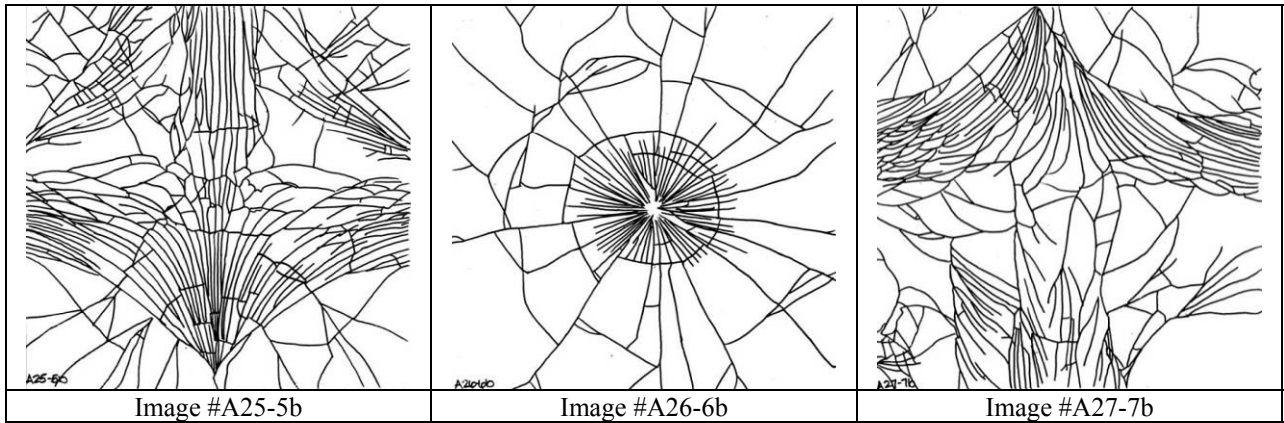
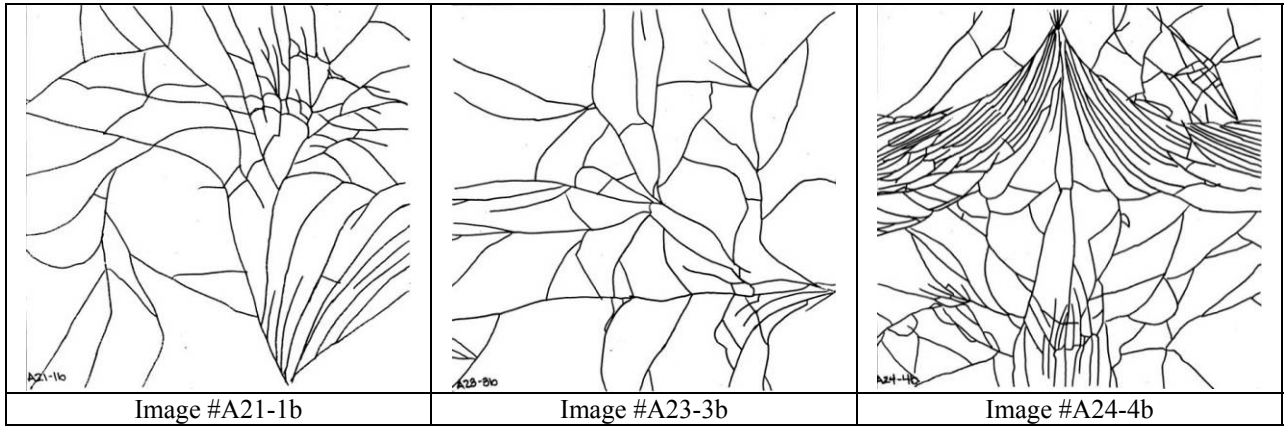
APPENDIX A
FRACTURE IMAGES

This section contains reduced images of all the specimens that were fractured in this research. These consist of glass pane fractures, glass bottle fractures, and plastic tail light lens fractures.

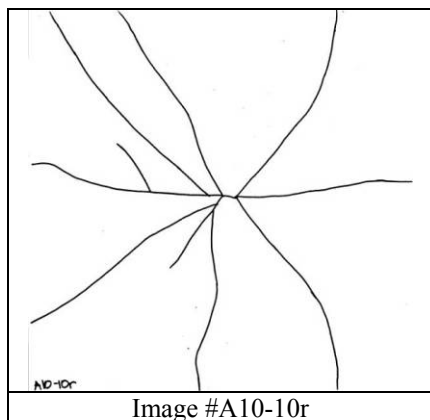
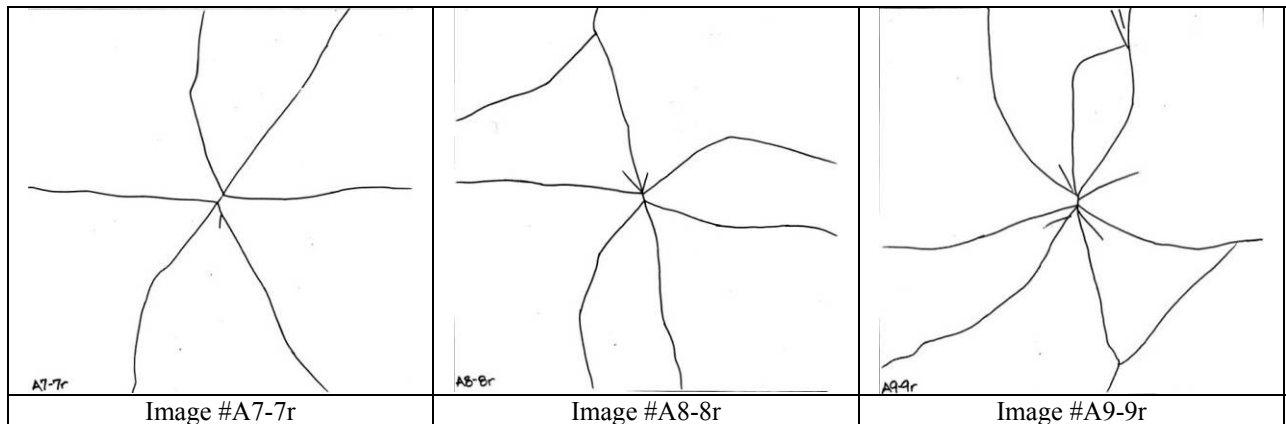
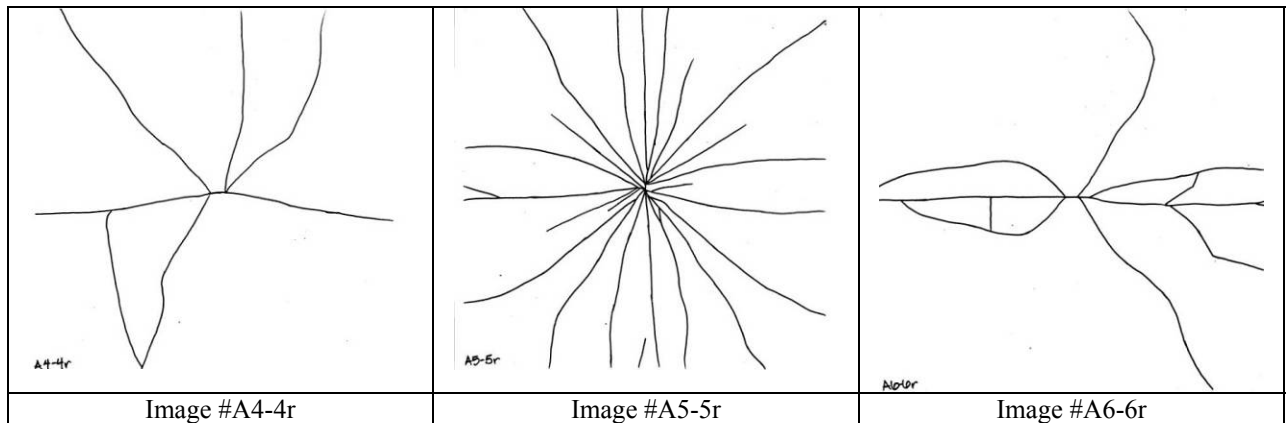
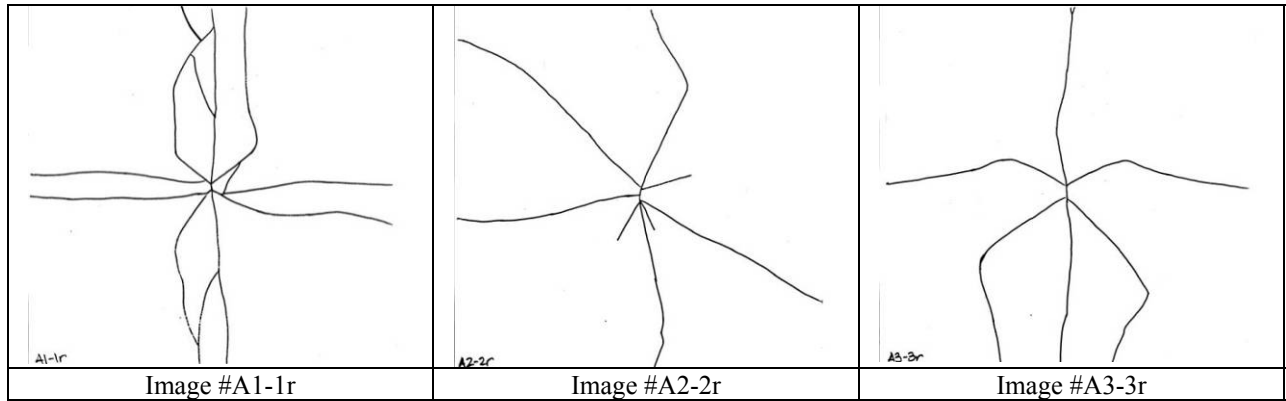
<u>Description</u>	<u>Page</u>
Glass Pane Impact Fracture - Blunt Tip	A-2
Glass Pane Impact Fracture - Round Tip	A-3
Glass Pane Impact Fracture - Sharp Tip	A-4
Glass Pane Compression Fracture - Blunt Tip	A-5
Glass Pane Compression Fracture - Round Tip	A-6
Glass Pane Compression Fracture - Sharp Tip	A-7
Glass Bottle Impact Fracture - Blunt Tip	A-8
Glass Bottle Impact Fracture - Round Tip	A-9
Glass Bottle Impact Fracture - Sharp Tip	A-10
Glass Bottle Compression Fracture - Blunt Tip	A-11
Glass Bottle Compression Fracture - Round Tip	A-12
Glass Bottle Compression Fracture - Sharp Tip	A-13
Plastic Lens Impact Fracture	A-14
Plastic Lens Compression Fracture	A-17

Note: Digital image copies (jpg) of the fractures are available from the authors.

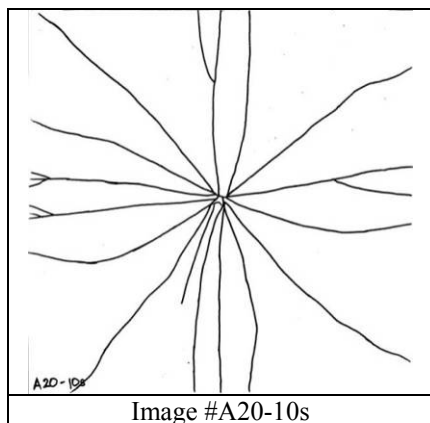
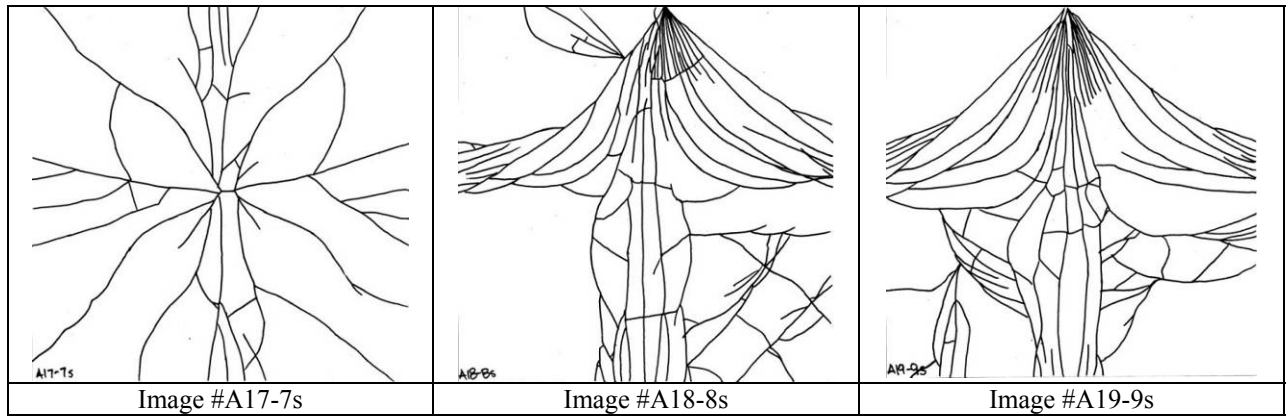
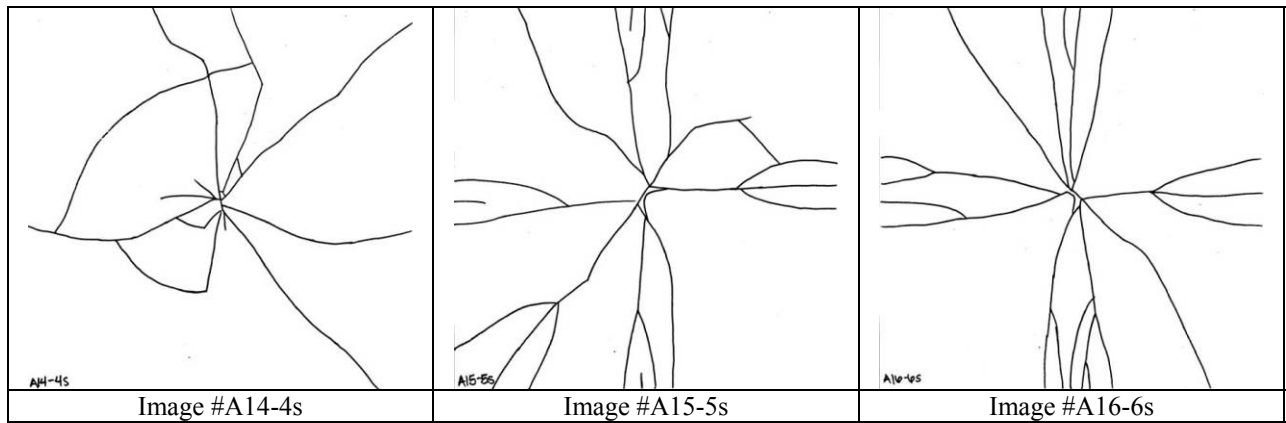
PANE FRACTURE IMAGES IMPACT FRACTURE - **BLUNT TIP**



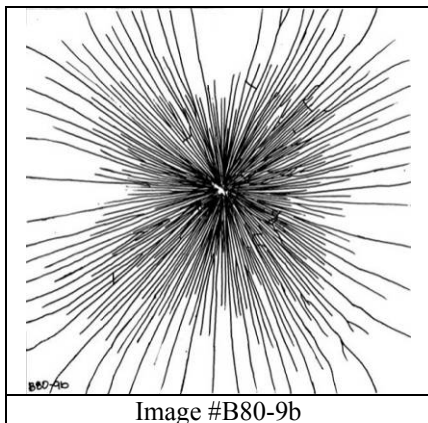
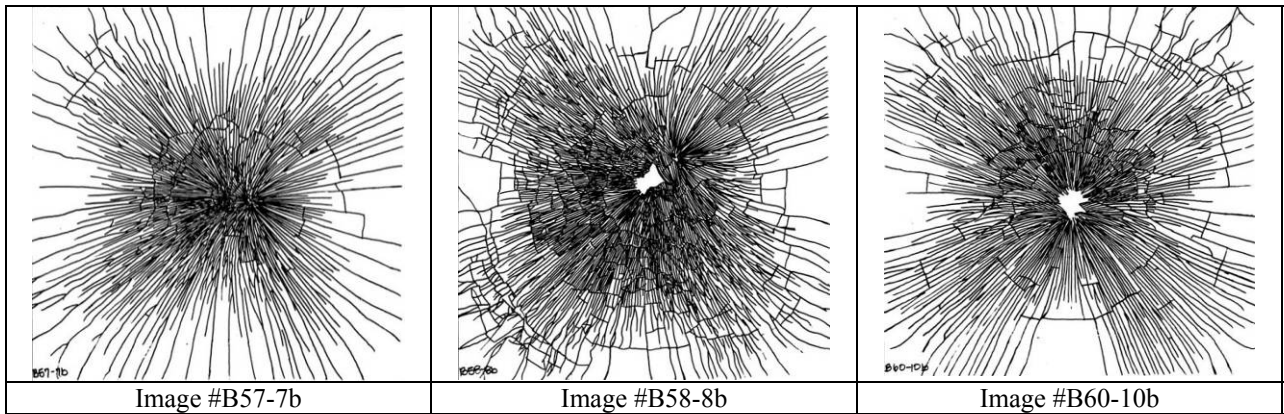
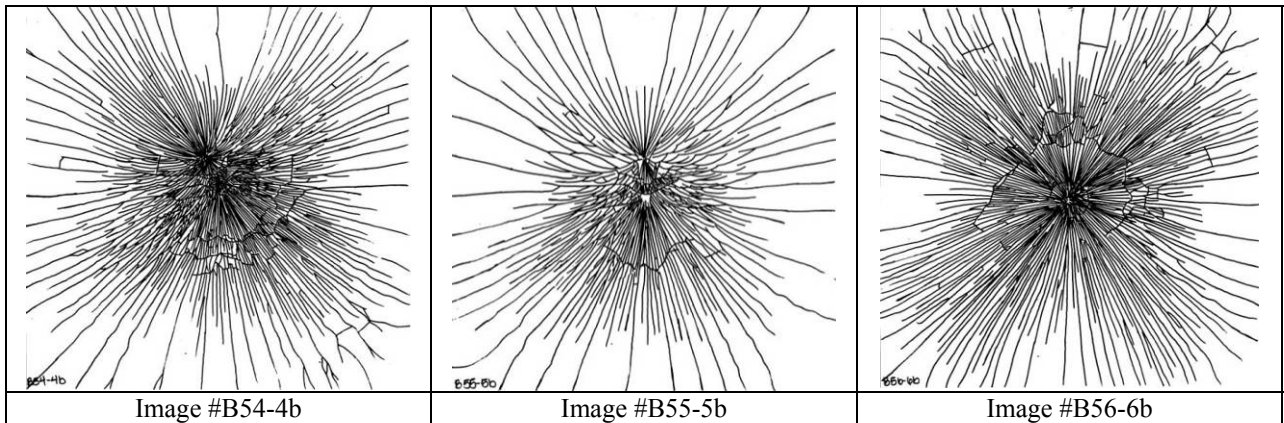
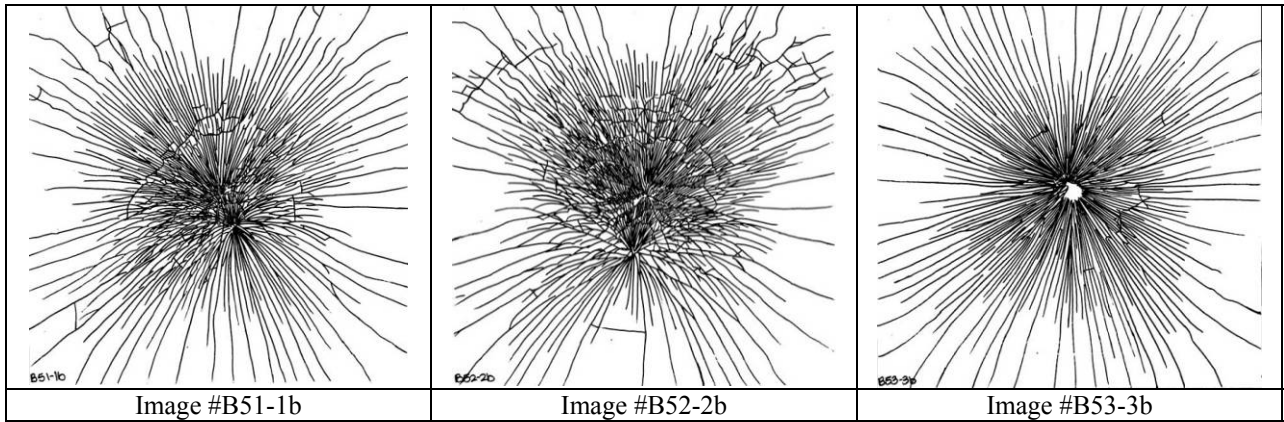
PANE FRACTURE IMAGES IMPACT FRACTURE - **ROUND TIP**



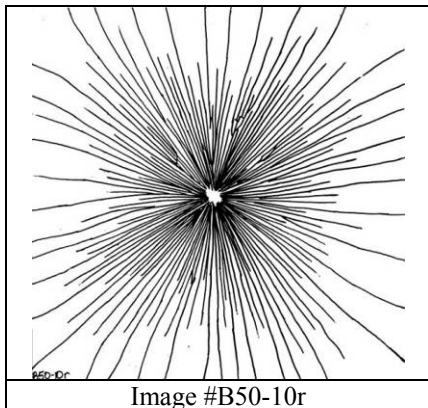
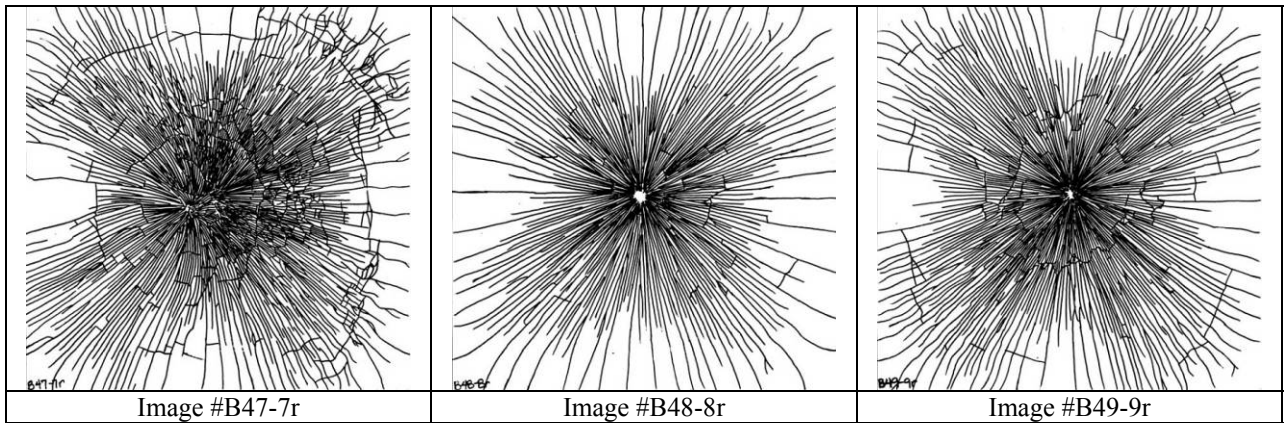
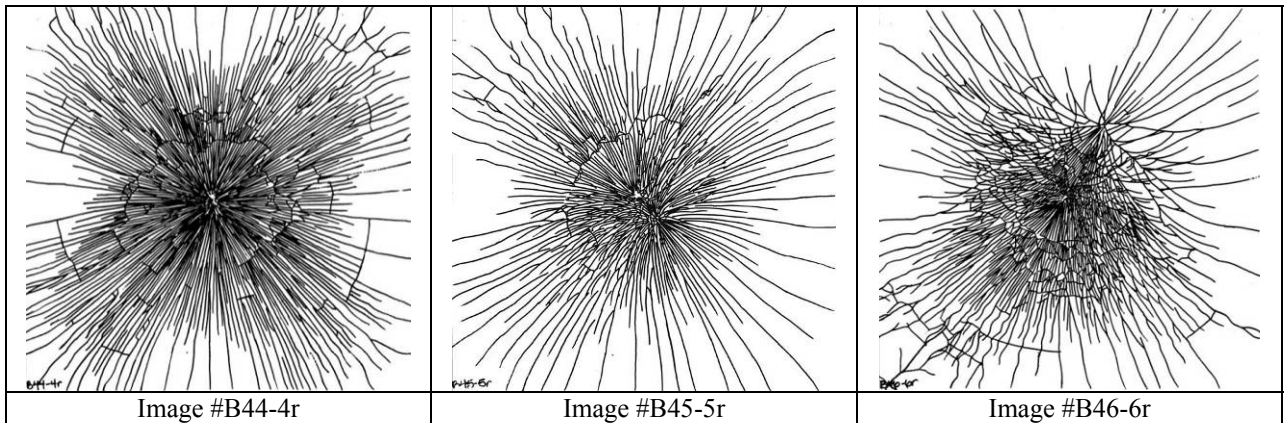
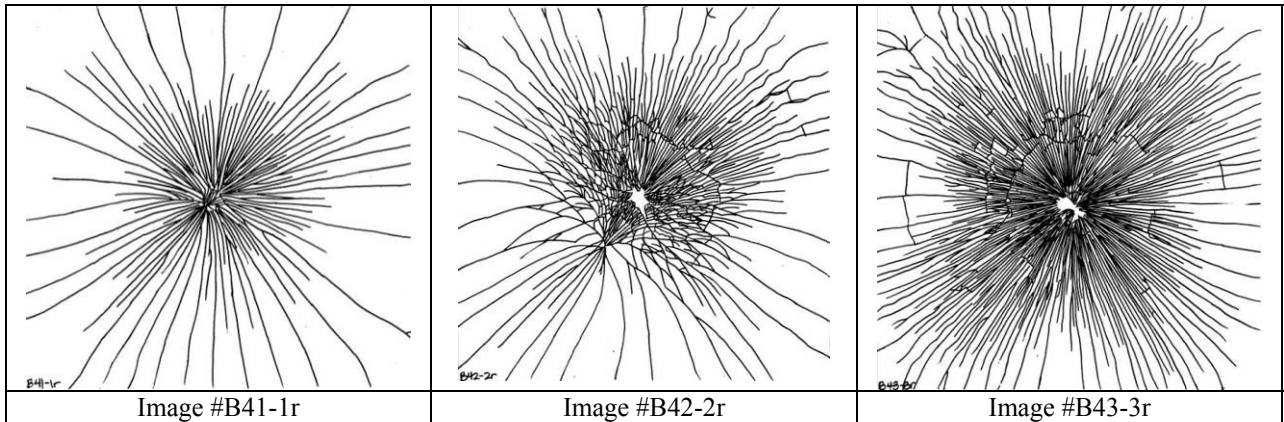
PANE FRACTURE IMAGES IMPACT FRACTURE - **SHARP TIP**



PANE FRACTURE IMAGES COMPRESSION FRACTURE - **BLUNT TIP**



PANE FRACTURE IMAGES COMPRESSION FRACTURE - **ROUND TIP**



PANE FRACTURE IMAGES COMPRESSION FRACTURE - SHARP TIP

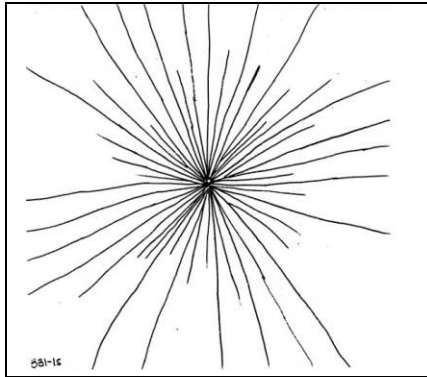


Image #B31-1s

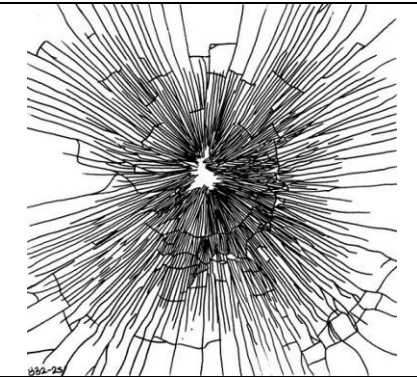


Image #B32-2s

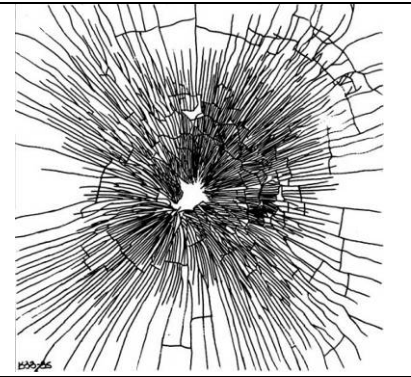


Image #B33-3s

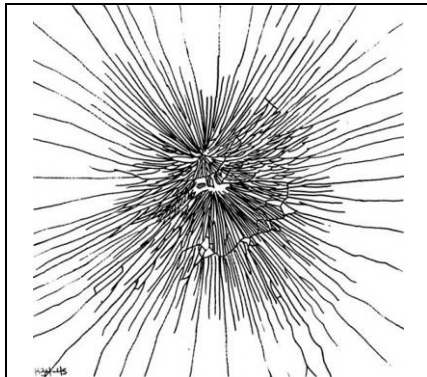


Image #B34-4s

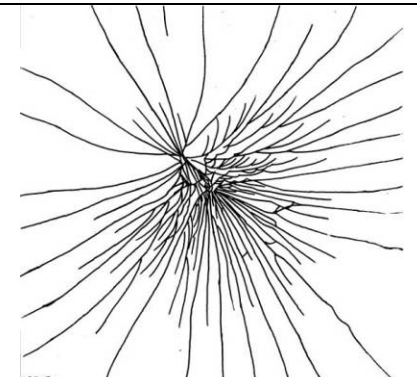


Image #B35-5s

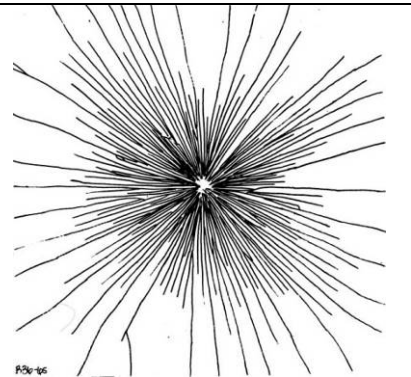


Image #B36-6s

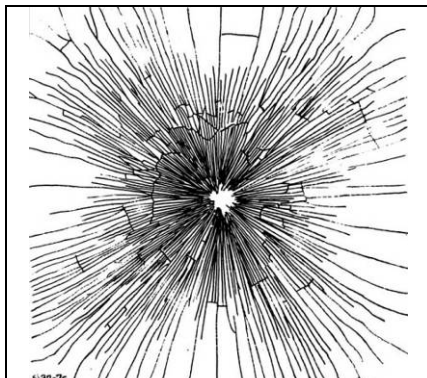


Image #B37-7s

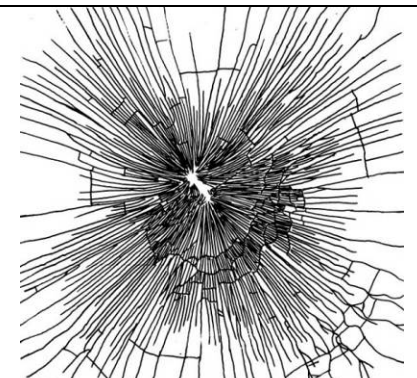


Image #B38-8s

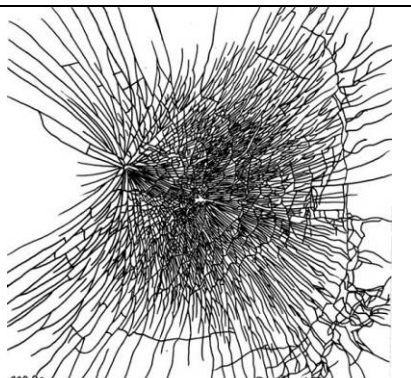


Image #B39-9s

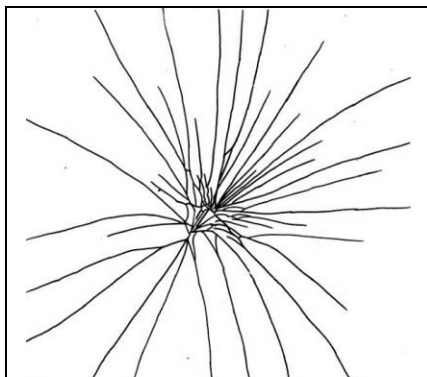


Image #B40-10s

BOTTLE FRACTURE IMAGES IMPACT FRACTURE - **BLUNT TIP**

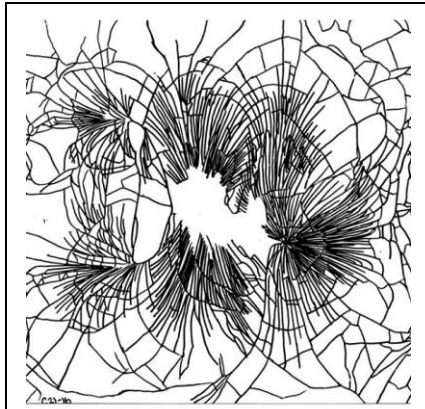


Image #C21-1b

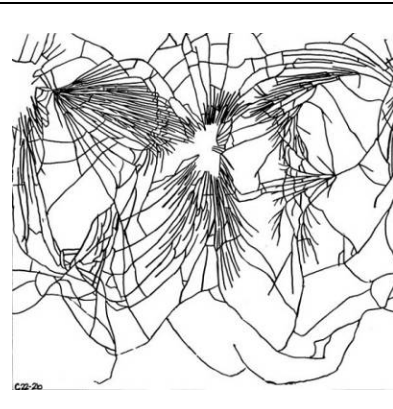


Image #C22-2b

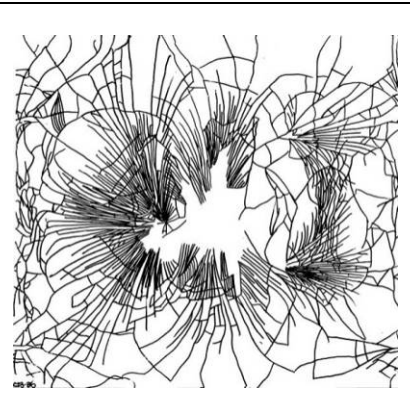


Image #C23-3b



Image #C24-4b



Image #C25-5b

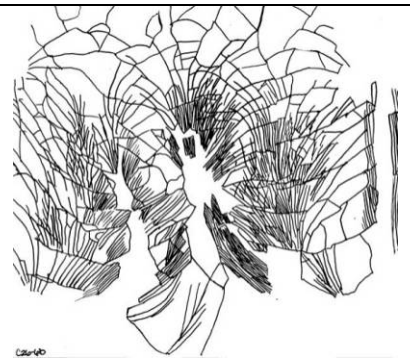


Image #C26-6b



Image #C27-7b



Image #C28-8b



Image #C29-9b

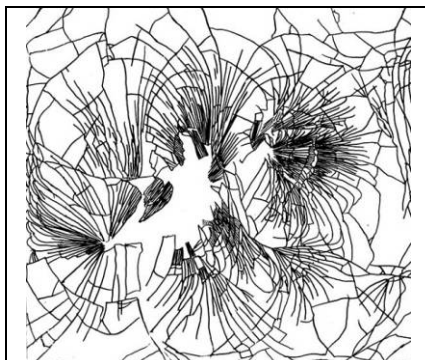
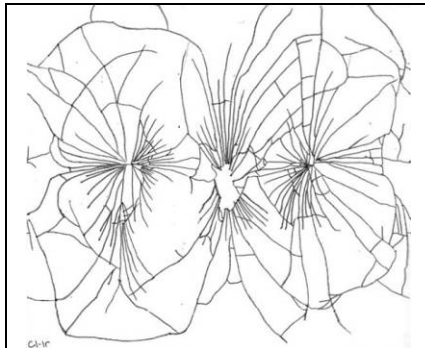


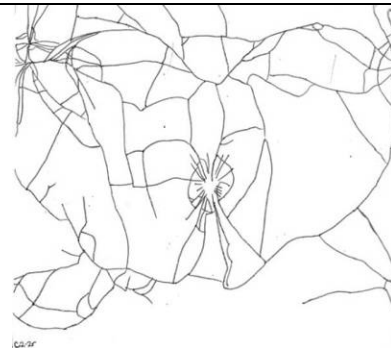
Image #C30-10b

BOTTLE FRACTURE IMAGES IMPACT FRACTURE - ROUND TIP



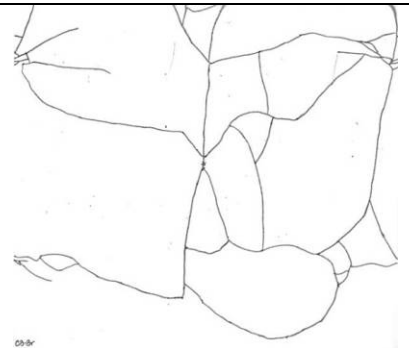
C1-1r

Image #C1-1r



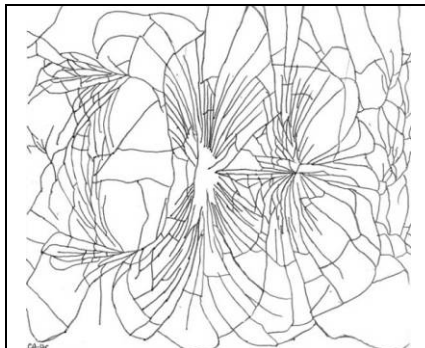
C2-2r

Image #C2-2r



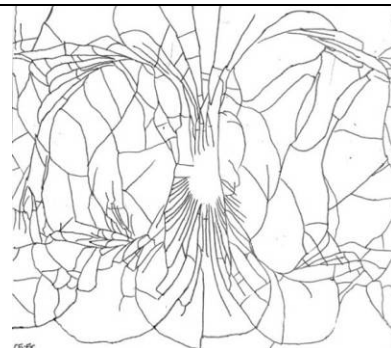
C3-3r

Image #C3-3r



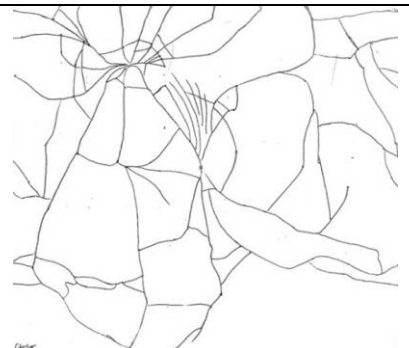
C4-4r

Image #C4-4r



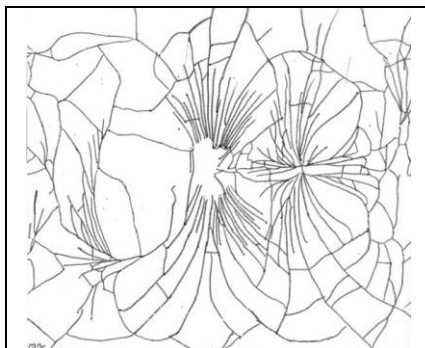
C5-5r

Image #C5-5r



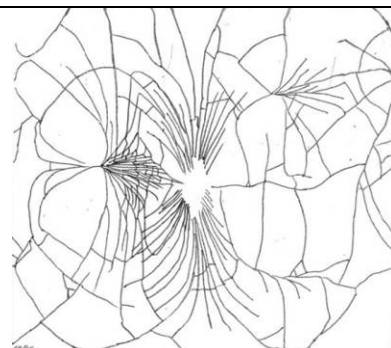
C6-6r

Image #C6-6r



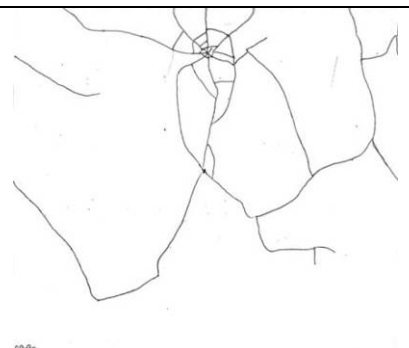
C7-7r

Image #C-7r



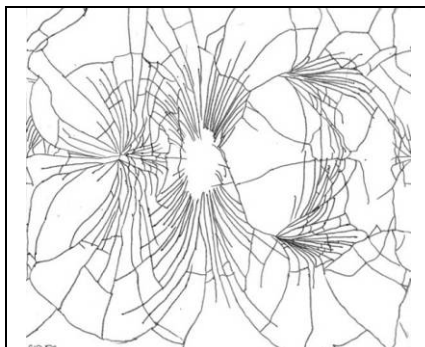
C8-8r

Image #C8-8r



C9-9r

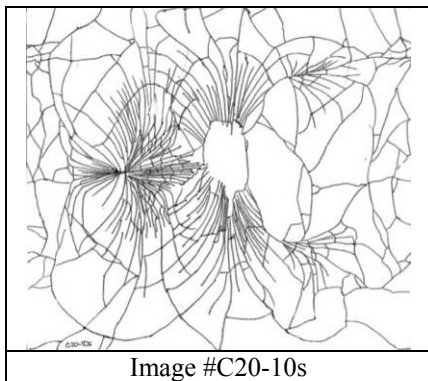
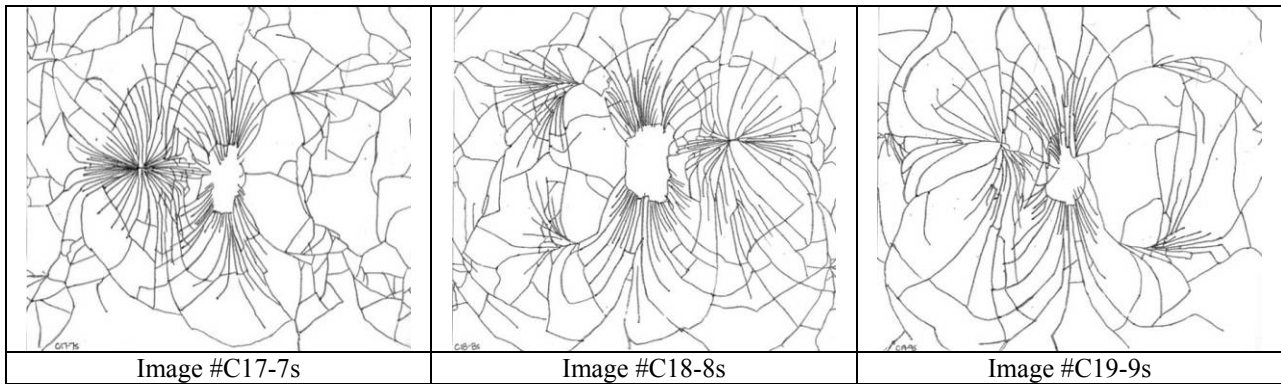
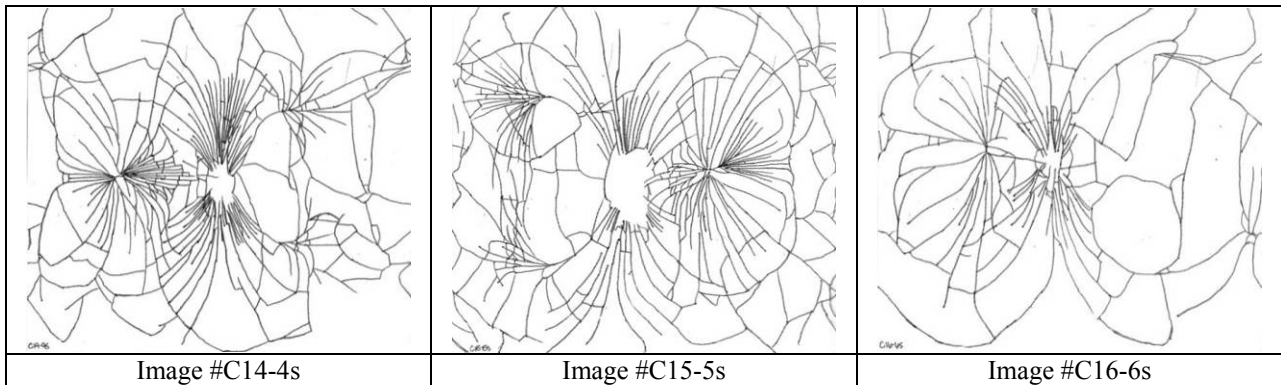
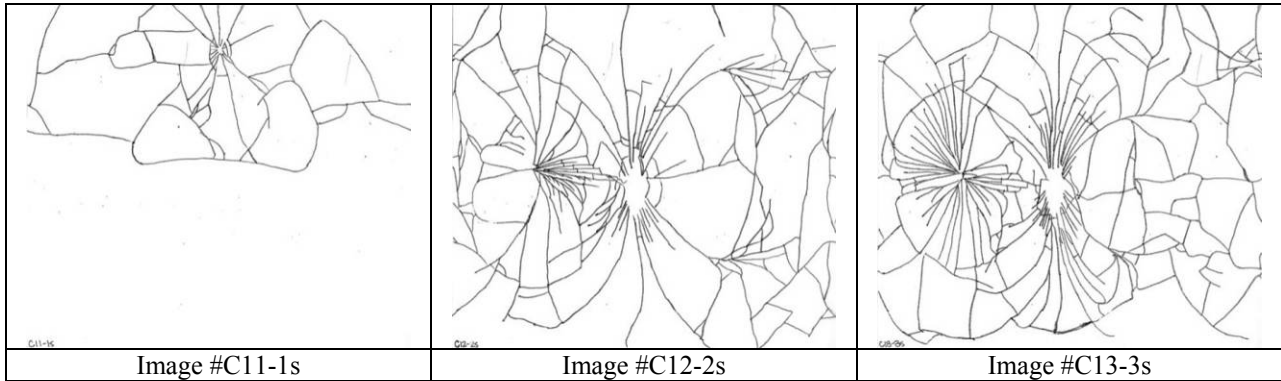
Image #C9-9r



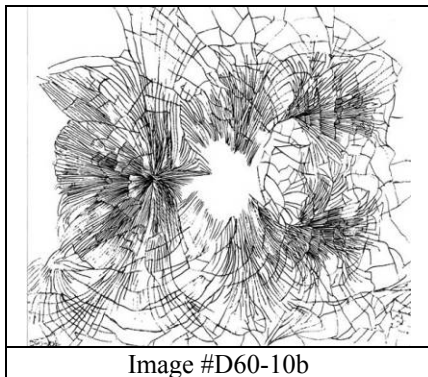
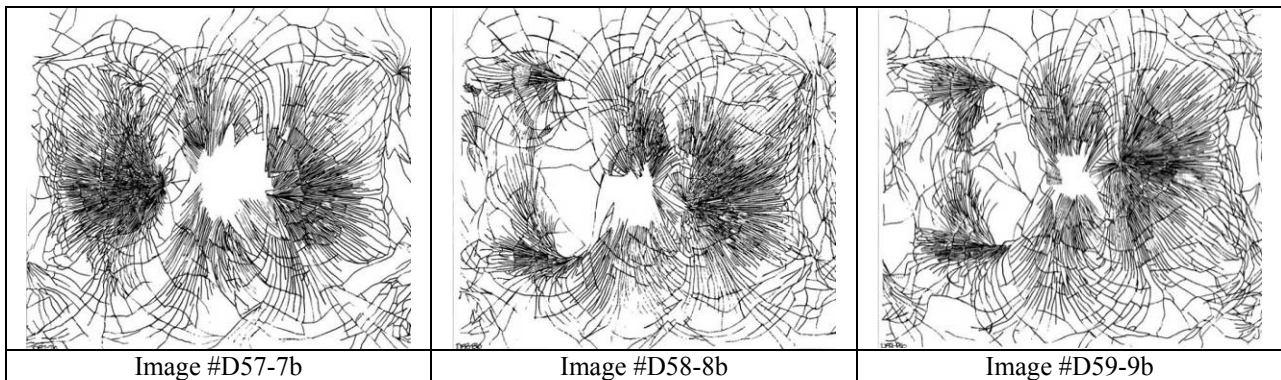
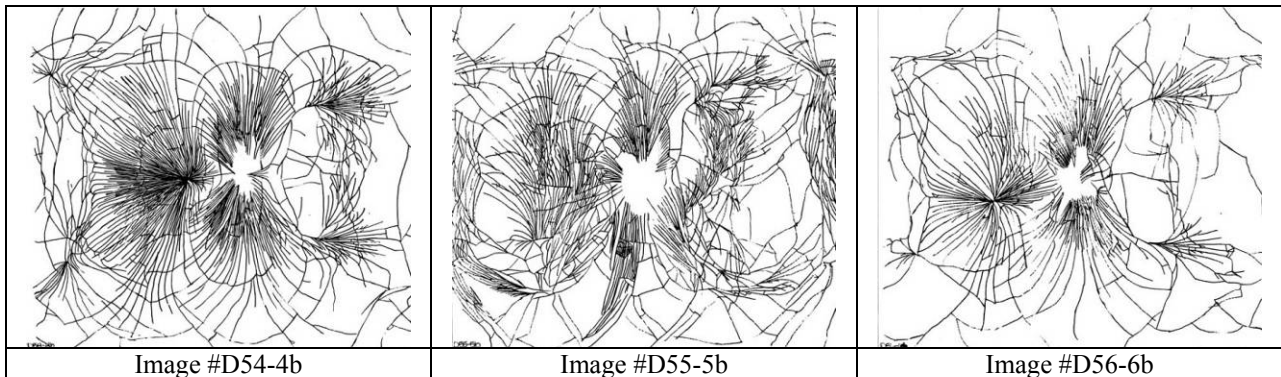
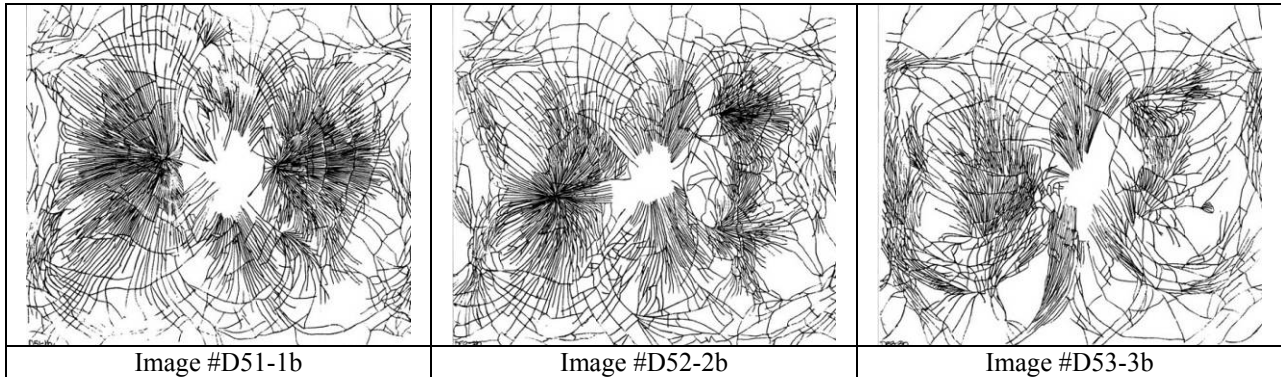
C10-10r

Image #C10-10r

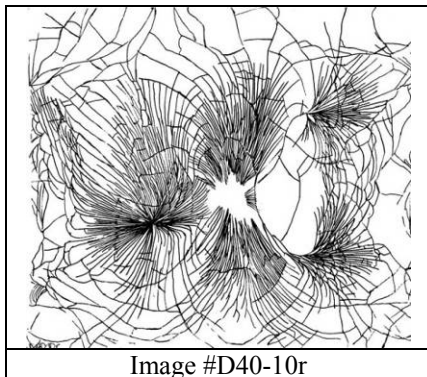
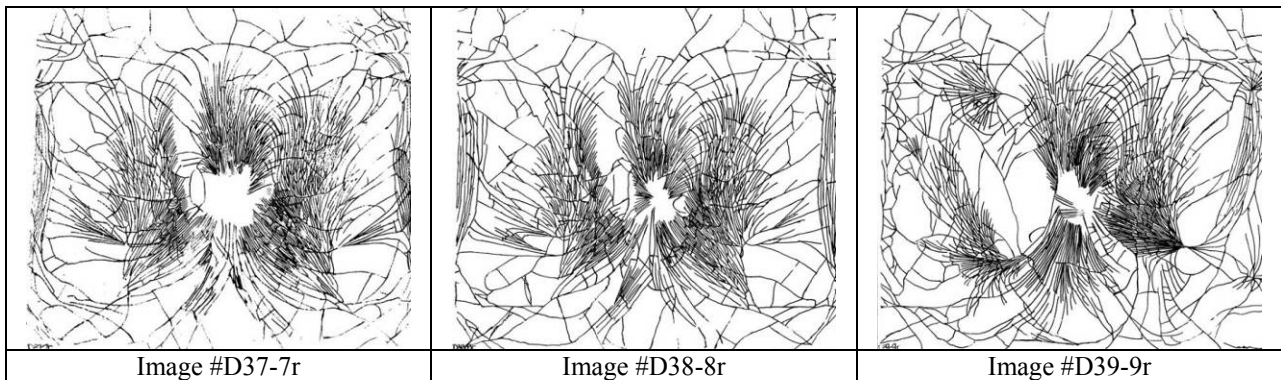
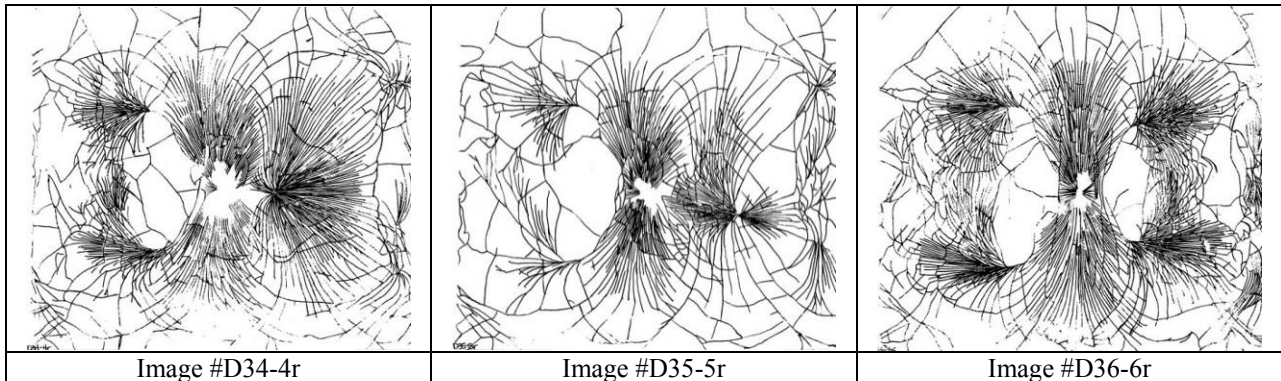
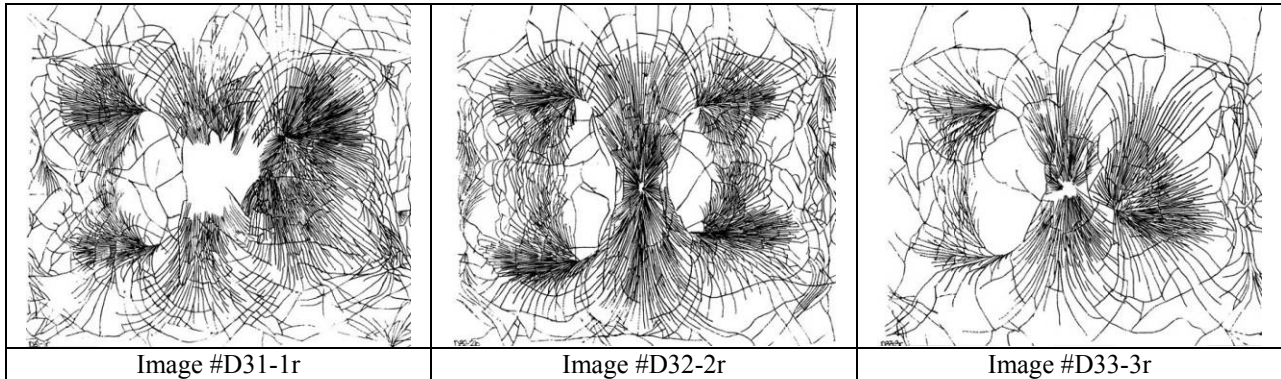
BOTTLE FRACTURE IMAGES IMPACT FRACTURE - SHARP TIP



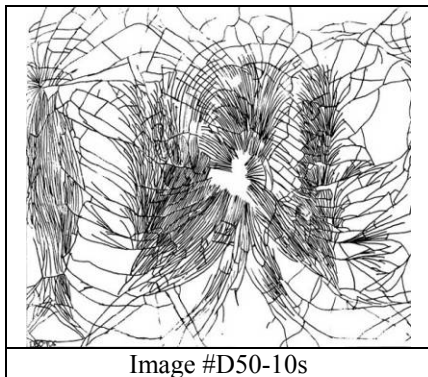
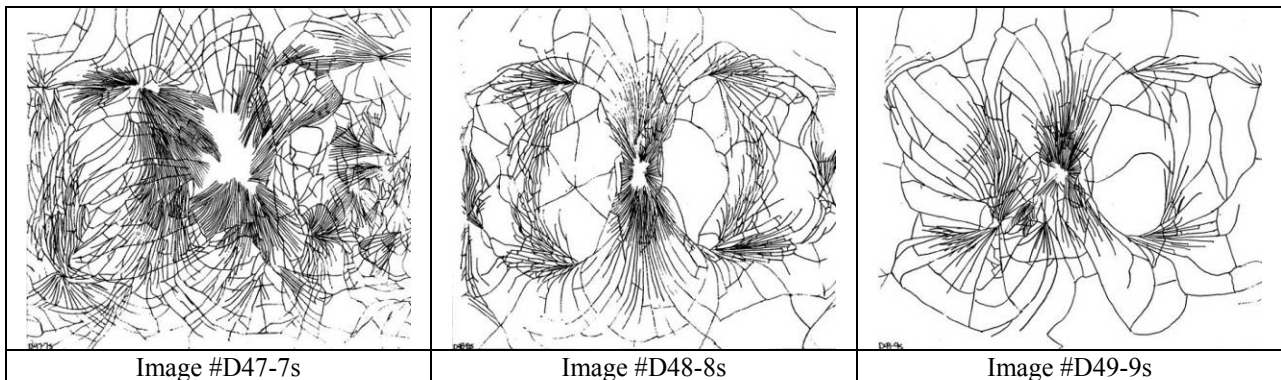
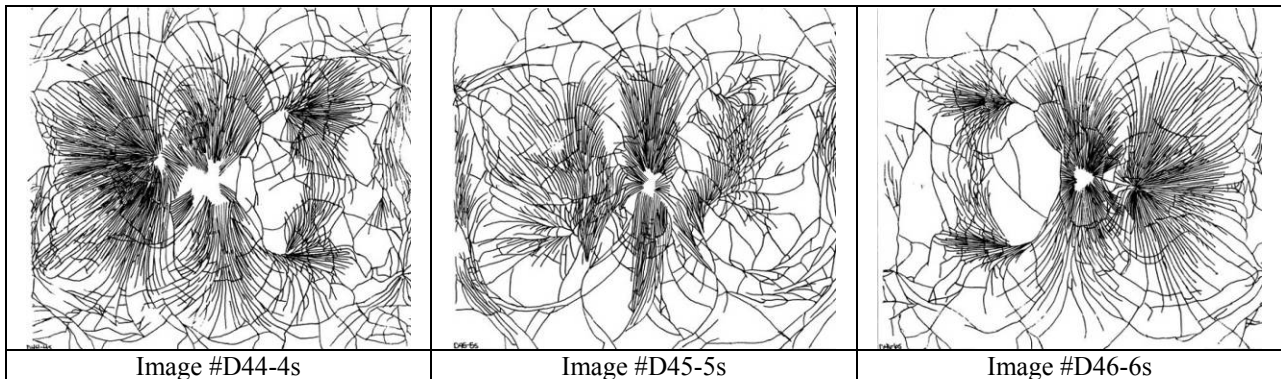
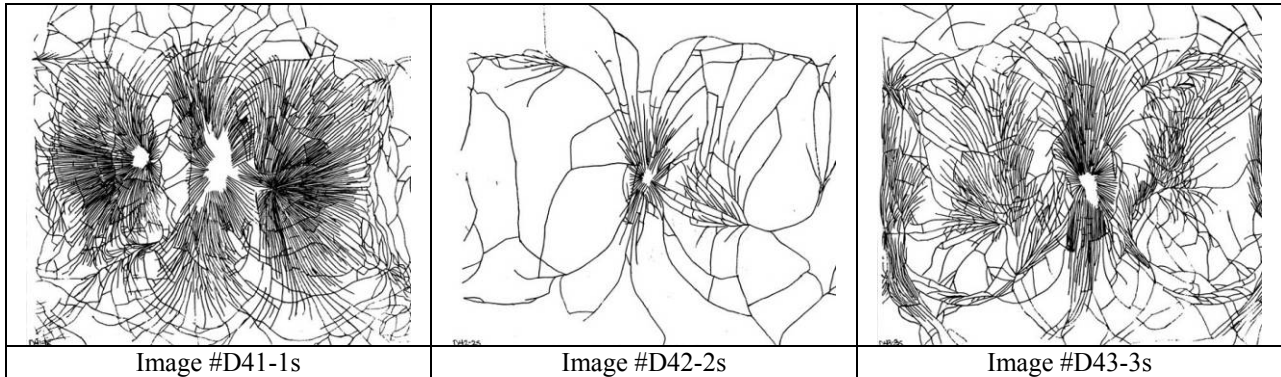
BOTTLE FRACTURE IMAGES COMPRESSION FRACTURE - BLUNT TIP



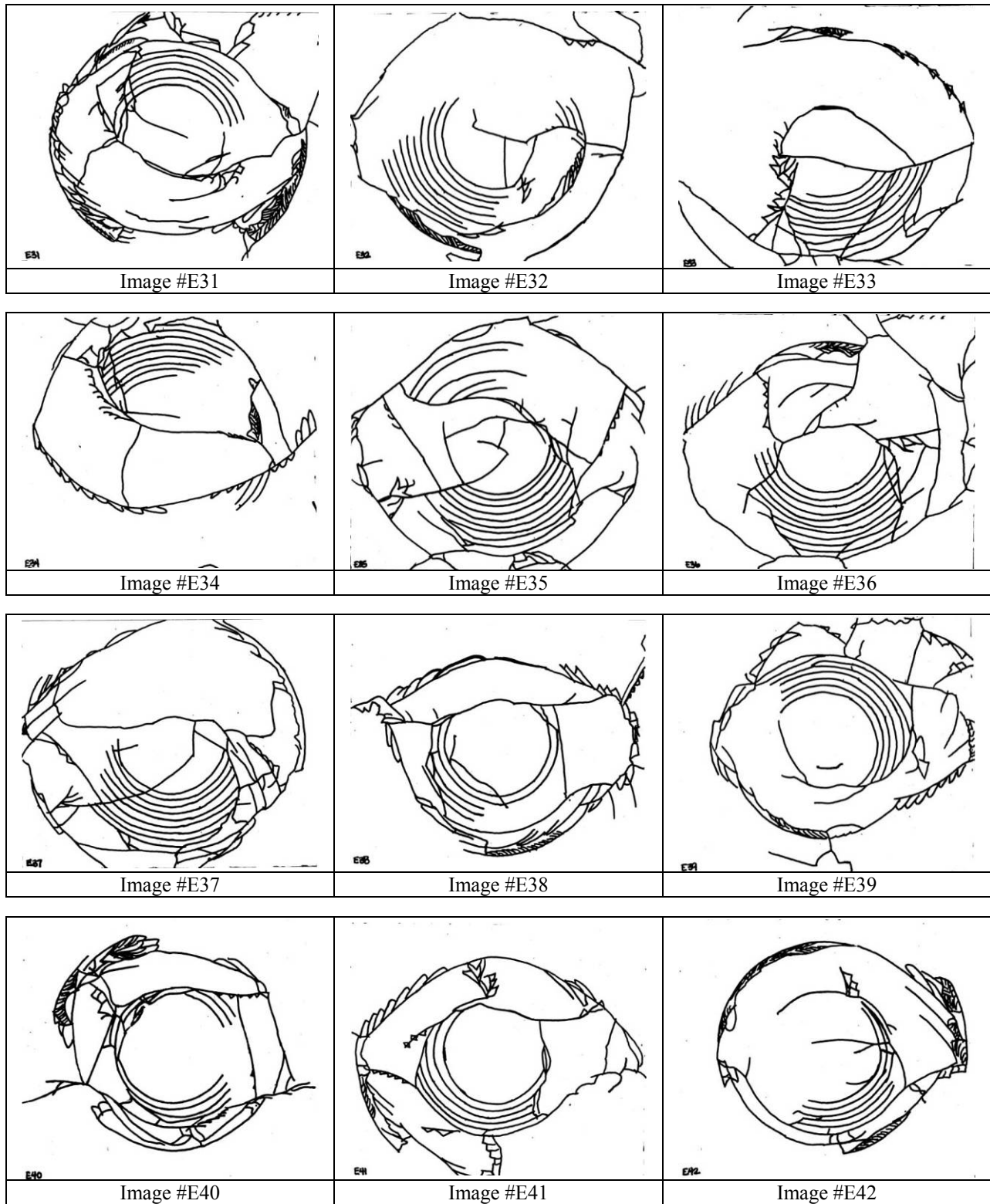
BOTTLE FRACTURE IMAGES COMPRESSION FRACTURE - ROUND TIP

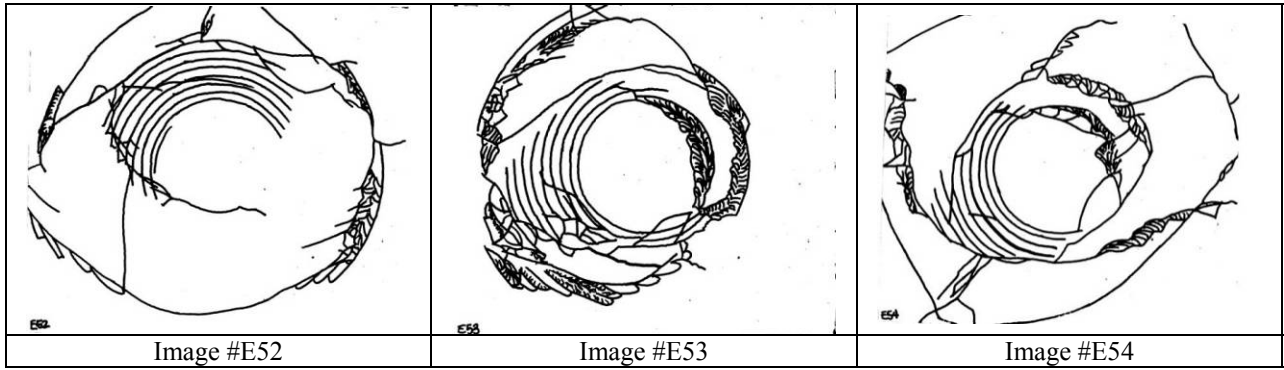
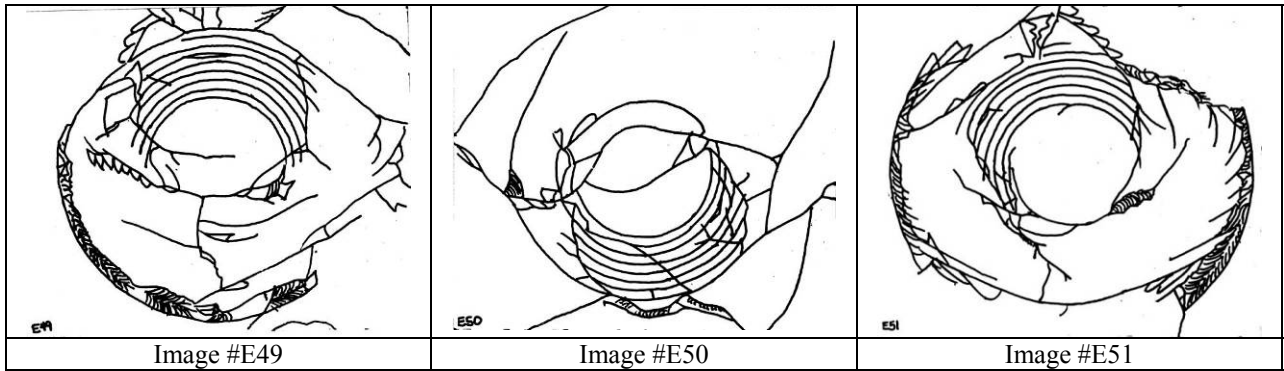
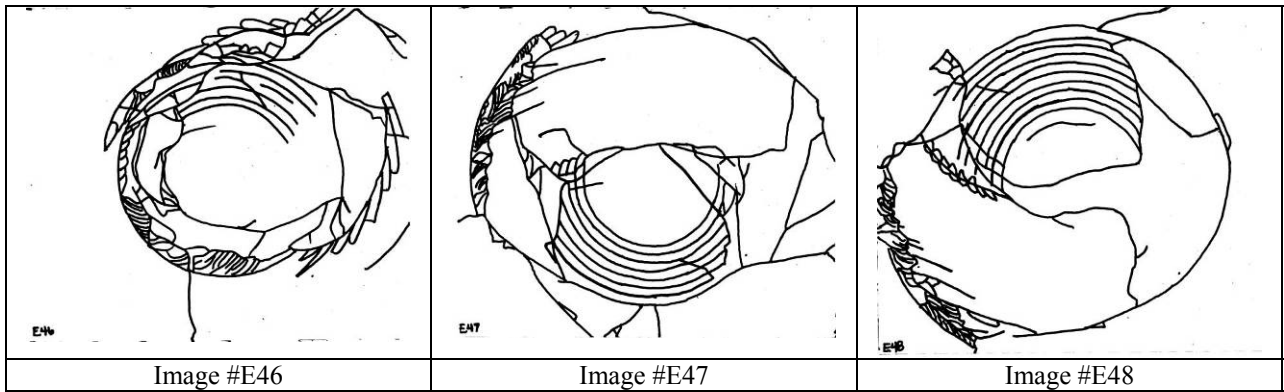
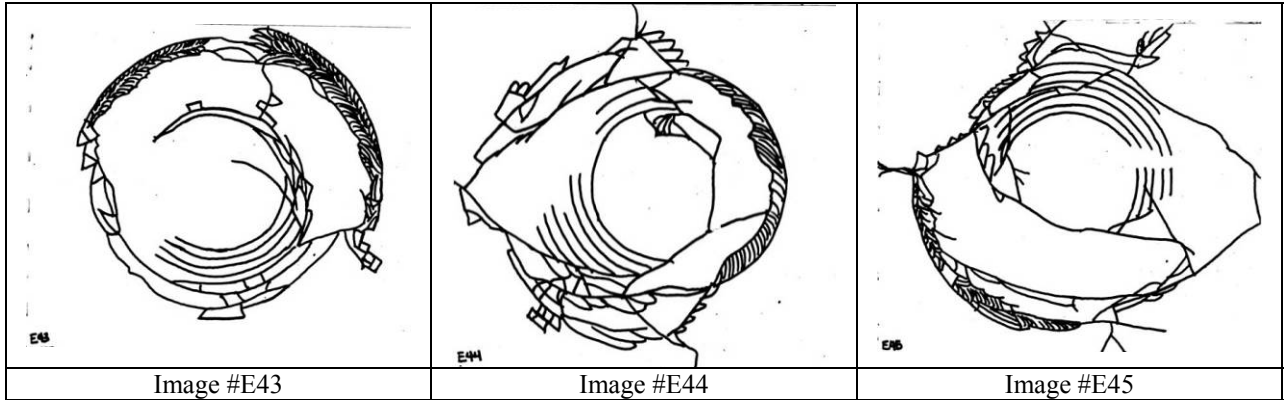


BOTTLE FRACTURE IMAGES COMPRESSION FRACTURE - SHARP TIP



PLASTIC LENS FRACTURE IMAGES - IMPACT FRACTURE





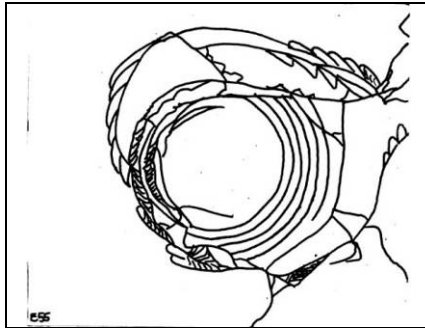


Image #E55

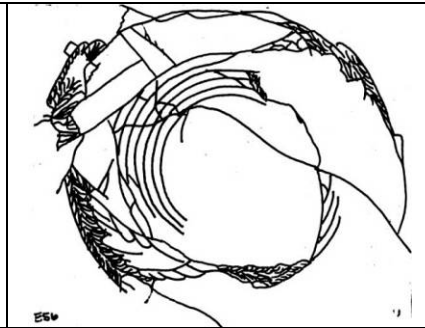


Image #E56

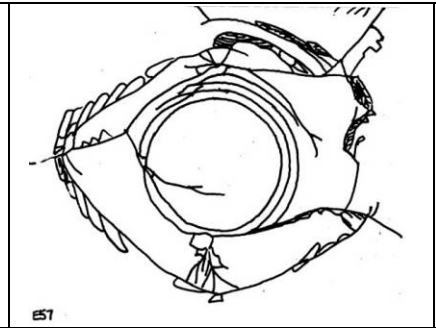


Image #E57

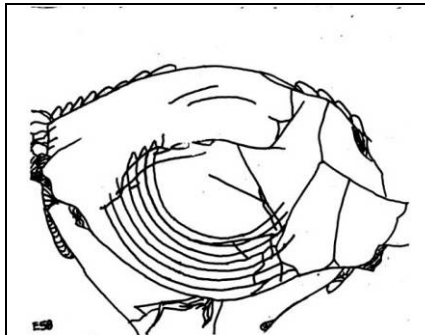


Image #E58

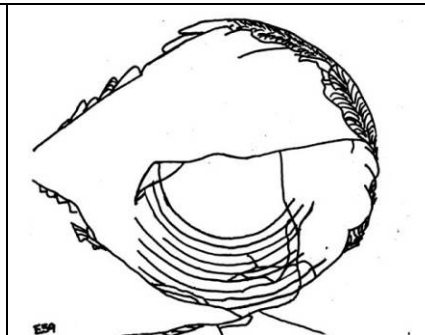


Image #E59

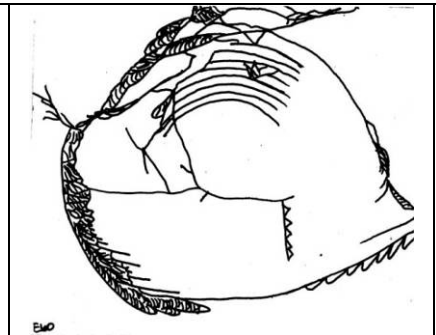
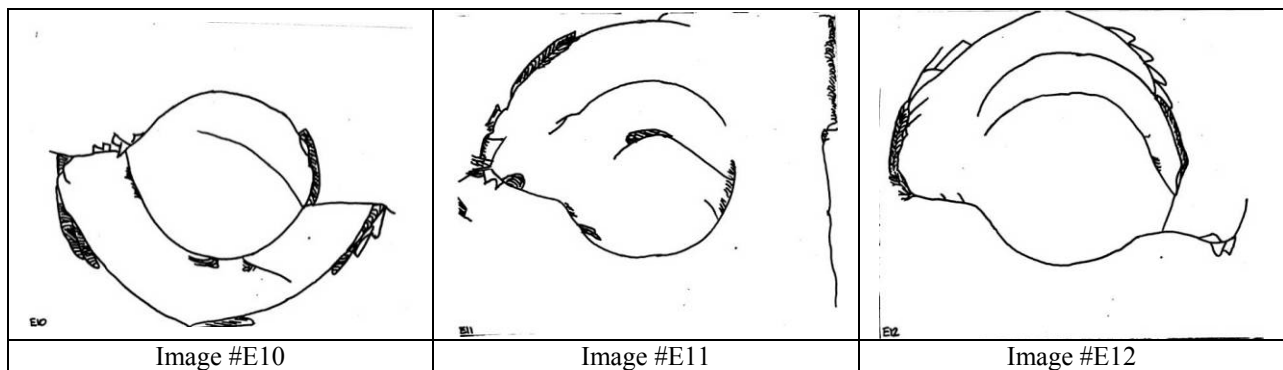
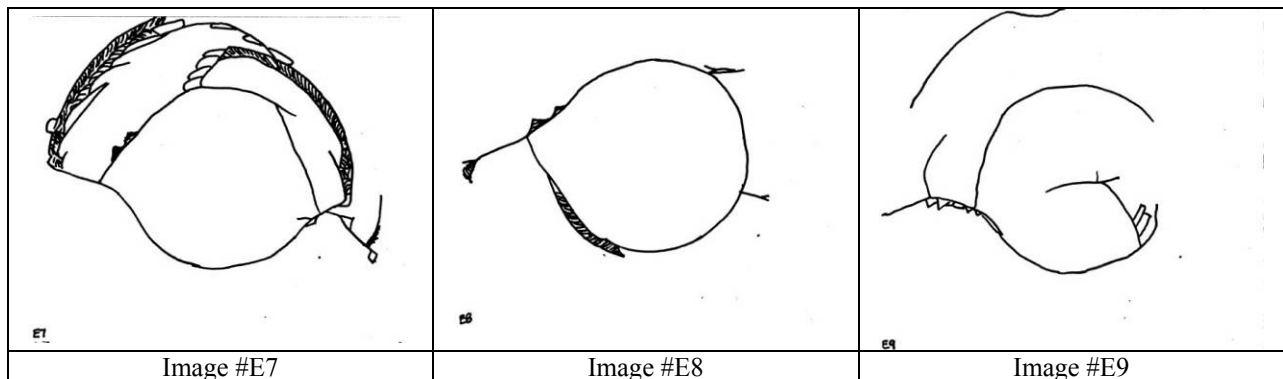
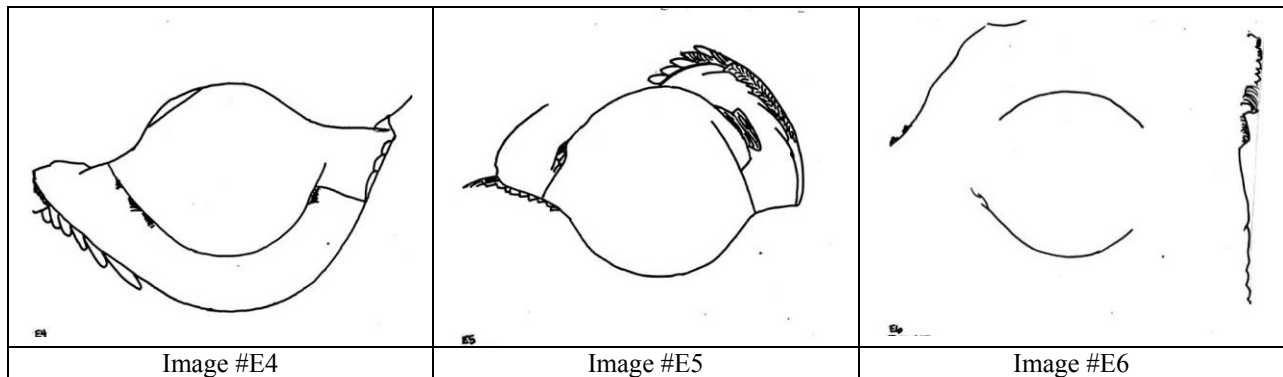
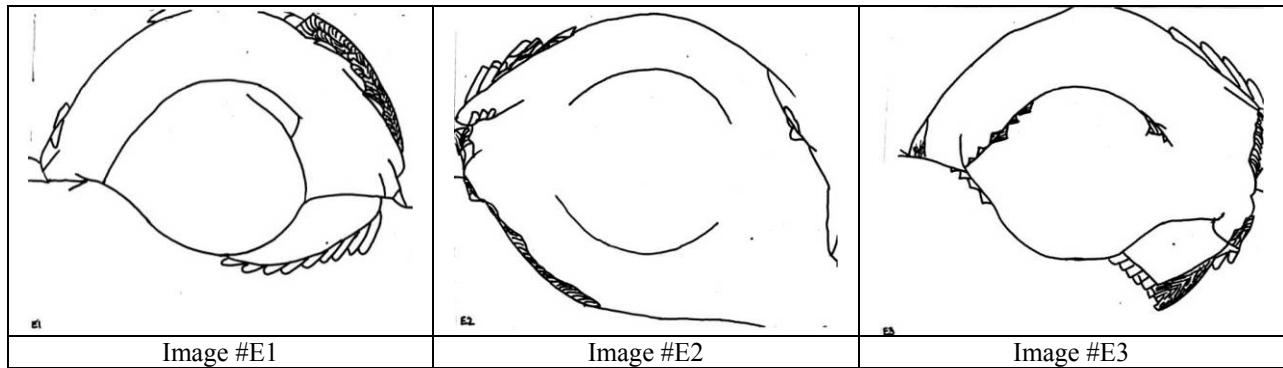


Image #E60

PLASTIC LENS FRACTURE IMAGES - COMPRESSION FRACTURE



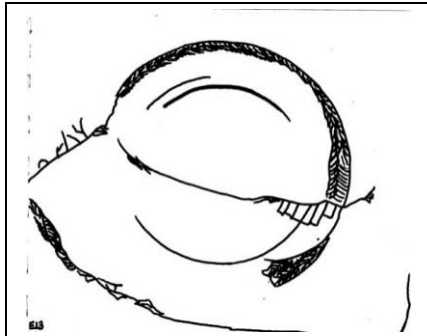


Image #E13

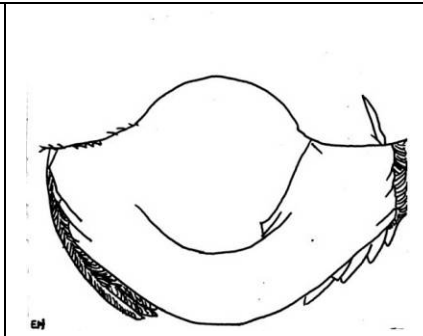


Image #E14

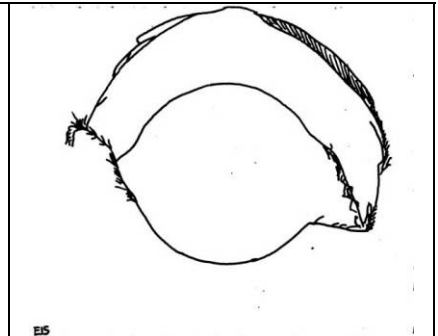


Image #E15

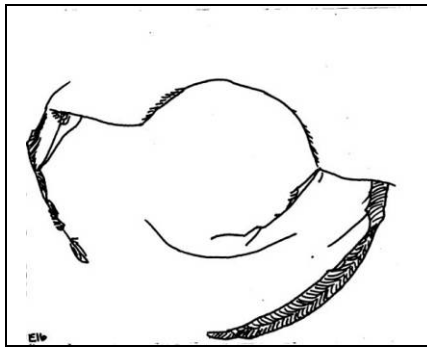


Image #E16

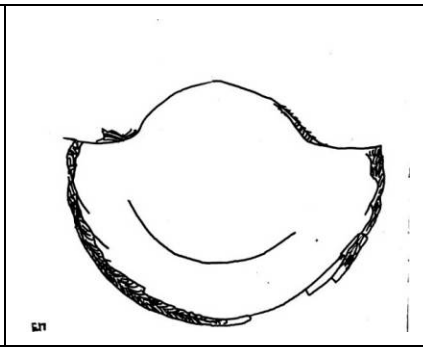


Image #E17

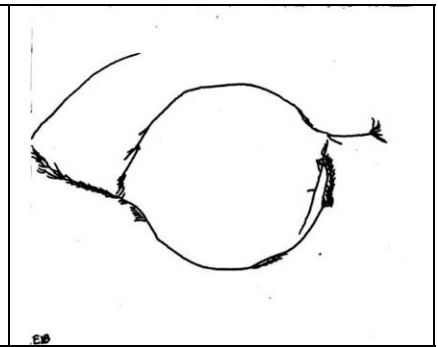


Image #E18

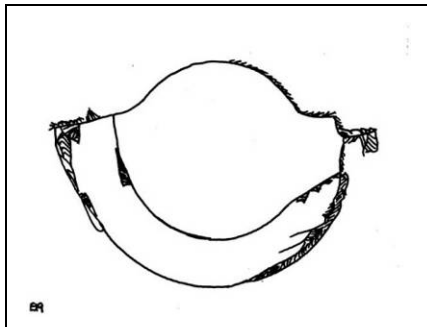


Image #E19

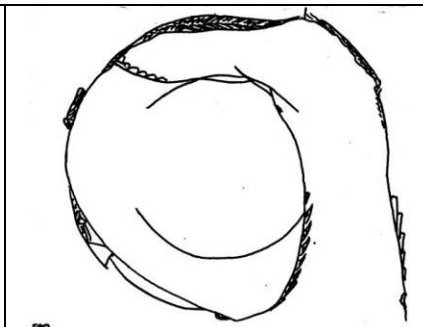


Image #E20

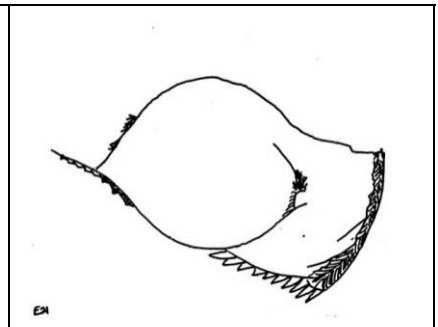


Image #E21

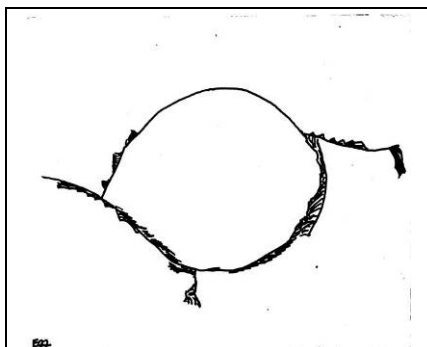


Image #E22

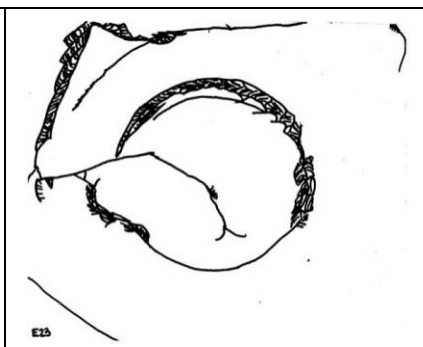


Image #E23

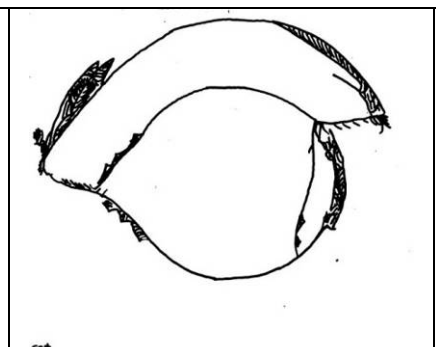
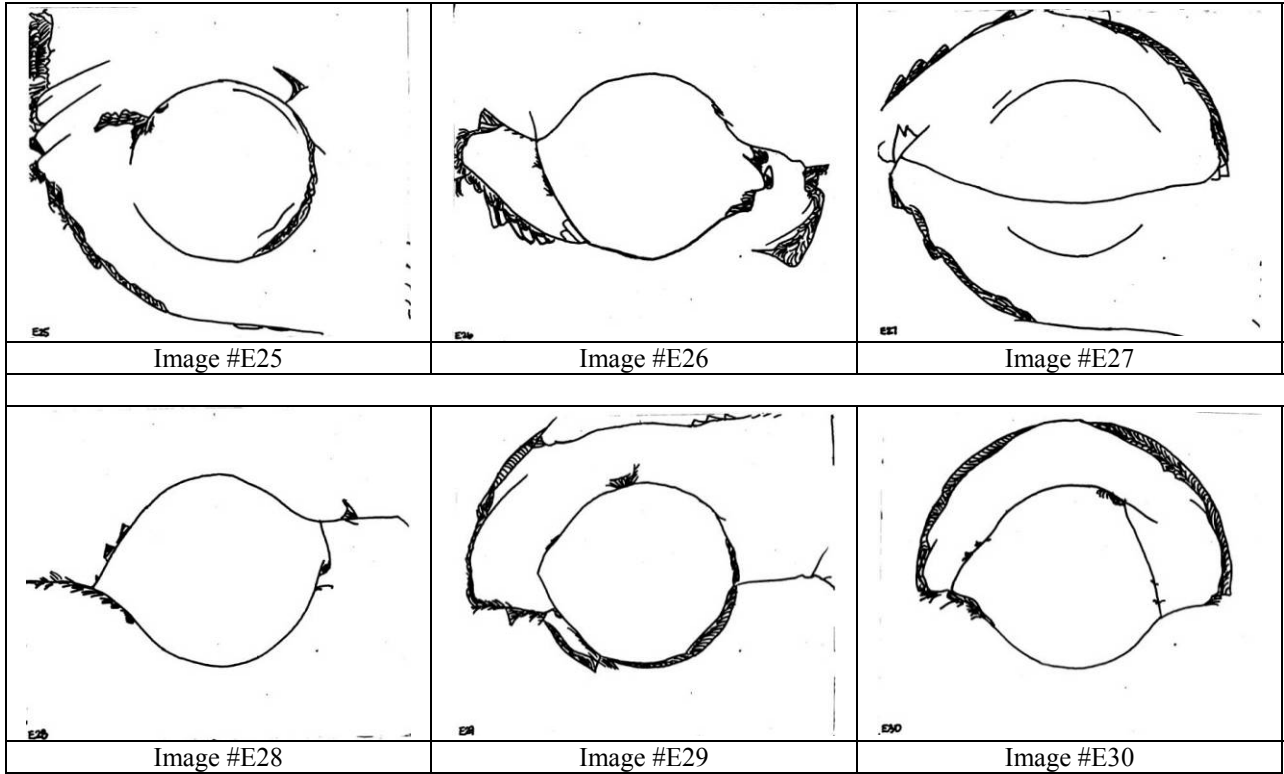


Image #E24



APPENDIX B

High Speed Video of the Fracture Sequence on a Glass Bottle and a Plastic Lens

Background

During the course of this study we had temporary access to high-speed video camera to document our velocity rates and image some of the actual impact fractures. We used a Phantom color high speed video camera (V. 7.3) to document the fracture sequence of a bottle using a sharp tip with impact fracture. The specifications for this camera are described in Table 1.

Model V7.3 Turbo Mode	Max Resolution	FPS	Exposure	Bits
High speed and high sensitivity. Can be configured with a 32GB of memory	800x600	6688	1 μ s	14
	512x512	11527		
	256x256	36697		
	128x128	88888		
	64x64 (T)	250000		
	32x16 (T) 6688	500000		

Table 1 Phantom Video camera specifications

The camera was primarily used to document the velocity of a dropping weight. To do this, we used a dropping weight labeled with a black dot. As we were interested primarily in velocity rate, we measured in triplicate, the velocity at different drop heights. The black dot on the dropping weight was used as a focus point for subsequent image analysis whereby a software routine from MATLAB[®] was used to track the time and position of the black dot. This routine then allowed us to derive the actual velocity at any position.

This appendix focuses on two sets of actual image fractures that were obtained during the study.

Some of the definitions that will be uses in this appendix are:

- Frame rate per second (**fps**) or camera frame rate
- A millisecond (**ms**) is a thousandth (10^{-3} or $1/1,000$) of a second.

- A microsecond (**μs**) is equal to one millionth (10^{-6} or $1/1,000,000$) of a second.
- A nanosecond (**ns**) is one billionth (10^{-9} or $1/1,000,000,000$) of a second.

Bottle Fracture Video

The conditions for this test were:

- Frame rate: 60,085 fps
- Seconds per frame: 1.664×10^{-5}
- Micro seconds per frame: 17 μs per frame
- Bottle length base to beginning of the shoulder: 20.3 cm

We were interested in looking at the crack propagation rate of a fracture on a glass bottle. We recorded two bottles undergoing such a dynamic fracture. The first bottle used a frame rate of ~ 31,007 **fps**. This rate proved to be insufficient to look at fracture propagation. Thus we increased the frame rate to 60,085 **fps**. The tradeoff for this increase is a reduction in image resolution. Both drops were made from a 3.66 meter height.

We used a sharp tip to break the bottle illustrated in Figure 1. We listed $T = 0$ as the point when we observed the tip touching the surface of the bottle. Due to the apparatus, we could not image the actual point of contact on the bottle from the top and had to settle for a side image. It is interesting to note that in both cases the point of impact is near the center of the bottle on the top surface; however, the first visible fracture we could observe was at the base at $T = 476 \mu\text{s}$.

This fracture appears to propagate in a circular manner from the right side of the base of the bottle. The bottle is in a Teflon™ milled, semi-circular cradle which is designed to only hold the bottle in place. The bottom of the bottle is in actual contact with the aluminum base plate.

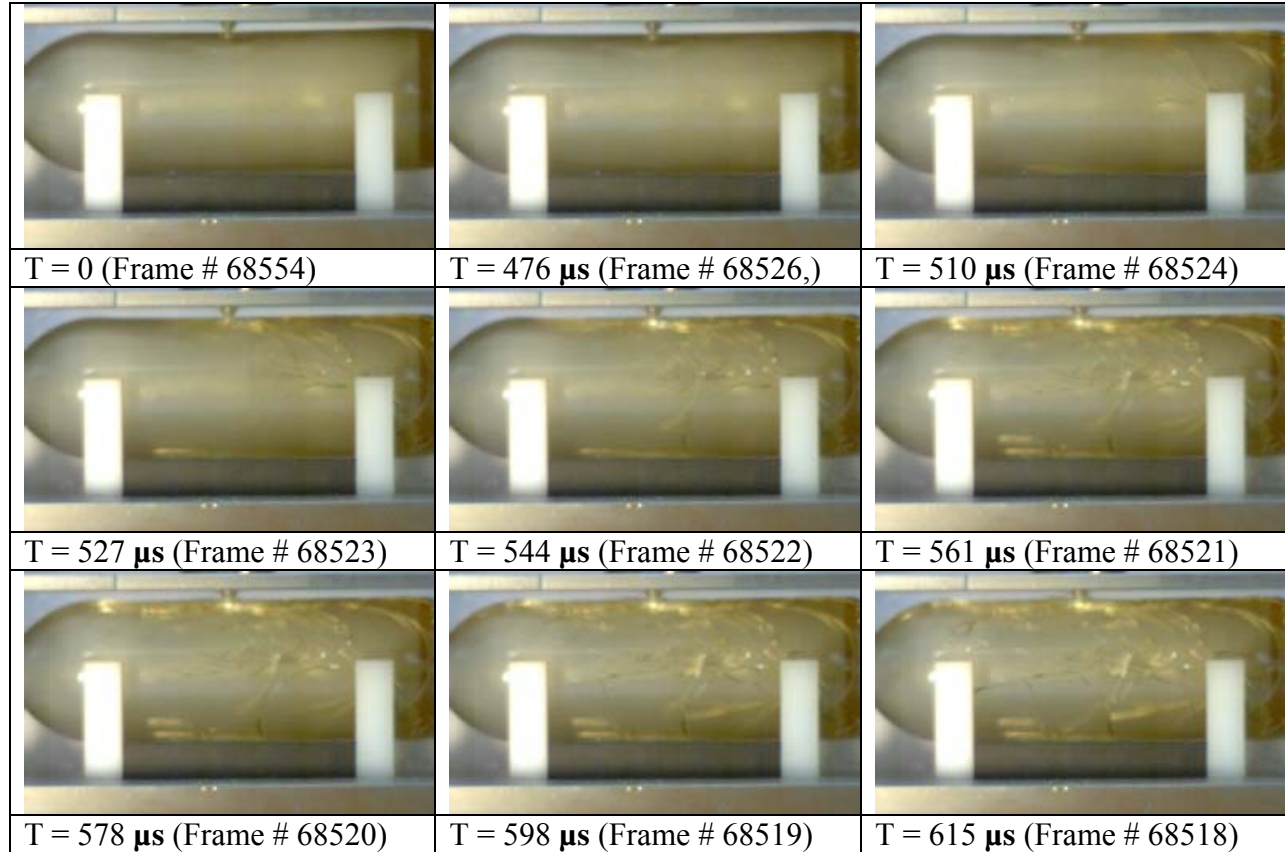


Figure 1 Bottle Fracture Images

Comment on the Fracture Video

The bottle length from the base to the beginning of the shoulder on the bottle is 20.3 **cm** or 0.203 **m**. In Figure 1, T = 0 is the time when we observed the tip touching the top surface of the bottle. T = 476 μs is the time we observed the first indication of a fracture near the bottom of the bottle. The fracture time, based on what is visible, is 139 μs for the 0.203 m bottle distance. This time can be converted same as 0.139×10^{-3} seconds. Alternatively, to find the fracture velocity, we divide the distance by the time interval ($0.203 \text{ m} / 0.139 \times 10^{-3} \text{ sec}$) and end up with a bottle fracture velocity of 1,460 **m/s**. We do not know if the fracture originated earlier at the point of impact as that area was not visible to the camera.

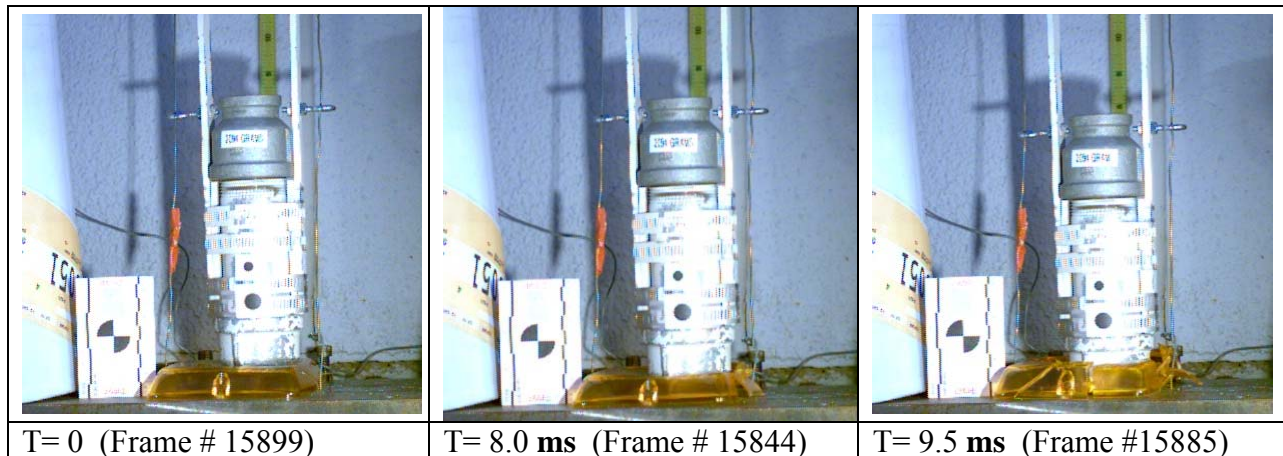
Plastic Lens Impact Video

For fracturing the plastic lens, we utilized a dropping pipe. This device is used by the California Criminalistics Institute (CALDOJ) as part of their Headlamp Examinations class. It is normally dropped from 20+ feet and upon impacting the ground, the resulting force will distort a filament. The system consisted of a pipe with end caps and two steel guide wires attached to a steel impact plate. The steel impact plate is under tension in order to tighten the two guide wires. The pipe can be raised to any height (up to 27 feet) with a rope pulley. When a predetermined level is reached, another trigger line is pulled which releases the pipe, thus allowing it to impact a steel plate.

The conditions for this test were:

- Frame rate: 7,000 fps
- Micro seconds per frame: 142.9 μ s
- Milli seconds per frame: 0.143ms per frame
- Drop height: 2.74 meters (9 feet)

Figure 2 illustrates the twelve sequences during the course of this drop showing the fracture on the plastic lens. The black dots on the pipe with a white background are reference marks for later video velocity analysis.



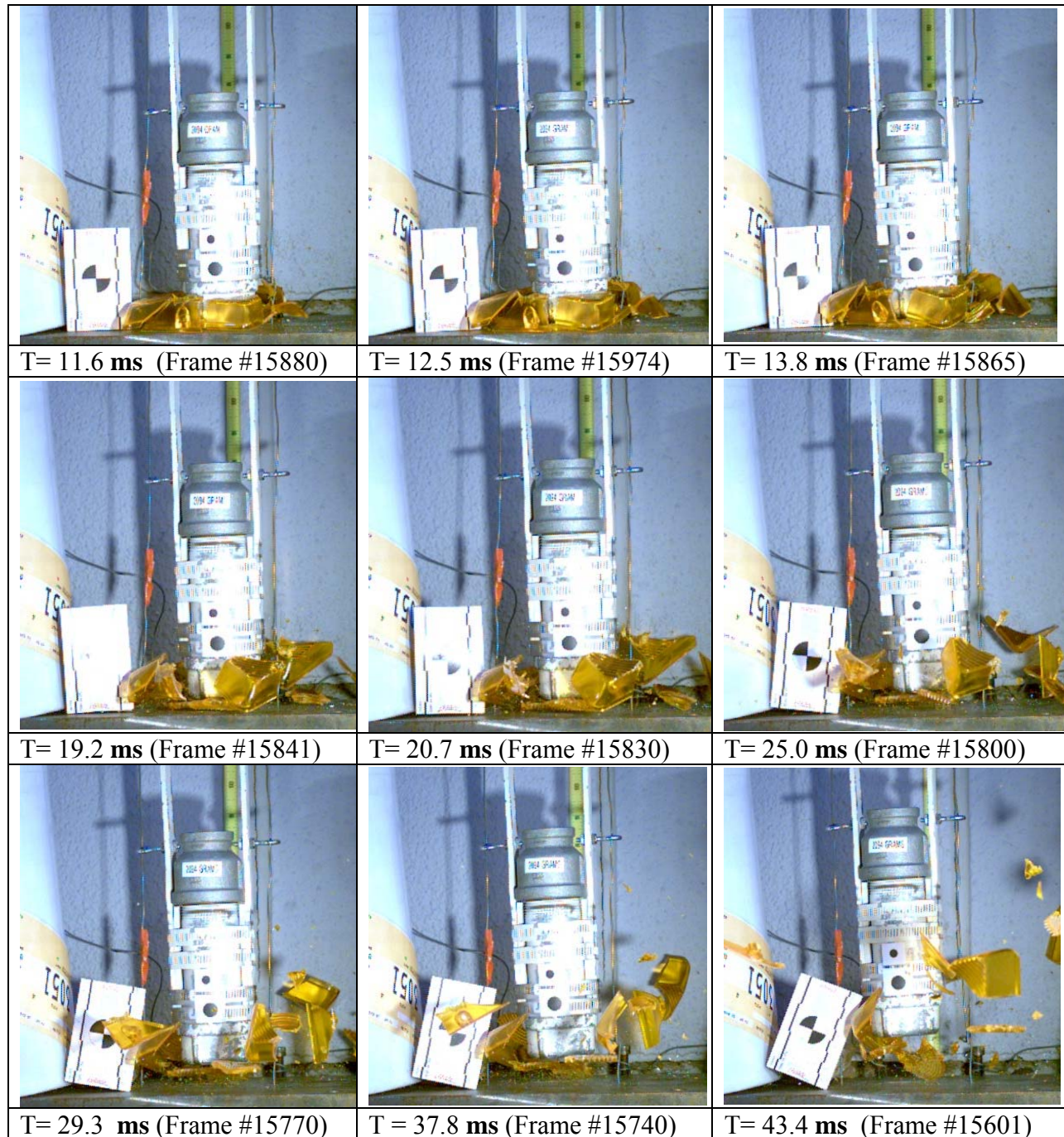


Figure 3 Plastic Lens Fracture

In this particular fracture test, the plastic tail light lens was on a steel plate when a lead filled pipe made the initial impact. By Frame 15830 the pipe is beginning to rebound and Frame 15601 illustrates some of the rebound from this impact while the lens fragments are still expanding upward and outward.

APPENDIX C

FRACTURE APPARATUS DESIGN

The fracture apparatus was designed so that it could be used for both glass pane and glass bottles. The logic behind this design was to develop a mechanism that would fracture the glass pane or the glass bottle without causing deep penetration. Thus, the design had to be adjustable in order to accommodate different heights and strong enough to absorb the impact of a heavy weight whose travel we wanted to arrest. Figure 1 illustrates the steel device we had machined for this research. The dimensions for the fracture device are illustrated in Figure 2. This design was predicated on the fact that we only wanted the tip to penetrate a fraction of an inch. The rest of the impact energy would be absorbed by the frame.

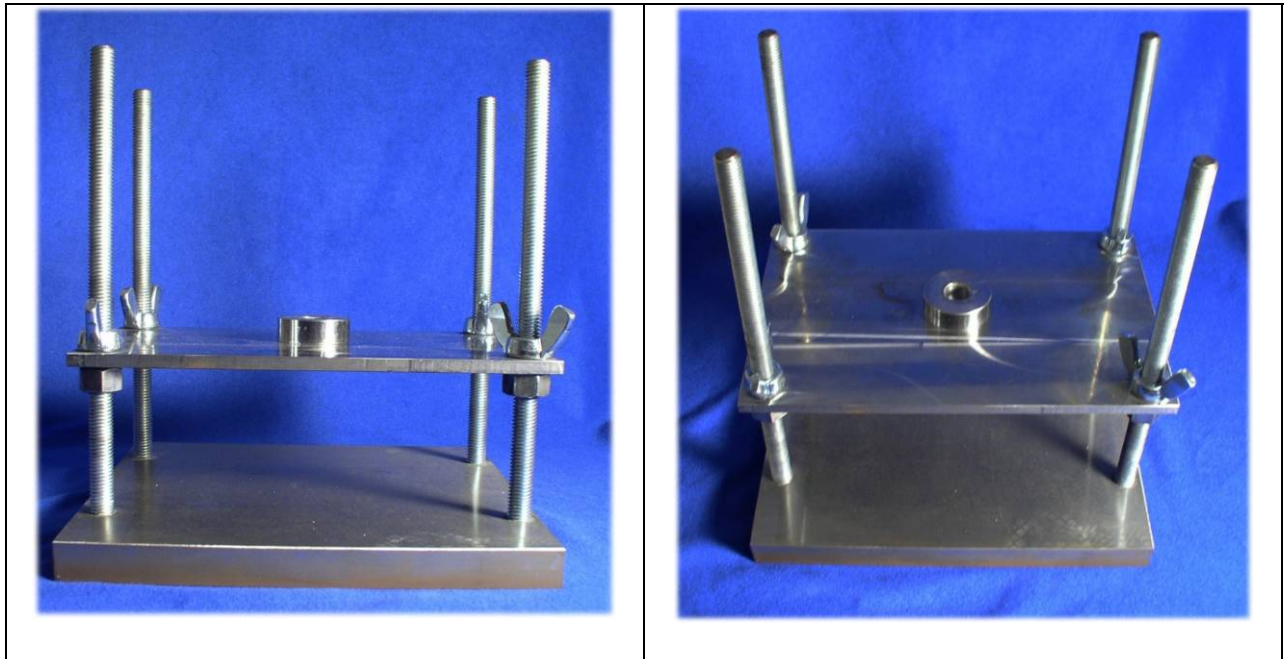


Figure 1 Two views of the fracture device

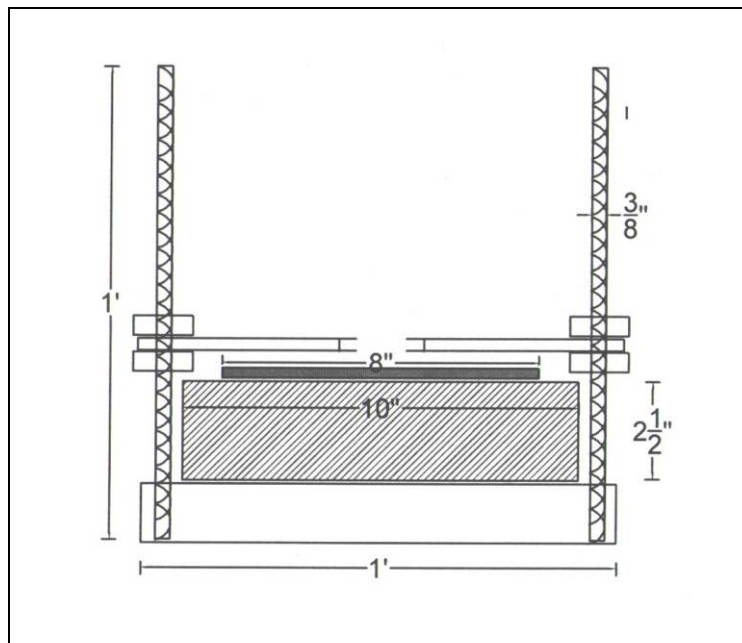


Figure 2 Fracture device dimensions

The cradle for the bottle was likewise designed to hold a bottle in place. This is illustrated in Figure 3.

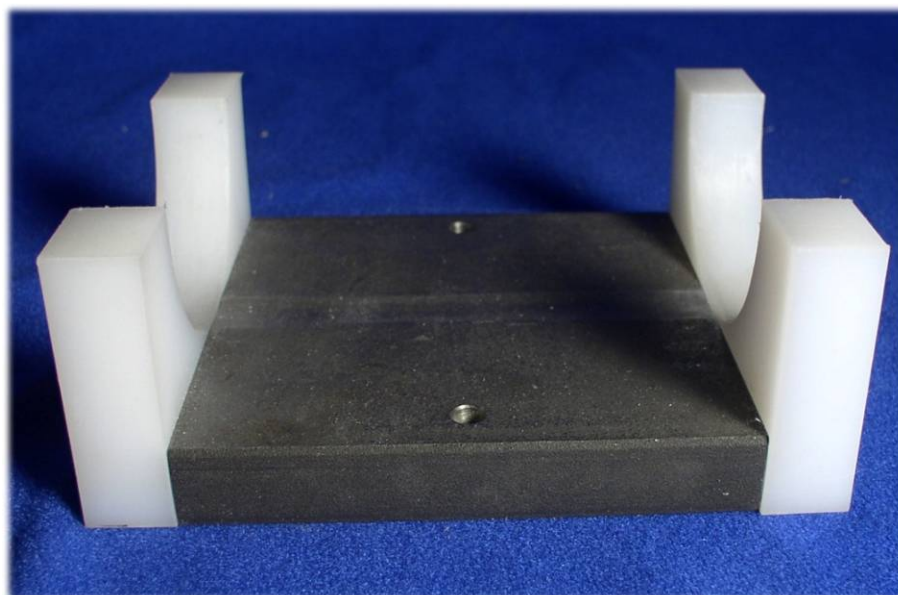


Figure 3 Bottle cradle with milled plastic Teflon® end pieces

The dimensions for this cradle are described in Figure 4.

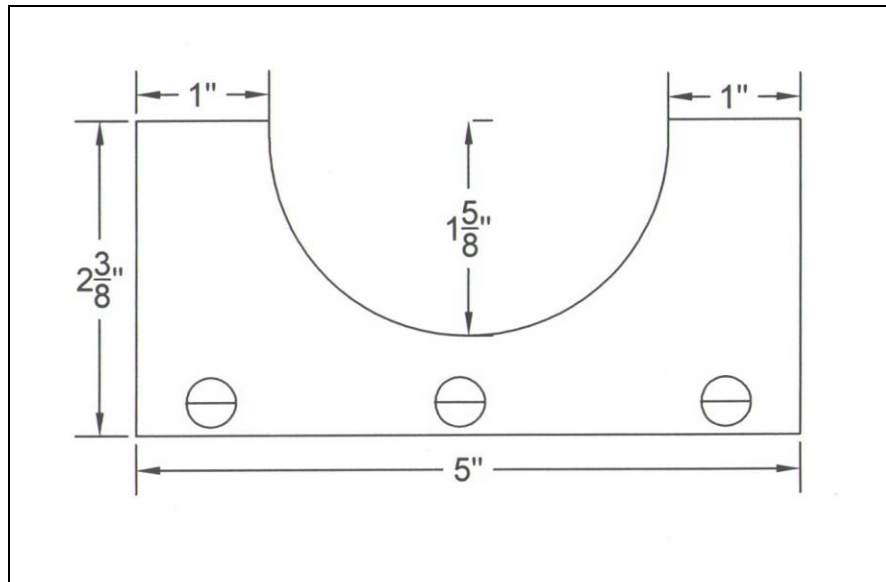


Figure 4 Cradle dimensions

The impact device was designed with replaceable tips having different surface profiles. Its dimensions are illustrated in Figure 5.

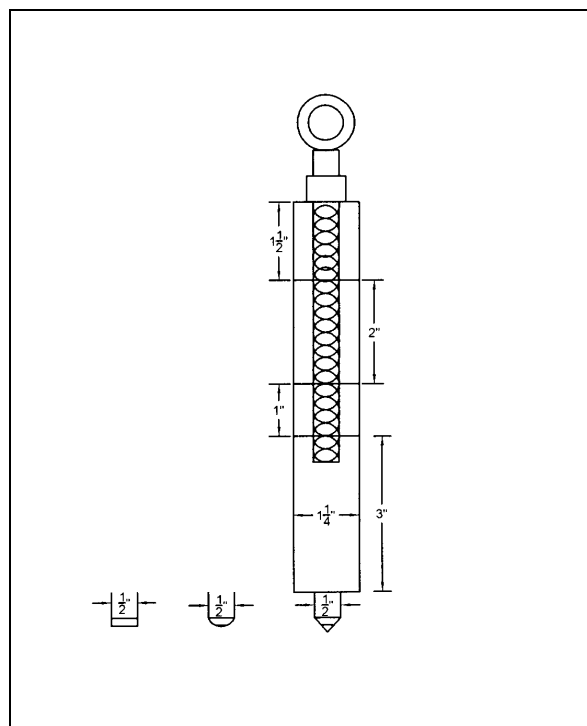


Figure 5 Indenter Dimensions

APPENDIX D

TIMING SYSTEM DESIGN

In order to measure the impact velocity by an alternative method, we decided on a timing system to measure the drop time of the falling impact weight over a given distance. So we designed a system from component off-the-shelf parts. This system uses optical emitters and sensors which send a start pulse and an end pulse to a timer whenever a light beam is interrupted. Figure 1 illustrates the component parts of this system.

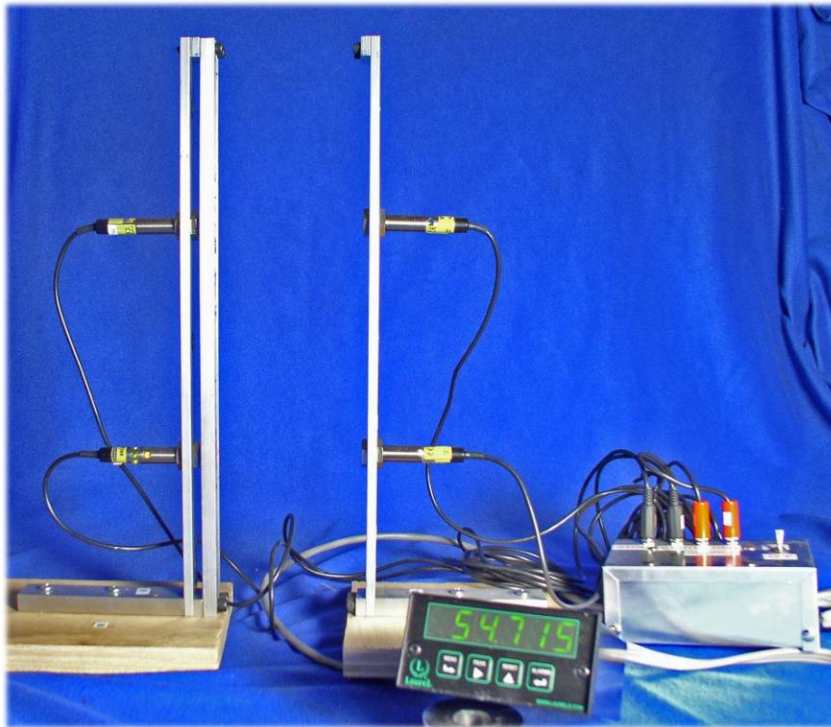


Figure 1 Component parts of the timing system

The system consisted of two aluminum brackets with the option for placing optical sensors at different heights by having a series of holes precisely drilled in the bracket. The right bracket contained the emitting light (660 nm visible red wavelength) and the left bracket was likewise arranged with the sensors with the addition of an aluminum plate which covered these sensitive sensors. In this plate are a series of very accurately predrilled 1/16" apertures spaced

three inches apart and centered over sensor slots. This arrangement allows for the precise measurement. When a falling object passes over the first 1/16" diameter aperture the timing begins. When the falling object interrupts the aperture of the second sensor, the sensor sends another signal ending the timing sequence. Figure 2 illustrates the brackets and the timing unit. Figure 3 is a close up of the sensor.

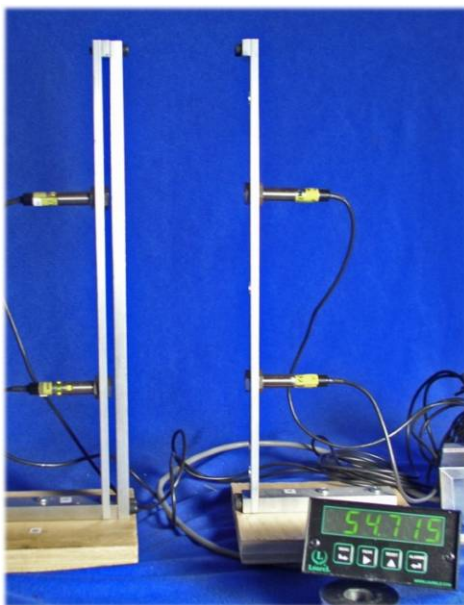


Figure 2 Bracket and timer



Figure 3 Sensor configuration

A line drawing of the timing system bracket is illustrated in Figure 4.

The timing system is capable of $0.2\mu\text{s}$ response over a one hour time frame. Its accuracy is limited to the response time of the sensors. With Banner M12E & M12NR sensors, the system will measure the time to $\pm 2\%$ at a 6 ft drop and $\pm 3.6\%$ at 20 ft. worst case scenario. Thus our accuracy is dominated by the $85\mu\text{s}$ repeatability spec on the photo sensor. The sensor specifications are listed in Table 2 and the timer specifications in Table 3.

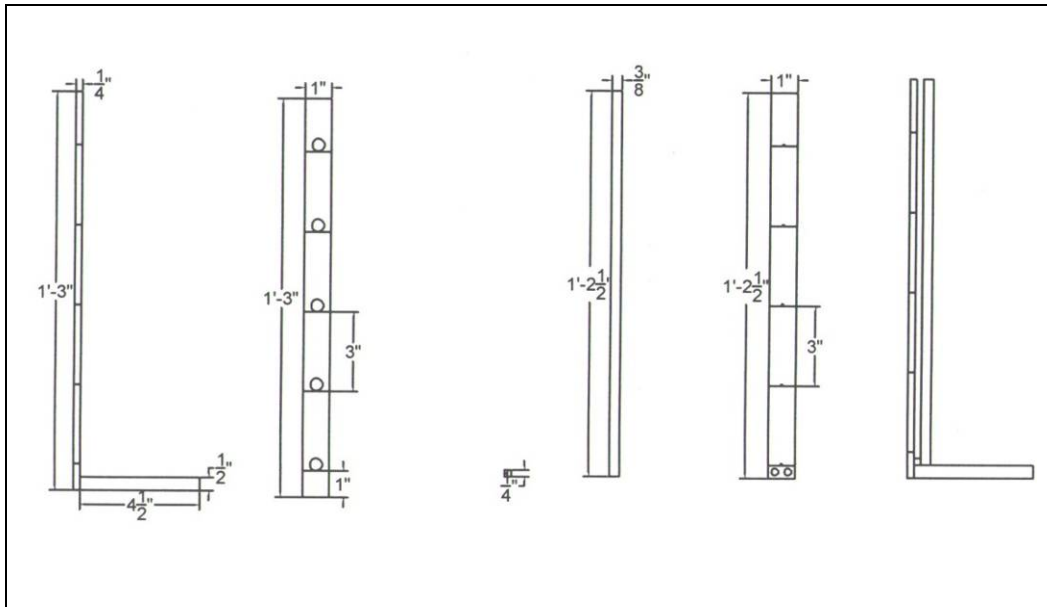


Figure 4 Timing bracket dimensions

Sensor Specifications

<p>Sensors: Model M12-PR Banner M12 Series Barrel Sensors Banner Engineering Corp. 9714 Tenth Avenue North Minneapolis, MN U.S.</p>	<p><u>Sensing Mode:</u> 660 nm visible red <u>Repeatability:</u> 85 microseconds <u>Sensor range:</u> 5 meters <u>Output:</u> Complementary (1 normally open and 1 normally closed) solid-state, NPN or PNP, <u>Output Response time:</u> 625 microseconds ON/375 microseconds OFF.</p>
--	---

Table 2 Sensor specifications

Timing Unit Specifications

<p>Digital Panel Timer Laurel Electronics Model L50000FR Timer SN 092211-154 3183-G Airway Avenue Costa Mesa, CA 92626,</p>	<p>Highest resolution is 0.2 us. The event time may be displayed H, M or S format with six-digit resolution or in HH.MM.SS clock format with 1 s resolution. The stopwatch display is updated during timing. Accumulated time from multiple events is also tracked and may be displayed to 999,999 hours.</p>
---	---

Table 3 Timer specifications

Accuracy Calculations

We developed some accuracy calculations using a spread sheet to see what the potential error rate was and deemed it would have no relevant impact our data. Table 4 illustrates a portion of that spread sheet.

Banner M12 Repeatability										
G =		32.174	ft/sec²					85.000	us	
					Worst Case Error			170.000	us	0.17
Drop	Drop	Time	Velocity	delta t	Measured					
inches	feet	Sec	ft./sec	for 2 in	V last 2 in		Low Time	Nom Time	High Time	Max Error
					Ft/sec		ms	ms	ms	%
0	0.00	0.0000	0.00							
2	0.17	0.1018	3.27	0.101786	1.64		101.616	101.786	101.956	0.17
4	0.33	0.1439	4.63	0.042161	3.95		41.991	42.161	42.331	0.40
6	0.50	0.1763	5.67	0.032351	5.15		32.181	32.351	32.521	0.53
8	0.67	0.2036	6.55	0.027273	6.11		27.103	27.273	27.443	0.62
10	0.83	0.2276	7.32	0.024028	6.94		23.858	24.028	24.198	0.71
12	1.00	0.2493	8.02	0.021723	7.67		21.553	21.723	21.893	0.78
14	1.17	0.2693	8.66	0.019977	8.34		19.807	19.977	20.147	0.85
16	1.33	0.2879	9.26	0.018594	8.96		18.424	18.594	18.764	0.91
18	1.50	0.3054	9.82	0.017464	9.54		17.294	17.464	17.634	0.97
20	1.67	0.3219	10.36	0.016518	10.09		16.348	16.518	16.688	1.03
22	1.83	0.3376	10.86	0.015710	10.61		15.540	15.710	15.880	1.08
24	2.00	0.3526	11.34	0.015011	11.10		14.841	15.011	15.181	1.13
26	2.17	0.3670	11.81	0.014398	11.58		14.228	14.398	14.568	1.18
28	2.33	0.3808	12.25	0.013854	12.03		13.684	13.854	14.024	1.23
30	2.50	0.3942	12.68	0.013367	12.47		13.197	13.367	13.537	1.27

Table 4 Calculation of sensor error rate